Assessment of seismic floor acceleration demands on non-structural components in limited ductility RC frame buildings designed according to NBC 2015

by

Reza SHEIKHZADEH SHAYAN

MANUSCRIPT-BASED THESIS PRESENTED TO ÉCOLE DE TECHNOLOGIE SUPÉRIEURE IN PARTIAL FULFILLMENT FOR A MASTER'S DEGREE WITH THESIS IN CONSTRUCTION ENGINEERING
M. A. Sc.

MONTREAL, JUNE 13, 2022

ÉCOLE DE TECHNOLOGIE SUPÉRIEURE
UNIVERSITÉ DU QUÉBEC

BOARD OF EXAMINERS

THIS THESIS HAS BEEN EVALUATED

BY THE FOLLOWING BOARD OF EXAMINERS

Mrs. Rola Assi, Thesis Supervisor
Department of Construction Engineering, École de technologie supérieure

Mrs. Ivanka Iordanova, President of the Board of Examiners
Department of Construction Engineering, École de technologie supérieure

Mr. Reda Snaiki, Member of the jury
Department of Construction Engineering, École de technologie supérieure

THIS THESIS WAS PRENSENTED AND DEFENDED

IN THE PRESENCE OF A BOARD OF EXAMINERS AND PUBLIC

JUNE 13TH, 2022

AT ÉCOLE DE TECHNOLOGIE SUPÉRIEURE

ACKNOWLEDGMENT

I am indebted to my supervisor, Professor Rola Assi, for her continued guidance through this project. I have benefited significantly from her wealth of knowledge and meticulous editing and review. I am also highly thankful for her financial support in carrying out this research.

I gratefully recognize the help of the Ph.D. candidate, Mr. Shahabaldin Mazloom, in providing the design sections of the studied buildings.

I am incredibly grateful for my parents, whose constant love and support keep me motivated and confident. My accomplishments and success are because they believed in me. My deepest thanks to my siblings, who keep me grounded, remind me of what is essential in life, and always support my adventures. Finally, I owe my deepest gratitude to my soulmate, Sheida. I am forever thankful for the unconditional love and support throughout the entire thesis process and every day.

ÉVALUATION DES ACCELERATIONS DE PLANCHER SISMIQUES SUR LES COMPOSANTS NON STRUCTURAUX DANS DES BATIMENTS EN BETON ARME A OSSATURE RESISTANT AUX MOMENTS DE DUCTILITE MOYENNE ET CONÇUS SELON LE CNB

Reza SHEIKHZADEH SHAYAN

RESUME

Cette recherche se concentre sur la quantification des demandes sismiques sur les composants non structuraux (CNS) sensibles à l'accélération attachés aux bâtiments à ossature RC résistant au moment avec une ductilité limitée et conçus selon le code national du bâtiment du Canada (CNB 2015). Un total de quatre structures de référence avec des hauteurs variables sont considérées dans cette étude, et la capacité sismique de ces bâtiments a été évaluée à l'aide d'une analyse statique non linéaire effectuée dans le logiciel SAP 2000. Des analyses dans le domaine du temps ont été effectuées sur des bâtiments élastiques et inélastiques en utilisant des séismes synthétiques compatibles avec les spectres d'aléa sismique uniforme de Montréal pour un sol ferme (sol classe C – CNB 2015) avec des périodes de retour de 475 et 2475 ans. Les demandes d'accélération sismique sur les CNS sont évaluées en déterminant les l'amplifications des accélérations maximales du plancher (PFA) et le facteur d'amplification des composants le long de la hauteur des bâtiments, par rapport aux dispositions de divers codes de bâtiment, y compris NBC 2015, ASCE7, EC8, NZS 1170.5 et ATC. Finalement, la performance sismique globale des CNS est discutée en évaluant le coefficient de force du composant, et un profil optimisé correspondant est proposé pour améliorer l'estimation des demandes d'accélération sismique sur les CNS dans une zone sismique modérée.

Mots-clés : Composants non structuraux, Demande d'accélération sismique, spectres d'aléa uniforme, Facteur d'amplification du composant, Facteur de force du composant

ASSESSMENT OF SEISMIC FLOOR ACCELERATION DEMANDS ON NON-STRUCTURAL COMPONENTS IN LIMITED DUCTILTY RC FRAME BUILDINGS DESIGNED ACCORDING TO NBC 2015

Reza SHEIKHZADEH SHAYAN

ABSTRACT

This research focuses on quantifying the seismic demands on the acceleration-sensitive non-structural components (NSCs) attached to the RC moment-resisting frame buildings with limited ductility and designed according to the National Building Code of Canada (NBC 2015). A total of four benchmark structures with varying heights are considered in this study, and the seismic capacity of frame buildings has been evaluated using nonlinear static analysis performed in the SAP 2000 software. Time-history analyses have been performed on elastic and inelastic buildings utilizing simulated ground motion records compatible with Montreal uniform hazard spectra for firm ground (site class C in NBC 2015) with 475 and 2475-year return periods. Seismic acceleration demands on NSCs are evaluated by assessing the amplification of horizontal peak floor acceleration (PFA) and the component amplification factor along the height of buildings, compared to the various building code provisions, including NBC 2015, ASCE7, EC8, NZS 1170.5, and ATC. Finally, the overall seismic performance of NSCs is discussed by evaluating the component force factor, and a corresponding optimized profile is proposed to improve the estimation of seismic acceleration demands on NSCs in a moderate seismic zone.

Keywords: Non-structural components, Seismic acceleration demand, Uniform hazard spectra, Component amplification factor, Component force factor

TABLE OF CONTENTS

Page

LIST OF TABLES

Page

LIST OF FIGURES

Page

LIST OF ABREVIATIONS

ASCE	American Society of Civil Engineers
CSA	Canadian Standards Association
EC 8	Eurocode 8
ESFP	Equivalent static force procedure
FEMA	Federal Emergency Management Agency
FRS	Floor response spectrum
GMR	Ground motion record
HVAC	Heating-ventilation-air conditioning
IO	Immediate Occupancy performance level
LS	Life safety performance level
MD	Moderately ductile
MDOF	Multi degree of freedom
MRF	Moment-resisting frame
NBC	National building code of Canada
N-S	North – South direction
NSCs	Non-structural components
OFCs	Operational and functional components
PCA	Peak component acceleration
PFA	Peak floor acceleration
PGA	Peak ground acceleration
RC	Reinforced concrete
SDOF	Single degree of freedom
SFRS	Seismic force resisting system
SRF	Stiffness reduction factor
UHS	Uniform hazard spectrum

LIST OF SYMBOLS

Greek alphabet

ΔLS	Displacement at life safety performance level
Δy	Yield displacement
ζ_0	Structural damping
ζ_{eq}	Equivalent damping
ζ_{hys}	Hysteretic damping
λ	Factor to account for low-density concrete
ϕ_y	Yield rotation
ω_i	Angular frequency at mode i

Lowercase Latin alphabet

a_0	Mass proportional coefficient
a_1	Stiffness proportional coefficient
a_g	Design ground acceleration on type A ground as per Eurocode 8
a_p	The dynamic amplification factor as per ASCE 7-16
b	Parameter of deformation capacity in component load–deformation curve given by ASCE 41-17

Uppercase Latin alphabet

A_r	The dynamic amplification factor as per NBC 2015
A_x	Height factor in NBC
D	Dead load
E	Earthquake load
E_C	Young modulus of concrete
E_S	Young modulus of steel

F_a	The acceleration-based site coefficient
F_p	Component seismic design force applied horizontally at the center of gravity of the component
F_t	Concentrated force applied at the top of the building
F_X	Portion of design base shear that is located at level x
h_i	The height above the base to level i
h_x	The height above the base to level x
I_E	The importance factor of the building as per NBC 2015
L	Live Load
M	Moment magnitude of an earthquake event
M_n	Nominal flexural resistance
M_p	Probable flexural resistance
M_r	Factored flexural resistance
M_v	Factor accounting for higher mode effect on the base shear force
M_y	Yield moment
R	Fault distance
R_d	Ductility-related force modification factor
R_O	Overstrength-related force modification factor
R_p	Component response modification factor
S	Snow load
$S_a(0.2)$	The spectral acceleration value for a period of 0.2 s
$S(T)$	The spectral acceleration value for a period of T
$S_T(T)$	Spectral acceleration of target spectrum
T_a	Building period defined by code expression
T_P	Non-structural component period
T_{1Bldng}	The fundamental period of the building
T_{iBldng}	The building period of mode i
T_{max}	The upper limit of period range *T*R
T_{min}	The lower limit of period range *T*R

T_R	Period range of interest for selection and scaling ground motion
$T_{90\%}$	The period of the highest vibration mode required to cumulate a minimum participating mass of 90% of the structure mass
V	Design base shear
V_{max}	Upper limit of design base shear
V_{min}	Lower limit of design base shear
V_y	Base shear force at yielding point
W	Seismic weight of building
W_i	Portion of W that is located at level i
W_P	Non-structural component weight
W_x	Portion of W that is located at level x

INTRODUCTION

Background and problem statement

There are generally two primary categories associated with the components in buildings based on their load-bearing capacity: structural components and non-structural components (NSCs), also known as Operational and Functional Components (OFCs) as per CSA S832-14 (2014b). NSCs are elements or subsystems that mainly do not contribute to the lateral load-bearing systems; however, the total operability of the buildings highly depends on the functionality of these components, specifically after seismic events. Generally, based on the location, method of construction or fastening, some NSCs may affect the total structural integrity of the building. NSCs are divided into three categories according to CSA (2014b) and Villaverde (1997): architectural ("internal" like interior partition walls, and "exterior" like cladding and parapets), Building or operational services, including mechanical systems (i.e., heating, ventilation and air-conditioning systems, elevators) electrical systems (i.e., transformers, battery racks), information technology and communication systems (i.e., telephone systems, cable trays), and building contents ("common" like supplies, computer systems, and "specialized" like fine arts, medical equipment).

Numerous amounts of research have been conducted during the years to evaluate the performance of the structural components, and plenty of deficiencies in cases of both designing and constructing the structural elements have been overcome. Although the improvement of structural components has prevented buildings from collapsing, it has been observed that due to the failure of NSCs, buildings may end up inoperable after even a moderate earthquake (Fierro et al., 2011; Miranda et al., 2012; Kazantzi A. K. et al., 2020). This phenomenon has shifted the interests of researchers toward assessing the seismic performance of NSCs to pave the way for reaching out to more effective seismic design methodologies as the major financial loss during a seismic excitation is related to the failure of NSCs (Miranda & Taghavi, 2003; Gupta & McDonald, 2008; Bradley et al., 2009; Anajafi et al., 2020; Rashid et al., 2021).

NSCs are commonly mounted on the building's floors or are attached to or hung from structural elements such as columns or slabs. In this case, NSCs are exposed to the amplified seismic excitation as both the primary structure and the NSC filter the ground motion experienced at the base of the structure (Petrone et al., 2016; Anajafi et al., 2020). The filtering effect of the supporting structure can drastically alter the frequency content of the original ground motion; therefore, the acceleration motion on each floor is different from the ground acceleration motion. Two crucial factors taking part in the first filtering effect are the floor level in which the NSC is attached relative to the base of the supporting structure and the inelasticity of the supporting structure that can considerably reduce the seismic acceleration demands on NSCs. Also, NSC filters the floor acceleration motion, such that the acceleration responses of NSCs are typically narrow-band and are markedly different from the broad-band characteristics of the original ground motion. Also, an essential component of the second filter is the ratio of the NSCs period to the fundamental period of the supporting structure, also referred to as the tuning ratio.

In this case, various studies have been conducted to evaluate the floor accelerations and the floor response spectra (FRS) in the elastic and inelastic buildings (Lin Jon & Mahin Stephen A., 1985; Sewell et al., 1986; Rodriguez et al., 2002; Singh M. P. et al., 2006; Sankaranarayanan & Medina, 2007; Wieser et al., 2013; Lucchini et al., 2014; Petrone et al., 2016; Merino et al., 2020; Haymes et al., 2020; Anajafi et al., 2020). The references mentioned above primarily compared the numerical results with various code provisions such as the proposed values for the height factor and the component amplification factor and have proposed novel equations to evaluate the floor spectral ordinates. Although the code-based formulations are commonly used to assess the seismic acceleration demands on NSCs, it has been observed that the building code provisions mostly fail to predict an adequate seismic performance of NSCs (Petrone et al., 2016; Kazantzi A. K. et al., 2020). This is primarily because the code provisions are based on the engineering judgment rather than the analytical or experimental results (Filiatrault & Sullivan, 2014).

Generally, recent studies on the seismic acceleration demands on NSCs mainly consider the ductility of the supporting structure and are mostly targeted at the US and European building code provisions. The ductility of the NSCs, which is also addressed by the code provisions to reduce the seismic acceleration demands on NSCs, is rarely considered. Moreover, few studies (Shooshtari et al., 2010; Asgarian & McClure, 2017, 2020a, 2020b) have been conducted to evaluate the seismic force demands of acceleration-sensitive NSCs attached to the buildings designed according to the National Building Code of Canada (NRCC, 2015). Furthermore, the effect of the severity of the input ground motion records (GMRs) on the acceleration demands on NSCs is not adequately addressed. Therefore, the shortcomings mentioned above have been investigated in this study, and more specifically, the obtained results are critically compared to the NBC provisions and other international building codes.

Objectives

The primary purpose of this study is to evaluate the seismic acceleration demands on non-structural components in moderately ductile RC moment-resisting frame buildings designed according to Canadian provisions. The specific objectives of this study are as follows:

1. Evaluate the effect of nonlinearity and height of the supporting structure on the seismic acceleration demand on NSCs, represented by the height factor, the recorded floor response spectra, the component amplification factor, and the component force factor.
2. Evaluate the effect of severity of the input GMRs on the seismic response of NSCs by using two sets of artificial GMRs with 475 and 2475-year return periods.
3. Evaluate the current code seismic provisions' accuracy in estimating the seismic demands on acceleration-sensitive NSCs.

Methodology

The following step by step procedure has been considered to achieve the objectives of this research:

1. Performing a comprehensive literature review on seismic response of NSCs.
2. Selection and modeling the reinforced concrete (RC) moment-resisting frame (MRF) buildings with varying height designed according to NBC 2015 (Mazloom & Assi, 2022).
3. Performing modal analysis on the 2D models via SAP2000 to obtain the fundamental periods of the selected buildings.
4. Determining the flexural capacity of the concrete sections by performing sectional analysis using Response 2000, defining the nonlinear properties of the concrete components according to ASCE 41-17, and assigning them to the structural elements.
5. Performing nonlinear static (Pushover) analysis to obtain the structures' nonlinear capacity and define the different structural limit states for each building model.
6. Selecting and scaling a set of suitable synthetic ground motion records compatible with the UHS in Montreal at 2% and 10% probabilities of exceedance per 50 years.
7. Performing linear and nonlinear time history analysis (NTHA) to obtain the height factor and component amplification factor.
8. Comparing the obtained results from elastic and inelastic analysis of the buildings with varying heights to evaluate the effects of the inelasticity and height of the supporting structure on the seismic acceleration demands on NSCs.
9. Comparing the obtained results from numerical analyses with the various building code provisions to evaluate the accuracy of the code-based formulations.

Limit of study

The limitations of this study are as follows:

1. The seismic acceleration demands on NSCs has been investigated on 2D frame building models created via SAP2000.

2. Only moderately ductile buildings have been studied in this research, and the effect of considering various ductility levels on the seismic response of NSCs is out of the scope of this research.
3. The acceleration-sensitive NSCs are solely selected to be investigated in this research, and the dynamic interaction between the NSCs and the supporting structure is neglected due to assuming that the total mass of the NSCs is less than 0.5% of the mass of the primary structure.
4. 5% damping ratio was considered for NSCs in this study. The effect of considering NSCs with smaller or larger damping ratios has not been investigated in this study.

Thesis organization

This thesis comprises four chapters in addition to the Introduction, conclusions, and recommendations. In the first chapter, a comprehensive literature review has been performed, and the seismic acceleration demands on NSCs in RC frame buildings have been critically reviewed. More specifically, the literature review is concentrated on the two crucial factors: the height factor and the component amplification factor. Also, the comparison of the obtained results from numerical analyses with various building code provisions is reviewed. In the second chapter, the salient characteristics of the selected buildings have been described. Also, the selection of the synthetic GMRs and the specific approach to scale them are elaborated. The third chapter discusses a detailed description of the nonlinearity in the concrete components in the frame buildings, details of performing pushover, and the linear and nonlinear time-history analyses. In the fourth chapter, a journal manuscript is presented. The seismic acceleration demands on NSCs are discussed in the forms of height factor and component dynamic amplification factor, and results are compared with the proposals of the various provisions. Also, the component force factor is investigated to evaluate the overall seismic acceleration demands on NSCs. Moreover, a corresponding optimized profile is proposed to improve the evaluation of the seismic acceleration demands on NSCs in RC frame buildings in moderate seismic zones. Finally, conclusions and recommendations for further studies are presented.

CHAPITRE 1

LITERATURE REVIEW

This section presents a brief explanation of the importance of NSCs and their contribution to the operability and functionality of buildings after seismic events. Furthermore, different parameters involved in estimating the design force of acceleration-sensitive NSCs are introduced. Moreover, the effect of considering ductility of the supporting structure, height levels, and the tuning ratio on the seismic response of NSCs has been discussed. Also, a detailed literature review has been conducted on the suggested formulations by multiple code provisions, including NBC 2015, ASCE7, EC8, NZS 1170.5, and ATC and the previous research works to evaluate the seismic demands of NSCs.

1.1 Introduction

The elements in buildings are divided into two groups depending on their load-bearing capacity: structural and non-structural components. The examples of various non-structural elements in buildings are illustrated in Figure 1.1 (CSA, 2014a). NSCs generally do not participate in load-bearing systems; however, the major operability disruption of the buildings after experiencing earthquakes with low to moderate intensity levels corresponds to the failure of NSCs (NIST, 2017). Although the failure of these components may not culminate with the total loss of the structural integrity or collapse, experiences from the past earthquakes show that several buildings shifted from their safe-serviceable range toward an inoperable state immediately after the earthquake due to the failure or severe falling hazard of NSCs. Figure 1.2 illustrates the damage to internal partitions and infill walls during the M_W 4.9 earthquake, which hit the northern part of Campania, Italy, in 2013 (Petrone et al., 2016). This condition can be critical, specifically for the buildings with high importance of occupancy level, such as hospitals (Naeim, 2004; Hur et al., 2017). Therefore, it becomes crucial to meet the total seismic performance requirements of a building, and it is essential to precisely estimate the floor acceleration demands imposed on NSCs in each story level (Taghavi & Miranda, 2005b; Vukobratović & Fajfar, 2017; Welch & Sullivan, 2017; González et al., 2019).

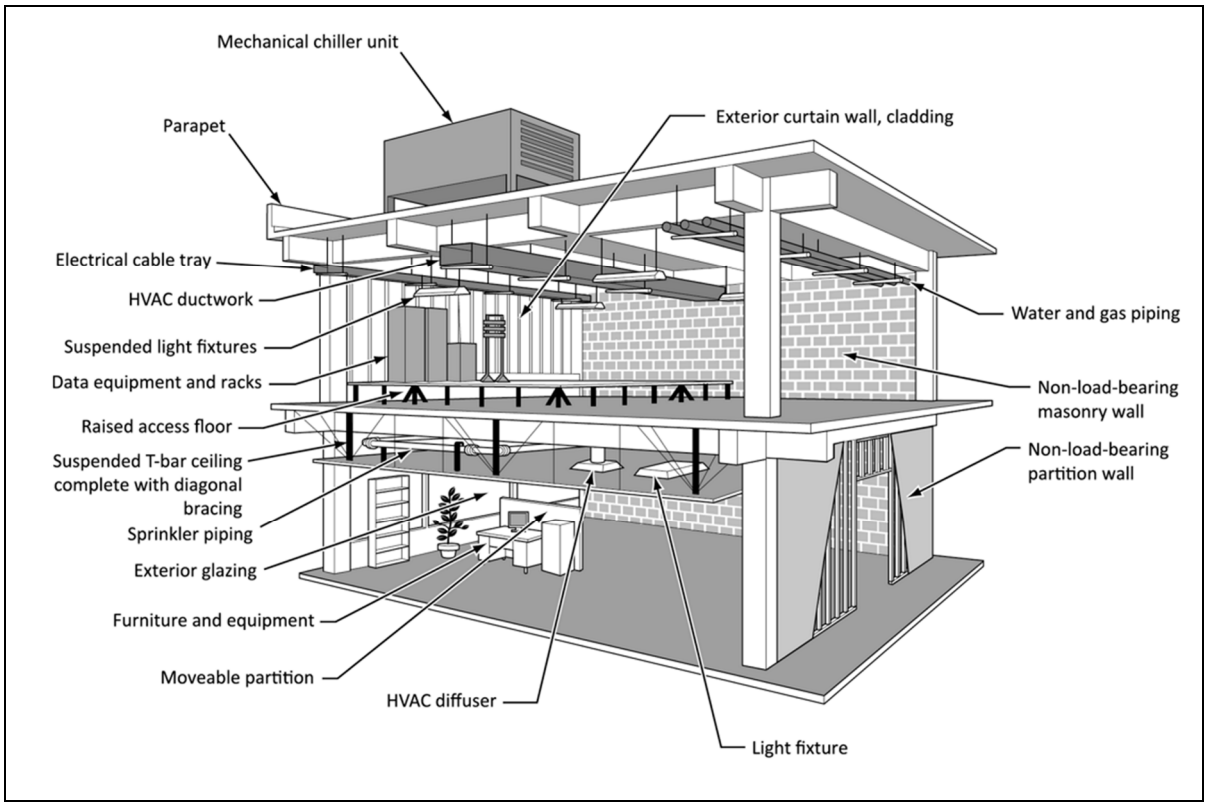

Figure 1.1 Examples of non-structural components in buildings

(a) (b)

Figure 1.2 Damage to (a) infill walls and (b) internal partition after M_w 4.9 earthquake in Italy, 2013

Based on the response parameters causing damages incurred to NSCs, there are two major classifications: acceleration-sensitive and displacement-sensitive components. When a seismic motion strikes a structure, vertical and horizontal floor accelerations trigger the inertia forces of the components mounted on the floor; hence, the components may overturn. In this case, the inertia forces govern the seismic design of NSCs. These components are considered acceleration-sensitive NSCs, such as anchored or free-standing mechanical and electrical systems for fire protection, heating-ventilation-air conditioning (HVAC), water distribution, piping systems, and ceiling systems. Examples of displacement-sensitive NSCs are wall partitions and glazing facades in which the induced damages to these components are due to the inter-storey drifts in the supporting structure.

1.2 Evaluation of seismic force demands on acceleration-sensitive NSCs

Different approaches can be utilized to investigate the seismic acceleration demands on NSCs:
1) Simplified formulations suggested by various building codes, including ASCE 7 (2013), NBC 2015 (2015), ATC (2018), Eurocode 8 (2005), and NZS 1170.5 (2016) to account for the horizontal seismic design force acting on the center of the mass of the NSCs. These formulations are based on the equivalent static methods, commonly utilized as a convenient tool when scant information about NSCs and supporting structure is available at the design phase.
2) A more common method to evaluate the seismic acceleration demands on NSCs is the floor response spectrum (FRS) approach: an uncoupled analysis between NSC considered a single-degree-of-freedom (SDOF) system and the primary structure.
3) The most accurate approach to investigate the seismic acceleration demands on NSCs is the coupled time-history analysis that requires the availability of the dynamic characteristics of the primary structure and the different types of NSCs. In this method, the dynamic interaction between NSCs and the primary structure is taken into account to consider the system integrity. However, this approach is rarely utilized due to significant modelling complexity.

1.3 Seismic force demands of NSCs according to the simplified code-based formulations

Design force formulations of NSCs suggested by seismic code provisions are mainly based on engineering judgment rather than the analytical or experimental results (Filiatrault & Sullivan, 2014). Therefore, several studies attempted to improve the various seismic regulations related to NSCs, specifically ASCE 7 and EC8. Also, building code formulations include several parameters that represent the seismic characteristic of NSCs, in which the two crucial factors, including the height factor and the dynamic amplification factor, have been extensively investigated in numerous studies. Various code provisions and the main components in the formulations are introduced in the following:

1.3.1 NBC 2015 and ASCE7-16

The seismic design force of NSCs addressed by NBC 2015 is presented in Equation 1.1.

$$V_P = 0.3F_aS_a(0.2)I_ES_PW_P \quad (1.1)$$

Where; $0.3F_aS_a(0.2)I_E$ is equivalent to the expected peak acceleration at the base of the building in which; F_a is the acceleration-based site coefficient; $S_a(0.2)$ is the spectral response acceleration value at 0.2 second; and I_E is the importance factor of the building. W_P is the operating weight of the component. S_P is the component response factor determined using Equation 1.2.

$$0.7 \leq S_P = C_PA_rA_x/R_P \leq 4.0 \quad (1.2)$$

Where; C_P is the element or component factor to account for the risk associated with the failure of component; A_r is the component force amplification factor that represents the dynamic amplification of the component relative to the position of its attachment.

A_r varies from 1.0 (no amplification) for the rigid components ($T_{NSC} < 0.06\ sec$) to 2.5 for the flexible ones ($T_{NSC} \geq 0.06\ s$). A_x is the height factor and it is equal to $1 + 2\,h_x/h_n$; in which the h_x is the NSC elevation in the building, and h_n is the total height of the building. The height factor represents the amplification of the acceleration from the base of the structure

to the height at which the component is attached with maximum value of 3.0 at the rooftop. Finally, R_P is the component response modification factor to recognize the energy dissipation capability of the component and its connection to the structure, it is equivalent to the reduction factor $R_d R_o$ used for buildings and varies from 1.0 to 5.0.

In United States, the seismic design force of NSCs is addressed in ASCE 7-16 by the Equation 1.3.

$$0.3 S_{DS} I_P W_P \leq F_P = \frac{0.4 a_P S_{DS} W_P}{R_P / I_P}\left(1 + 2\frac{z}{h}\right) \leq 1.6 S_{DS} I_P W_P \tag{1.3}$$

Where; a_P is the component amplification factor equivalent to A_r in NBC 2015, S_{DS} is the 5% damped site-specific design spectral acceleration at short period (0.2 sec); W_P is the component operating weight; z is the height of the attachment point of the NSC with respect to the base of the structure; h is the total height of the structure; R_P is the component response modification factor that corresponds to the capacity of NSCs to absorb energy (1.0 – 12); and I_P is the component importance factor (1.0 or 1.5).

1.3.2 Eurocode 8

In the EC8, the seismic design force of NSCs can be determined using the Equation1.4.

$$F_a = \frac{S_a \cdot \gamma_a}{q_a} W_a \tag{1.4}$$

With the seismic coefficient S_a, given by the Equation 1.5.

$$S_a = \frac{a_g}{g} S \left[\frac{3(1 + z/H)}{1 + (1 - T_P/T_1)^2} - 0.5\right] \leq \frac{a_g}{g} S \tag{1.5}$$

Where; γ_a is the component importance factor (1 or 1.5); W_a is the weight of the component; q_a is the component behavior factor (1.0 or 2.0); a_g is the design ground acceleration; g is the acceleration of gravity; S is the soil factor; z is the height of the NSC with respect to the base of the structure; H is the total height of the building; T_P is the fundamental period of the NSC; and T_1 is the fundamental period of the supporting structure. As illustrated in Equation 1.5, the

component amplification factor is dependent on the ratio of the period of the NSC to the fundamental period of the host structure (T_P/T_1). Moreover, EC8 does not account for the higher modes effect.

1.3.3 NZS 1170.5

According to the NZS 1170.5, the horizontal seismic design force of NSCs can be determined by the Equation 1.6.

$$F_{Ph} = C_P(T_P)C_{Ph}R_P W_P \leq 3.6W_P \tag{1.6}$$

Where; T_P is the component period, C_{Ph} is the horizontal response factor of the component; R_P is the component risk factor that varies regarding the failure consequences of the component; and W_P is the weight of the component. Also, $C_P(T_P)$ is the horizontal design coefficient of the component and can be determined using the Equation 1.7.

$$C_P(T_P) = C(0)C_{Hi}C_i(T_P) \tag{1.7}$$

The site hazard coefficient at $T = 0$ can be calculated using the Equation 1.8.

$$C(0) = C_h(0)ZRN(T, D) \tag{1.8}$$

Where; C_{Hi} is the floor height coefficient for level i; $C_i(T_P)$ is the spectral shape coefficient of the component for level i; $C_h(0)$ is the spectral shape factor at $T = 0$, Z is the hazard factor; R is the return period factor that can vary from 0.25 to 1.8 regarding the importance level of the supporting structure; and N is the near fault factor.

1.3.4 ATC approach (NIST.GCR.18-917-43)

Based on the recorded floor motions from the instrumented buildings and numerical investigations, the Equation 1.9 has been suggested by the Applied Technology Council in the USA (2018):

$$\frac{F_P}{W_P} = PGA\left[\frac{(\frac{PFA}{PGA})}{R_{\mu bldg}}\right]\left[\frac{(\frac{PCA}{PFA})}{R_{Pocomp}}\right]I_P \quad (1.9)$$

Where; PFA/PGA is the floor amplification factor and can be determined using the Equation 1.10.

$$\frac{PFA}{PGA} = 1 + a_1[z/h] + a_2[z/h]^{10} \quad (1.10)$$

With;

$$a_1 = (1/T_{abldg}) \leq 2.5 \quad (1.11)$$

$$a_2 = \left[1 - (0.4/T_{abldg})^2\right] > 0 \quad (1.12)$$

Where; W_P is the weight of the component, PGA is the peak ground acceleration; PFA is the peak floor acceleration; $R_{\mu bldg}$ is the reduction factor to account for building global ductility; R_{Pocomp} is the inherent component reserve strength margin factor; I_P is the component importance factor; z is the height of the NSC with respect to the base of the structure; h is the total height of the supporting structure; and T_{abldg} is the fundamental translational period of the supporting structure, can be determined using Equation 12.8-7 given in ASCE/SEI 7-16. Unlike ASCE 7 in which the floor amplification factor varies linearly from PGA at the base of the supporting structure to 3.0 times the PGA at the rooftop level, ATC approach suggested a nonlinear equation for the floor amplification. Also, the term PCA/PFA is dependent on the location of the component in the building, with values ranging between 1.4 and 4.0.

1.4 Summary of acceleration demands of NSCs according to building codes

As it is discussed earlier, two essential factors to investigate the seismic acceleration demands on NSCs are height factor and the component amplification factor. The height factor (A_x) accounts for the magnification of the floor acceleration, described as the ratio of PFA over PGA. The definition of height factor described by different code provisions is compared in

Figure 1.3. In the PFA/PGA distribution illustrated in Figure 1.3, a typical 9-storey building with the total height of 27 m is considered.

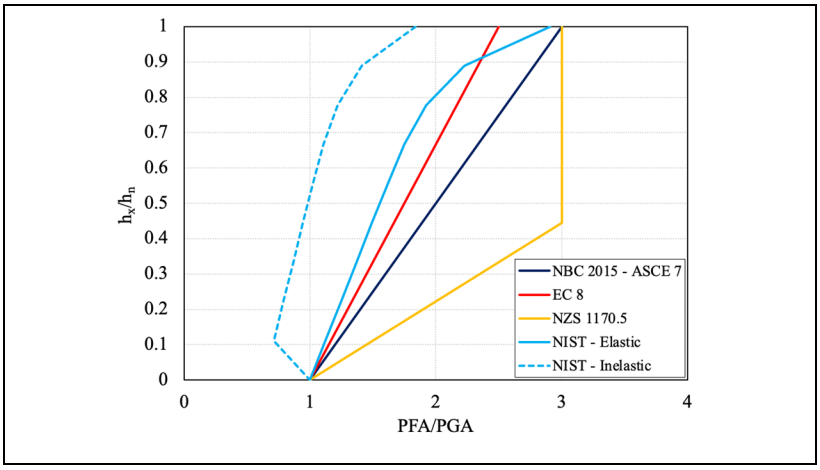

Figure 1.3 The PFA/PGA distribution

Also, the component dynamic amplification factor denoted by A_r in NBC represents the dynamic amplification of the component relative to the position of its attachment. It can be computed as the floor response spectrum (FRS) normalized by the peak floor acceleration (PFA) at a given building level. The variation of the component amplification factor proposed by various building codes at the rooftop of the buildings is illustrated in Figure 1.4.

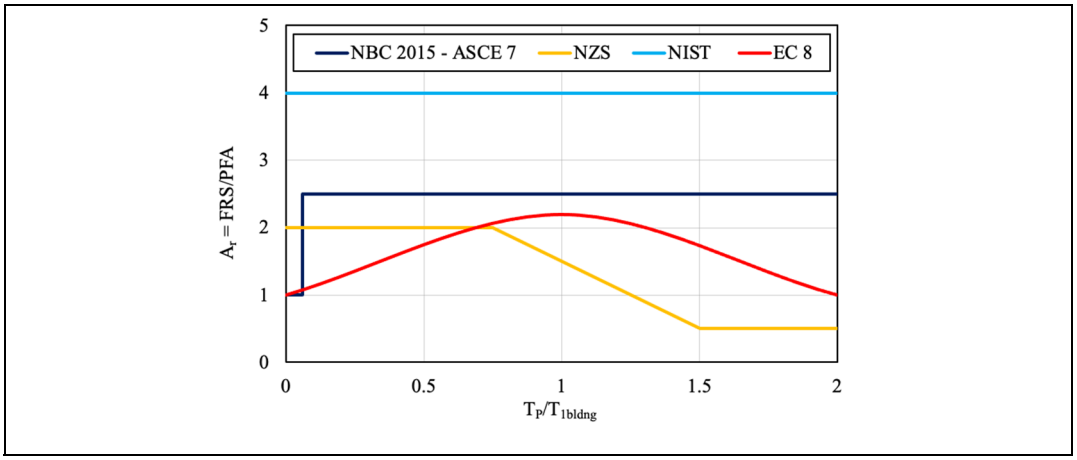

Figure 1.4 The component dynamic amplification factor in different design codes, proposed at the rooftop level

In general, except for the inelastic ATC approach, the current code formulations propose the linear profile for floor amplification and do not consider the higher modes' effect in determining the component amplification factor. In this case, utilizing the code formulations may result in either over-or-underestimation of the seismic acceleration demands on acceleration-sensitive NSC. In the following, a summary of the crucial findings of the previous studies regarding height factor, floor response spectra and the component amplification factor compared to the code provisions are discussed.

1.4.1 Height factor

In this context, Fathali and Lizundia (2011) proposed Equation 1.13 to determine the PFA demands of NSCs. It was discussed that compared to the straight PFA profile proposed by ASCE 7, Equation 1.13, which has a nonlinear trend and lets the relative height (z/h) varies exponentially, would give a better insight into the PFA demand.

$$\frac{PFA}{PGA} = 1 + \alpha(z/h)^{\beta} \tag{1.13}$$

Where: α and β are the functions of the PGA and fundamental period of the primary structure and are presented in Table 1.1.

Table 1.1 Values of parameters α and β

	Period range (s)	0.4SDS = PGA < 0.067g	0.067 ≤ 0.4SDS = PGA < 0.2g	0.4SDS = PGA ≥ 0.2g
α	$T_{Bldg1} < 0.5$	1.26	1.04	0.99
	$0.5 < T_{Bldg1} < 1.5$	1.52	1.02	0.65
	$T_{Bldg1} > 1.5$	0.90	0.72	0.00
β	$T_{Bldg1} < 0.5$	1.09	1.29	0.89
	$0.5 < T_{Bldg1} < 1.5$	1.57	1.63	1.55
	$T_{Bldg1} > 1.5$	1.69	3.00	1.00

Petrone et al. (2016) investigated seismic acceleration demands on the light acceleration-sensitive NSCs attached to the elastic and inelastic RC frame buildings with a high level of

ductility and varying height, designed according to EC8. Time-history analyses were performed using a set of frequent earthquake ground motions with a 63% probability of exceedance per 50 years and compared the obtained values of floor amplification with the proposals of EC8 and ASCE 7 provisions. As is shown in Figure 1.5, the elastic PFA/PGA ratio follows a linear trend relative to the height of the buildings. Also, the PGA is de-amplified in the lower floor levels of the taller buildings; however, PFA/PGA ratio is significantly amplified in the topmost level of all the buildings.

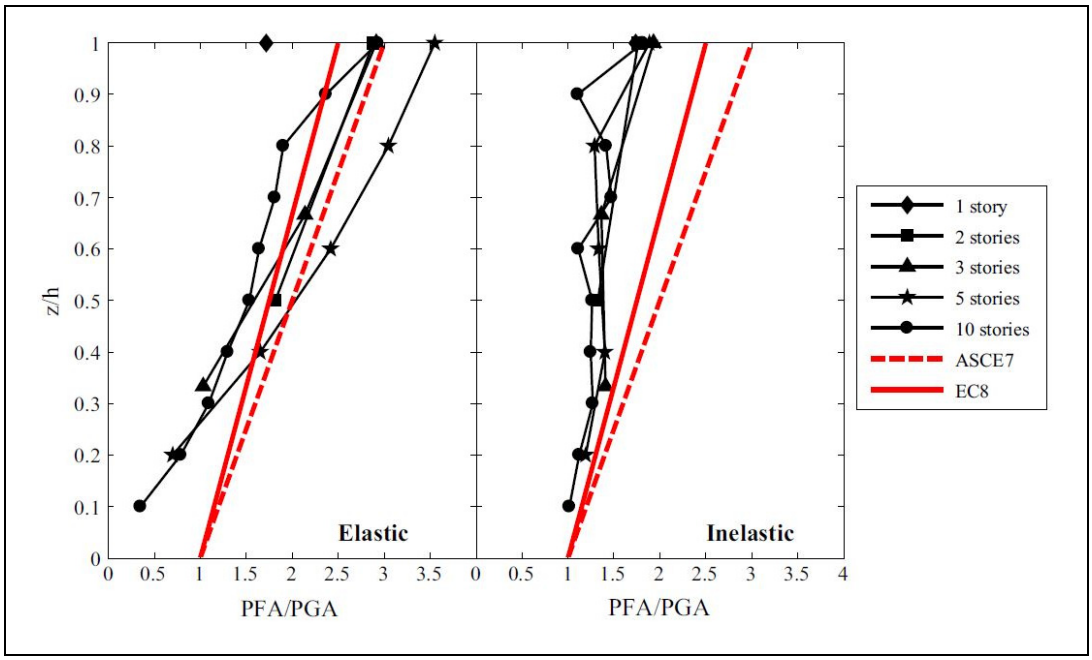

Figure 1.5 Floor amplification factor versus relative height of the different studied buildings compared to ASCE7 and EC8

Similarly, the PFA/PGA ratio has a linear trend along the height of the inelastic buildings. The floor acceleration response in the inelastic buildings is less amplified than elastic buildings due to the period elongation effect due to considering the inelasticity in the buildings.

Moreover, the PFA at the rooftop level of the buildings is dominated by the contribution of the higher modes, which causes the whiplash effect. This result was in accordance with the observation of Rodriguez et al. (2002) and Taghavi and Miranda (2005a); however, due to the low ductility demand of the studied buildings, the effect of this phenomenon on the results is

not noticeable. It was also discussed that both the ASCE 7 and EC8 provisions provided a safe floor amplification factor envelop for the inelastic structures, which are more adequate than the elastic ones.

In another research, Berto et al. (2020) investigated seismic acceleration demands of NSCs attached to RC buildings with slender cantilever wall (CW) and moment-resisting frame (MRF) as the seismic force-resisting systems (SFRS), as shown in Figure 1.6.

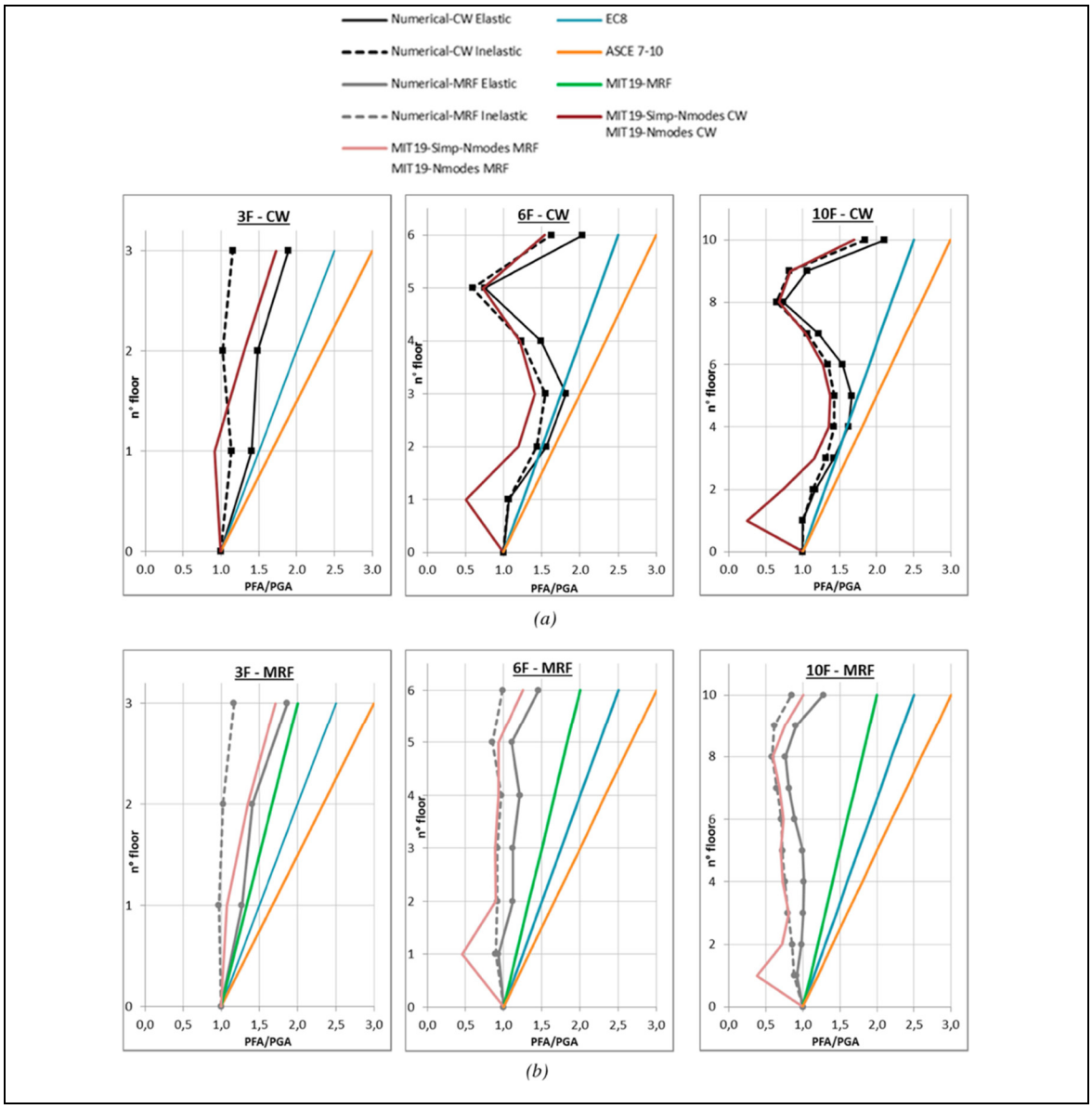

Figure 1.6 The PFA/PGA ratio for a) CW and, b) MRF buildings, compared with different code provisions

In this case, linear and nonlinear time-history analyses were performed on buildings with varying height levels by utilizing two different sets of 30 ground motion records to cover the wide range of frequency contents.

The PFA/PGA ratio profiles for different buildings were obtained and compared with ASCE 7 and EC8 provisions, and also two other proposals referred to as MIT19-MRF (MIT, 2019), which has been derived from the works of Petrone et al. (2016) and Fathali & Lizundia (2011), and MIT19-simp-Nmodes which has been exploited from the recent studies (Lagomarsino, 2015; Abbati et al., 2018) and have been presented in the commentary of Italian standard (MIT, 2019).

It can also be seen that for both CW and MRF buildings, the ASCE 7 proposal overestimated the values for the floor amplification, even when considering elastic buildings. On the other hand, the EC8 provision has estimated a safe-sided floor amplification compared to the numerical results. A good agreement between the obtained results and the MIT19-simp-Nmodes proposal derived based on the modal superposition approach is observed, specifically in the higher floor levels. However, this proposal overestimated floor amplification in the lower levels, even the elastic buildings. Moreover, the MIT19-MRF has also suggested conservative values of floor amplification for the MRF buildings.

Agrahari and Pathak (2021) investigated the seismic acceleration demands on NSCs in RC-MRF buildings with varying heights and utilized a wide range of ground motion records. The floor amplification factor for different buildings considering ground motions ranging less than 0.067 g was obtained and compared with ASCE 7 and Fathali and Lizundia's (2011) proposal, as depicted in Figure 1.7.

The 2-storey building represents buildings with a natural period of less than 0.5 second. For the buildings with a lower natural period, ASCE 7 overestimated the floor amplification factor, while Fathali and Lizundia (2011) showed 7% higher values for the mean amplification factor. Generally, ASCE 7 gives a better insight into the amplification factor for the buildings with a natural period below 1.0 sec, while it is conservative for the buildings with a natural period higher than 1.0 sec. Moreover, as the height of the building increases, the proposal of Fathali and Lizundia significantly overestimated the seismic demands. Finally, it is observed that by

considering the ground motion records ranging below 0.067 g, the proposed model by Fathali and Lizundia (2011) showed inadequate results.

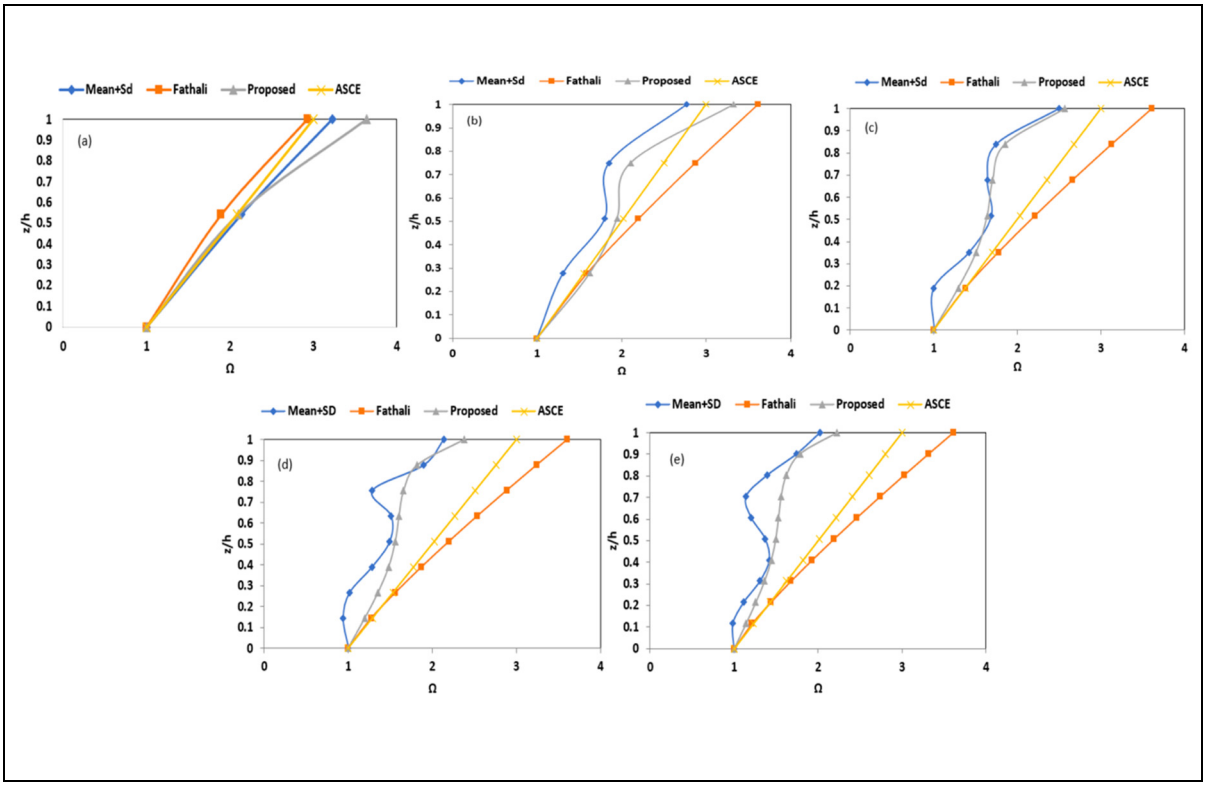

Figure 1.7 The floor amplification for buildings with a) 2, b) 4, c) 6, d) 8, and e) 10-storeys, compared with codes

Furthermore, Shang et al. (2022) calculated PFA/PGA ratio along the building height through performing elastic time-history analysis on the ductile RC-MRF buildings with varying heights. The obtained results from numerical analysis of individual buildings and the comparison of the results with ASCE 7, EC8, and GB 50011 (2010) are illustrated in Figure 1.8.

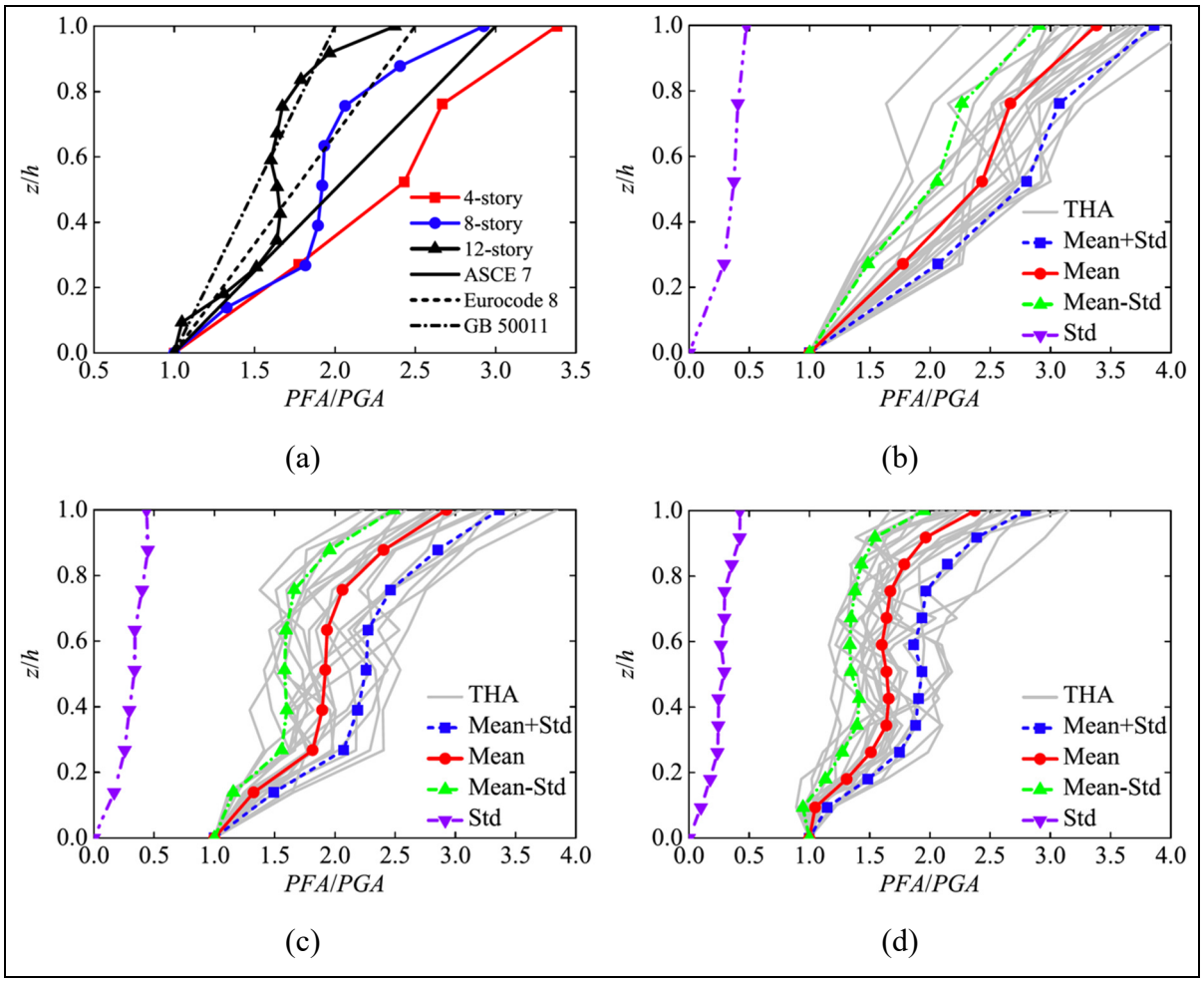

Figure 1.8 The PFA/PGA ratio, (a) comparison between the numerical results and current codes, (b) PFA/PGA in the 4-story frame, (c) PFA/PGA in the 8-story frame, (d) PFA/PGA in the 12-story frame

The variation of the mean PFA/PGA along the height of the building has a nonlinear trend. The structures with longer periods (i.e., the 12-storey frame) generally correspond to smaller PFA/PGA values than those with shorter periods (i.e., 4-storey frame). Moreover, a comparison of the results with the current codes shows that the ASCE 7 envelops the numerical results, except for the 4-storey frame. Also, GB50011 significantly underestimates the PFA demand over the height of the buildings. In general, it was concluded that the linear trend proposed by the current codes over-or under-estimates the PFA/PGA ratio along the building height.

1.4.2 Floor response spectra approach

The floor response spectra method is a simplified yet accurate analysis procedure to estimate the seismic acceleration demands on flexible NSCs. This approach is an uncoupled analysis between NSC, a single-degree-of-freedom (SDOF) system, and the primary structure. The NSCs usually have a small mass compared to the supporting structure (i.e., 0.5% of the total mass of the primary structure), so the dynamic interaction between NSCs and the primary structure can be neglected (Taghavi & Miranda, 2008).

Considering NSCs with a larger mass or those with the fundamental period tuned to the modal period of the supporting structure, which highlights the resonance phenomenon, the FRS method would result in an upper-bound seismic acceleration demands on NSCs (Kazantzi A. K. et al., 2020)

In this approach, seismic acceleration demands on NSCs can be directly assessed through generating FRS from the absolute acceleration response of the floor of a structure excited by shaking events (Wang et al., 2021), as illustrated in Figure 1.9. When a structure is struck by ground motion, the building modifies the frequency content of the base excitation as a filtering action and transfers it to the building floors. In this case, the recorded floor motion can describe seismic demands on NSCs mounted on or hung from building floors in terms of filtering and magnification parameters.

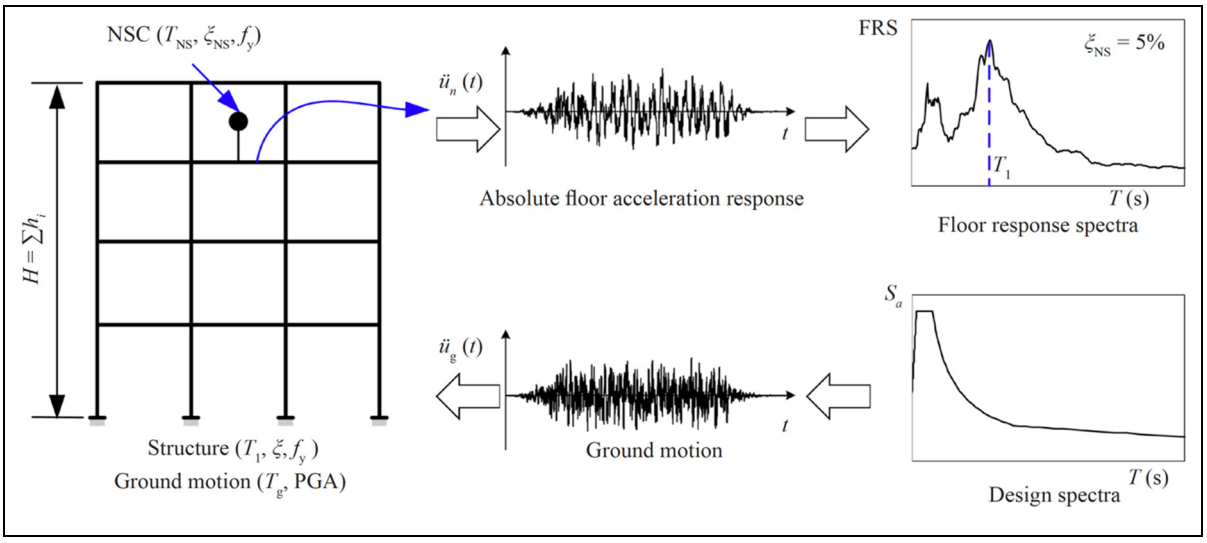

Figure 1.9 Generation of the FRS

Different methods have been developed to generate FRS that can be categorized into four groups; FRS based on SDOF models, FRS based on MDOF models, amplification factor methods, and directly defined FRS. Figure 1.10 (Wang et al., 2021) shows the schematic illustration of generating FRS based on different methods.

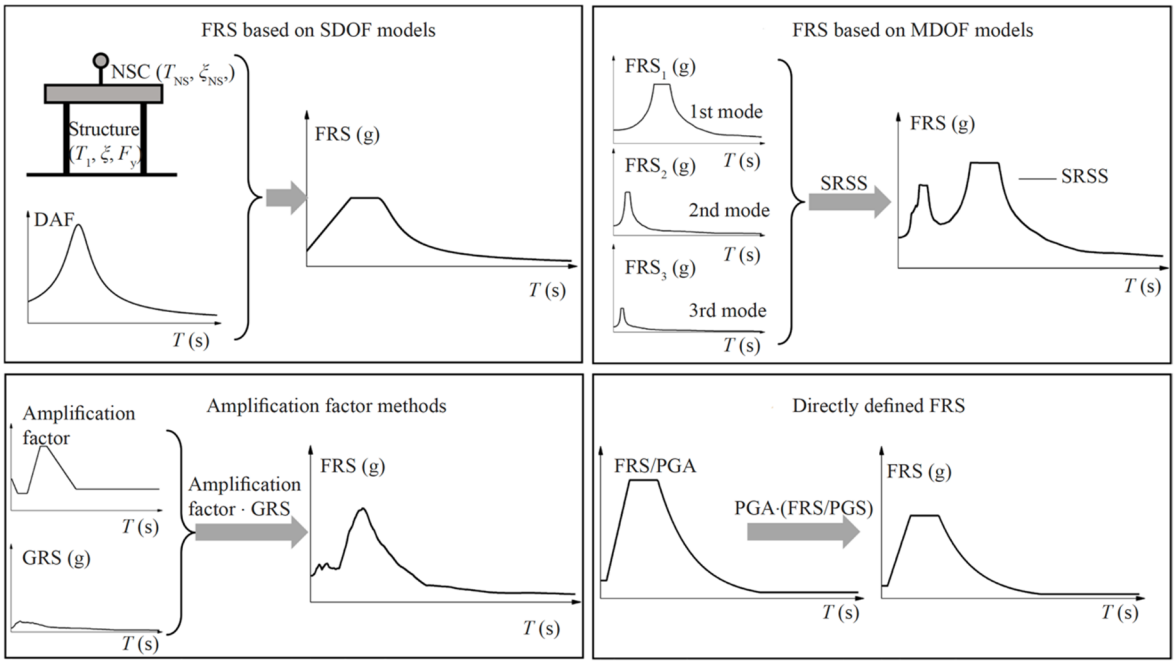

Figure 1.10 Definition of FRS based on different methods

Several studies have been conducted to evaluate the seismic demands of NSCs through implementing various methods to generate FRS. It has been observed that FRS has been rigorously affected by several parameters associated with the primary structure and NSCs characteristics (Wang et al., 2021). The most pivotal factors include the nonlinearity in the supporting structure (Wieser et al., 2013; Anajafi & Medina, 2018b, 2019a; Surana, 2019), the nonlinearity in the NSCs (Vukobratović & Fajfar, 2017; Obando & Lopez-Garcia, 2018; Kazantzi et al., 2018; Anajafi et al., 2020), the location of the NSCs in the supporting structure (Petrone et al., 2016; Anajafi & Medina, 2018b), the ratio of the NSCs period to the fundamental period of the supporting structure (Medina et al., 2006; Anajafi & Medina,

2019a), and the damping ratio of both NSC and supporting structure (Clayton & Medina, 2012; Sullivan et al., 2013; Obando & Lopez-Garcia, 2018; Anajafi & Medina, 2019b).

Petrone et al. (2016) proposed a novel three-branch FRS formulation illustrated in Figure 1.11 and compared the numerical results obtained from inelastic analysis with the proposed FRS, as is shown in Figure 1.12. The parameters a, b, and a_P were determined based on the fundamental period of the reference structure, as shown in Table 1.2.

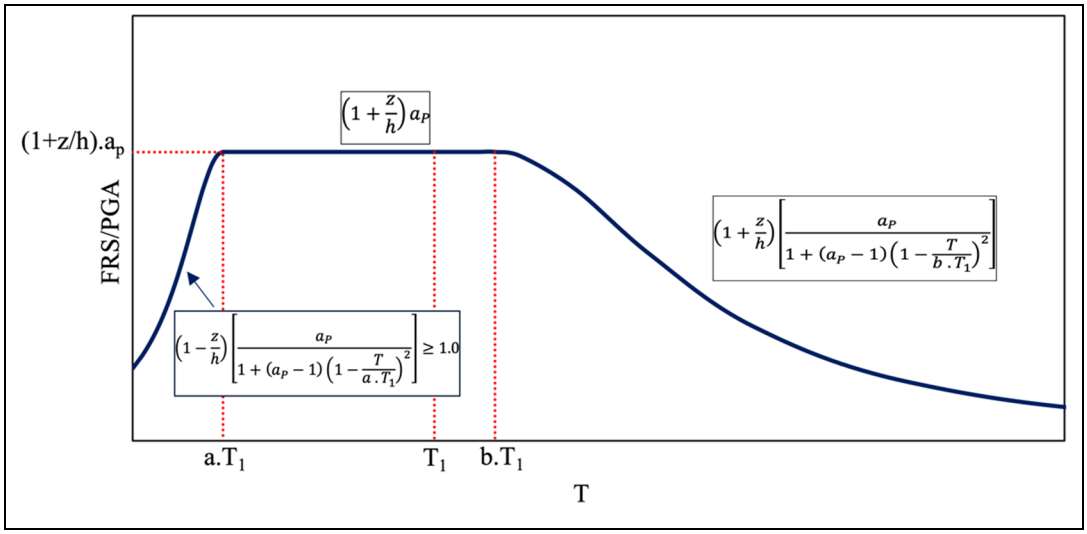

Figure 1.11 Shape of the proposed FRS

Table 1.2 Values of the parameters of the proposed FRS

Fundamental Period	a	b	a_P
$T_1 < 0.5\ s$	0.8	1.4	5.0
$0.5\ s < T_1 < 1.0\ s$	0.3	1.2	4.0
$T_1 > 1.0\ s$	0.3	1.0	2.5

Branches no. 1 and 3 are similar to the FRS shape proposed by EC8. The flat branch no. 2 covers the peak FRS values corresponding to the first and higher modes. The flat branch overestimates the FRS specifically for NSCs tuned to the fundamental period of the supporting building; however, it considers the uncertainties in determining the modal periods of both

reference structure and NSCs. This formulation is limited to the frame buildings designed according to EC8; thus, further modification is needed for different building types. The numerical results obtained from inelastic analysis were compared to the proposed formulation and EC8, as depicted in Figure 1.12. It was observed that the proposed formulation is generally safe-sided; however, it would give a more precise estimation of acceleration demands on NSCs compared to EC8.

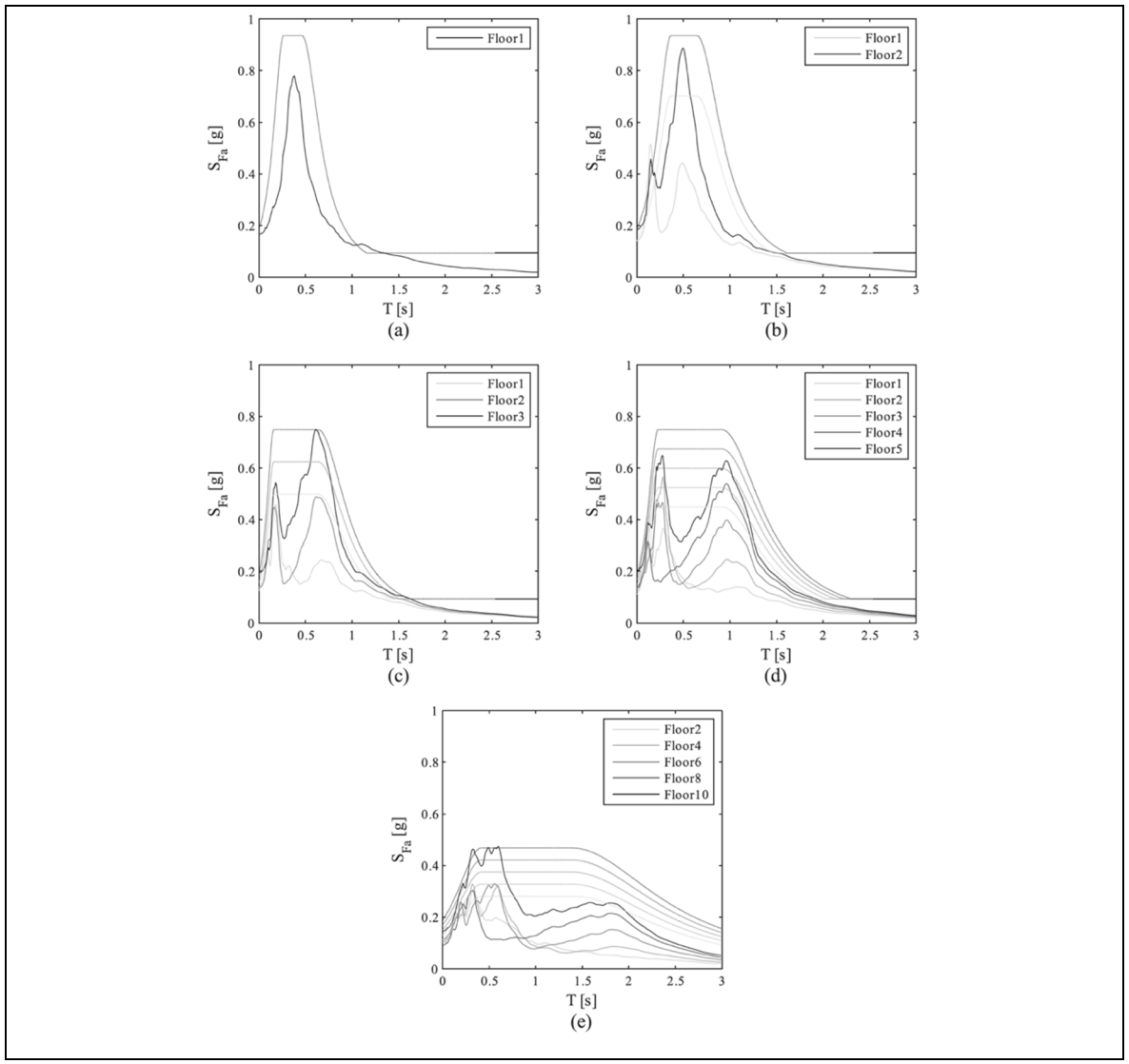

Figure 1.12 Inelastic FRS (solid lines) compared with the proposed floor spectra (dashed lines) for the (a) 1-storey, (b) 2-storey, (c) 3-storey, (d) 5-storey, and (e) 10-storey structures

Vukobratović and Fajfar (2015, 2016, 2017) observed that the FRS values are utterly different in the resonance and off-resonance regions. Therefore, they developed a method that Yasui et al. (1993) initially proposed to generate the FRS from single-storey and multi-storey structures. The resonance region was defined as the period range of the supporting structure where the peak FRS values occur with ±15% broadening of the peak FRS values to account for the uncertainties related to the determination of modal periods of the reference structure. Considering multi-storey buildings, FRS is determined through the combination of the calculated floor spectra for individual vibrational modes using the SRSS modal superposition method.

Shang et al. (2022) proposed a method for a more accurate generation of FRS based on modifying the existing methodology proposed by Vukobratović and Fajfar (2015, 2016, 2017), as illustrated in Figure 1.13.

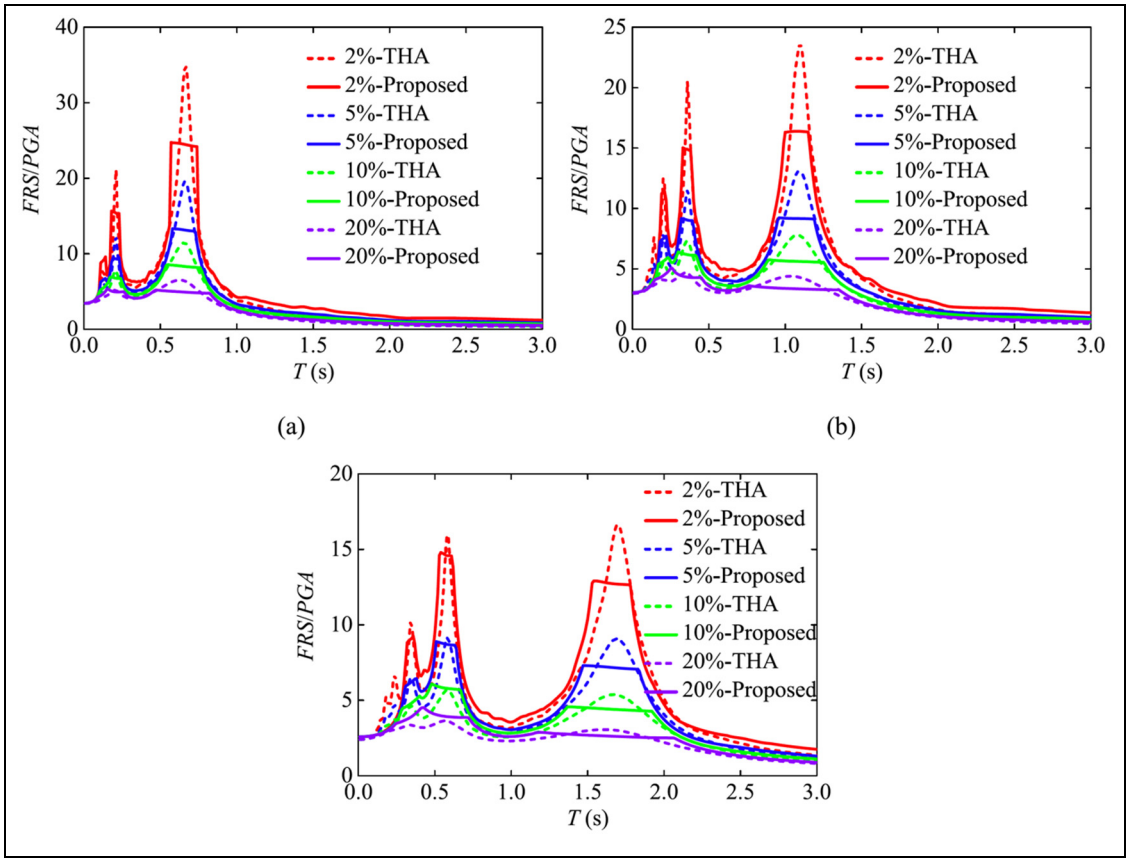

Figure 1.13 The top-floor FRSs for NSCs with different damping ratios:
a) 4-storey frame; b) 8-storey frame c) 12-storey frame

In this case, time-history analyses were performed on three elastic concrete frame buildings designed according to the Chinese code. It was suggested that using the algebraic summation of the first three vibrational modes would result in a more accurate estimation of the floor spectra. Moreover, a comparison of the obtained results from time-history analysis and the proposed method was made. It was observed that the proposed method could give a better estimation of the floor spectral acceleration of NSCs in the off-resonance period range.

1.4.3 Component amplification factor

The validity of the methodologies presented in ASCE 7 and EC8 to estimate the seismic acceleration demands on NSCs was evaluated by Kazantzi et al. (2020). In this research, 47 instrumented buildings in California, with storeys ranging from 2 to 52 and different SFRSs including steel, reinforced concrete, and masonry walls, have been studied. 113-floor motion records with 5% damped spectral acceleration and different frequency contents, have been employed from the instrumented buildings. Analytical results have been exhibited in terms of component amplification factors. Figure 1.14 (a) illustrates the component amplification factor for eight different instrumented buildings by the transparent gray lines and the median, 16%, and 84% percentiles.

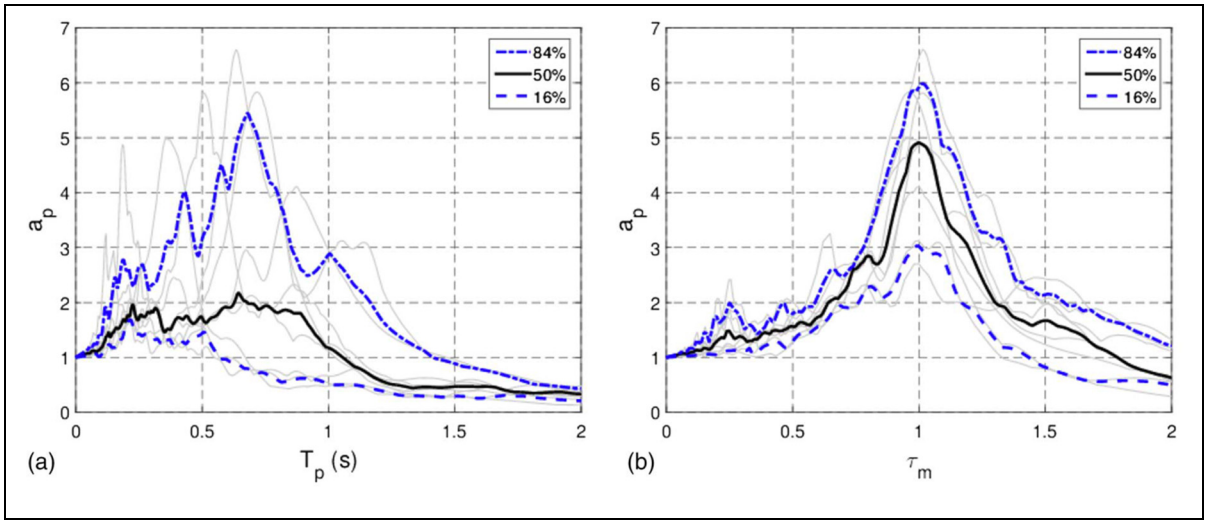

Figure 1.14 The component amplification factor for different studied buildings as a function of (a) component period, and (b) normalized component period

Due to the inherent dispersion in the results, no clear peak value could be recognized in the mean amplification spectra, so a rational estimation could not be made. In this case, the horizontal axis is normalized by the supporting structure's modal period, and the result is depicted in Figure 1.14 (b). In this case, the maximum peak component amplification value depicted by the median spectrum is about 5.0, which is within the realistic range of the component amplification factor. It was concluded that neglect of the normalizing component period by the fundamental period of the supporting structure led to a drastic underestimation of the acceleration demands on NSCs. Also, the component amplification factors for different buildings are illustrated in Figure 1.15, considering two different component damping levels.

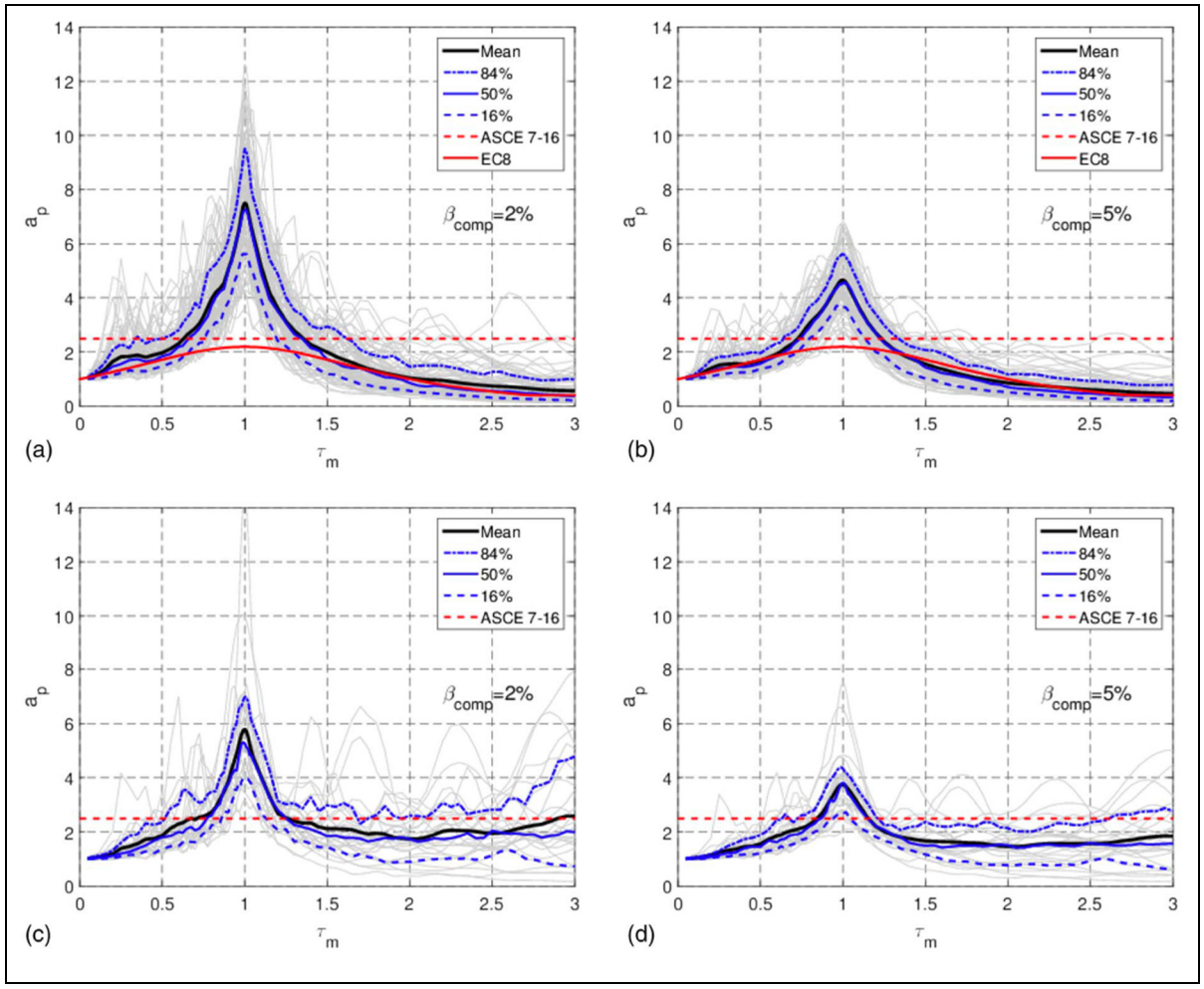

Figure 1.15 Floor amplification factor considering different recorded floor motions and component damping levels

The horizontal axis corresponds to the component period normalized by the first modal period of the supporting structure as depicted in Figure 1.15 (a, c), and by the second or third modal period of the supporting structure as depicted in Figure 1.15 (b, d). Moreover, by comparing the results with both ASCE 7 and EC8 provisions, it is concluded that the resulted acceleration amplification values are greater than the proposed values by provisions for a wide range of component periods.

In another research carried out by Anajafi et al. (2020), the component dynamic amplification factor has been evaluated to design acceleration-sensitive NSCs. In this case, buildings with different SFRSs, including special steel moment-resisting frame (SMRF) and reinforced concrete shear wall (RCSW), have been selected to consider various stiffness ranges of SFRSs. The results are illustrated in Figure 1.16, in which the component acceleration response and component ductility are denoted as S_{ac} and μ_c, respectively.

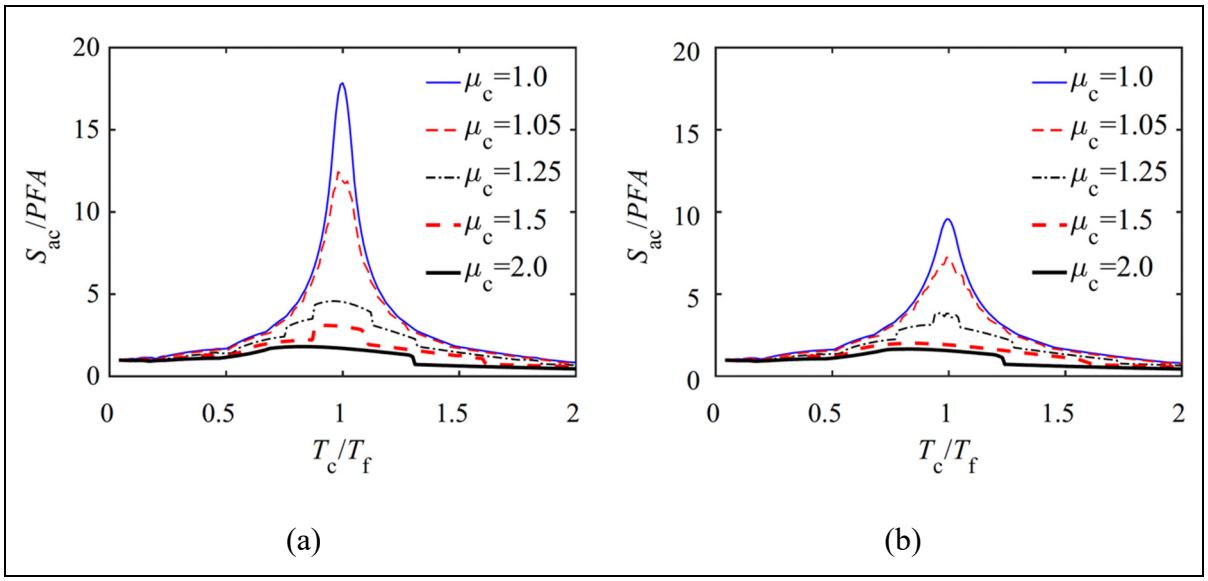

Figure 1.16 Component amplification factor considering components with different ductility and damping levels a) 2%-damped, and b) 5%-damped

In this study, two sets of ground motion records (GMRs) have been utilized to perform inelastic time-history analysis. The first group was 20 far-field GMRs compatible with the 5% damped site-specific target spectrum. The wavelet technique (Al Atik & Abrahamson, 2010) was implemented to match the motions with the target spectrum to reduce the inherent dispersion of the structural responses due to the record-to-record variability. However, it was formerly indicated in another research that the dispersion is yet considerable even by utilizing the spectrum matching technique. So using a greater number of records is inevitable (Anajafi & Medina, 2018a). The second group of GMRs included 44 far-field records taken from FEMA P-695 (2009). The values of the component amplification factor considering various component ductility levels and different damping levels were obtained from the nonlinear time-history analysis.

As illustrated in Figure 1.16, the maximum amplification has occurred in the range of component periods tuned to the period of the fundamental mode of the supporting structure. Significant reduction in acceleration amplification resulted from the components with higher ductility levels. According to the obtained numerical results, it was also concluded that considering elastic components with a 5% damped spectral ordinate results in a remarkable reduction in the component amplification factor compared to the case of considering a 2% damping level with the component amplification factor is about 10.

Shang et al. (2022) investigated the seismic acceleration demands on NSCs through calculating the component dynamic amplification factor and comparing the numerical results with various building codes, as illustrated in Figure 1.17.

It was discussed that the dynamic amplification factor is significantly dependent on the NSC damping ratio. The higher the damping ratio of NSC, the lesser the dynamic amplification factor. Also, the effect of the damping ratio is more pronounced on or in the vicinity of one of the resonating periods of the reference structure. However, the influence of the NSC damping ratio is negligible for NSCs with very long or very short periods.

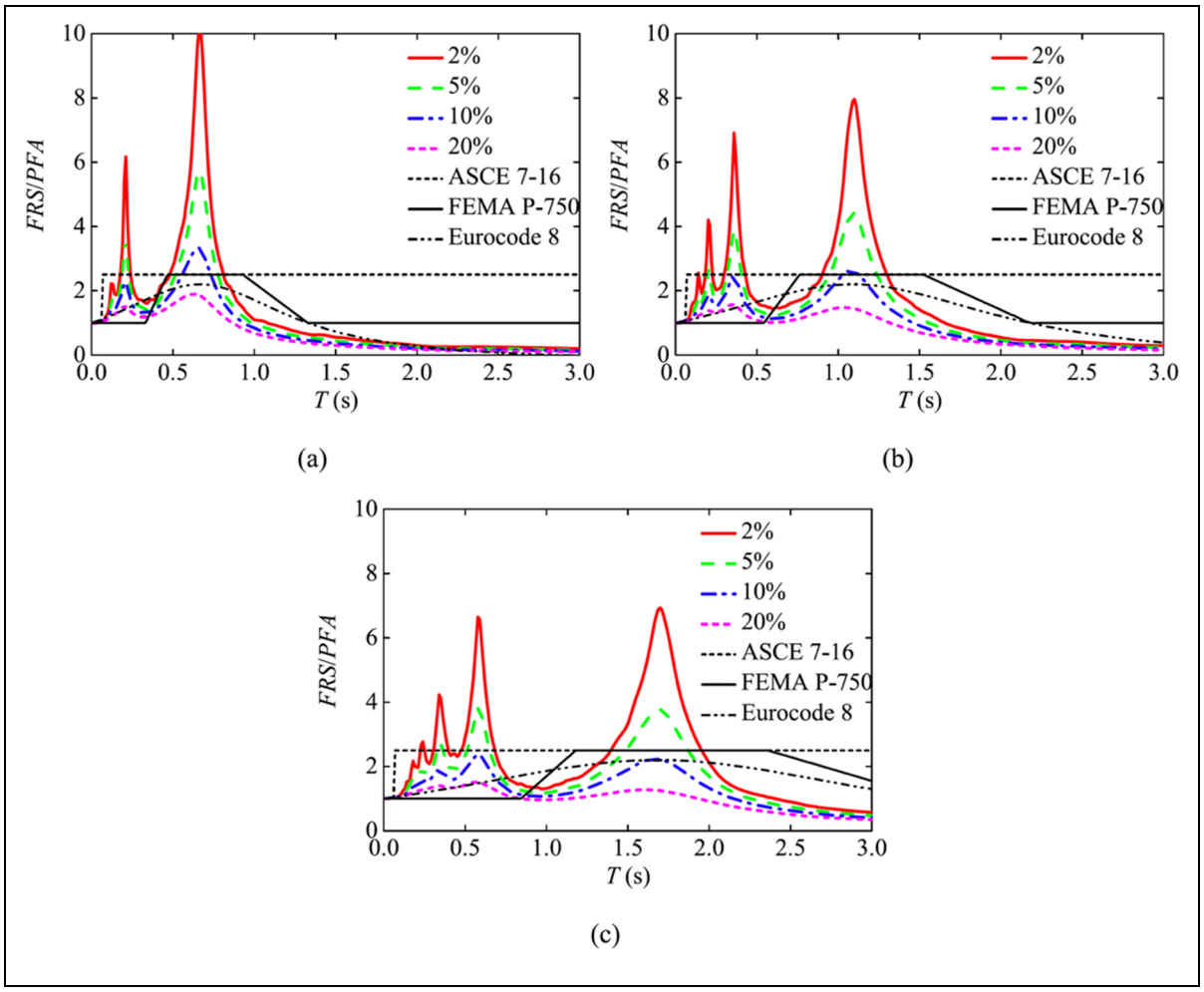

Figure 1.17 The rooftop dynamic amplification factor at different NSC damping ratio, a) 4-storey, b) 8-storey, c) 12-storey

Moreover, Asgarian and McClure (2020a, 2020b) proposed a practical approach for generating NSC floor design spectra, considering different damping ratios for NSCs. In this case, the dynamic characteristics of buildings were determined based on the ambient vibration measures. The obtained results illustrated in Figure 1.18, showed that NBC 2015 and ASCE 7 significantly underestimated the component amplification factor in the low and medium-rise buildings. It was also observed that the NSC damping ratio considerably affects the component acceleration response.

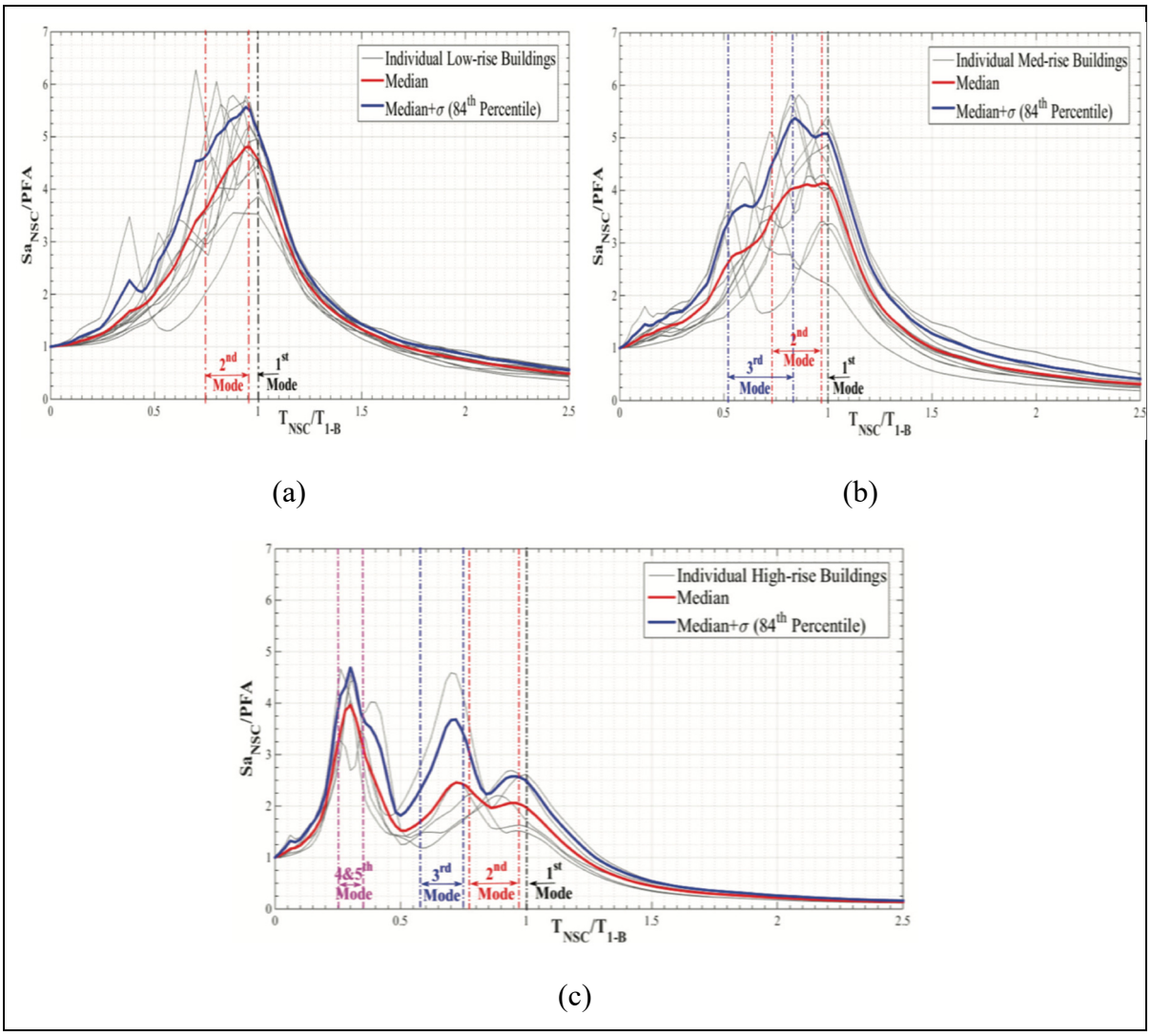

Figure 1.18 The component amplification factor in the roof of the buildings, a) low-rise buildings, b) medium-rise buildings, c) high-rise buildings

1.5 Summary

This chapter discussed the importance of NSCs and their contribution to the buildings' overall seismic response. It was lightened that although NSCs are not designed to carry loads; however, the major inoperability of buildings corresponds to the failure of NSCs even after moderate seismic activities. Therefore, a detailed description of the seismic acceleration demands on acceleration-sensitive NSCs has been provided by evaluating the height and component amplification factors. Also, the comparison between the numerical results and

various building code formulations was reviewed. It was discussed that the current methodologies proposed by different code provisions generally under- or overestimate the seismic acceleration demands on NSCs.

Moreover, it was highlighted that very few research had been conducted to investigate the seismic force demands of NSCs on the buildings designed according to the Canadian code. Moreover, it was shown that several factors corresponding to structural and non-structural characteristics play a crucial role in predicting the adequate seismic demands of NSCs. However, this literature review was limited and explicitly devoted to those related to the objectives of the present study. Specifically, the findings of the previous studies regarding the height factor and the component amplification factor were comprehensively reviewed.

CHAPITRE 2

DESCRIPTION AND MODELING OF THE SELECTED BUILDINGS AND THE INPUT GROUND MOTION RECORDS

In this chapter, a detailed description of the selected buildings, the modelling in the elastic range and the procedure of selecting and scaling the synthetic ground motion records are explained.

2.1 Description of the buildings and modelling assumptions

Multi-storey reinforced concrete (RC) moment-resisting frame (MRF) buildings designed according to NBC (2015) and CSA A23.3-14 (2014a) with limited ductility with 3, 6, 9, and 12-floors have been selected (Mazloom & Assi, 2022). The selected buildings consist of three 7-meter bays in North-South (N-S) and East-West (E-W) directions. Also, each floor has 3-meters of typical height. The elevation view of the 6-storey building is shown in Figures 2.1. Modelling and parametric details of the selected buildings are described in the following paragraphs. Also, the determination of the modal periods and the seismic base shear of the frame building are presented in Appendix I.

Typical concrete material with 28 days of compressive strength ($\acute{f_c}$) of 35 MPa is utilized for all the sections. Also, the yield stress of the selected steel material for reinforcements is 400 MPa for both the longitudinal (f_y) and transverse (f_{yt}) rebars. The structures have a typical building configuration and do not have irregularity in the plan or the height of the buildings. The buildings are assumed to be located in Montreal, QC, and on a stiff soil of class C as per NBC 2015, with a normal importance factor.

The buildings are modelled utilizing SAP2000 (CSI, 2019), and modal analysis has been performed for each structure to obtain the fundamental period of the buildings. Bare frames are considered without modelling non-structural components with the regular distribution of the mass and stiffness. The first three fundamental periods of the studied structures have been

obtained from 2D modal analysis and are shown in Table 2.1. Also, the effect of cracking in the concrete elements is taken into account by considering 40% and 70% of the gross moment of inertia of the beams and columns, respectively, as recommended by CSA A23.3-14 (2014a).

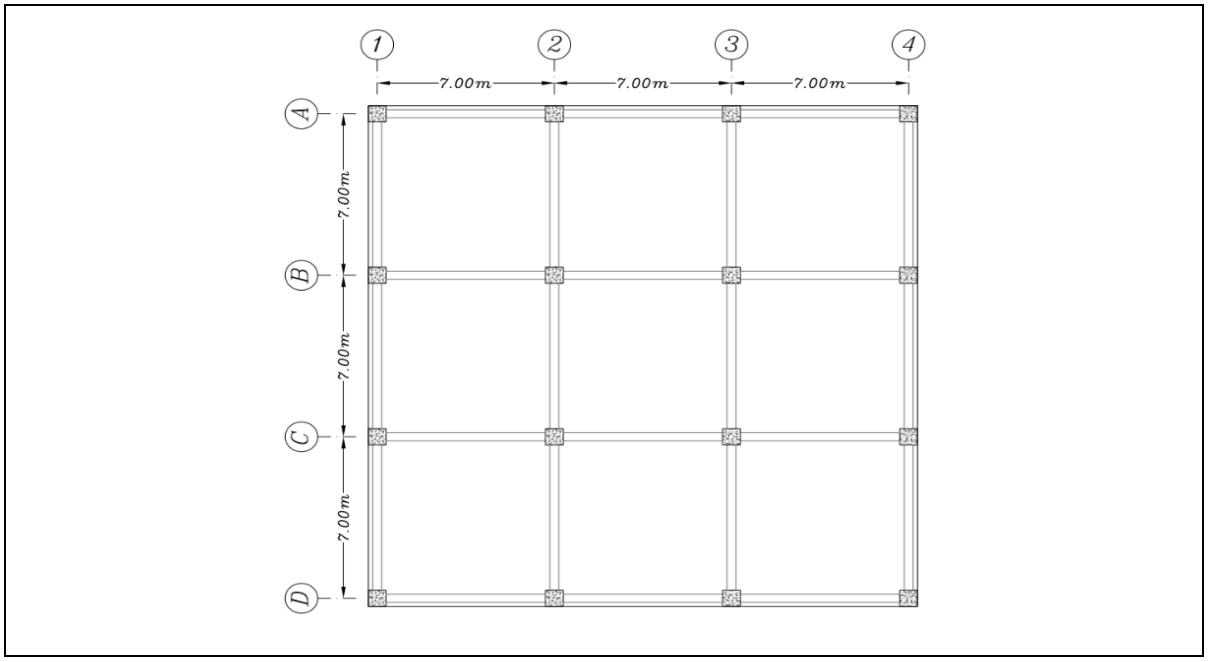

Figure 2.1 Typical floor plan of the 6-sorey building

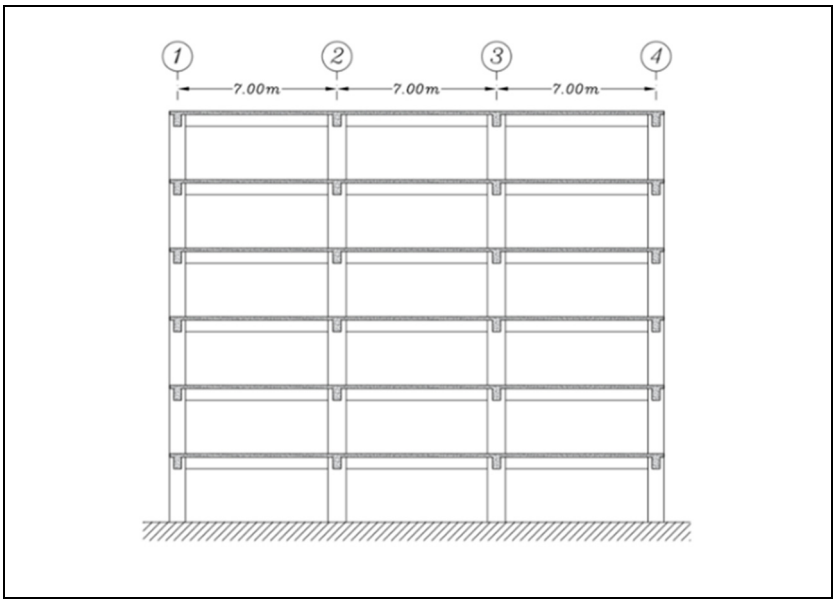

Figure 2.2 Elevation view of the 6-sorey building

Table 2.1 Fundamental periods of the studied buildings

Number of Storeys	T_1	T_2	T_3
3	0.972	0.264	0.128
6	1.07	0.324	0.165
9	1.364	0.426	0.229
12	1.463	0.469	0.260

Unit is Second

2.2 Selection and scaling of the ground motion records

This section presents the selection and scaling procedure of the input ground motion records utilized in the time-history analysis. The ground motion records have been selected based on the Method-A described in commentary J, NBC2015 and harvested from the synthetic ground motion records database for the eastern and western regions of Canada provided by Atkinson (2009), which are available in the engineering seismology toolbox website (www.seismotoolbox.ca).

Commentary J of NBC2015 proposes methods A and B to select and scale the ground motion records. Based on method A, the synthetic ground motion records are selected and scaled to match the target spectrum ($S_T(T)$) proposed by NBC 2015 for periods greater than or equal to 0.5 sec. For the periods less than 0.5 sec, the spectral acceleration is the product of the 5% damped response spectral accelerations ($S_a(T)$) at the periods of T = 0, 0.05, 0.1, 0.2, and 0.3 sec times the site coefficient values at the corresponding periods ($F(T)$), using the linear interpolation for the intermediate periods. The target spectrum with 2% and 10% probabilities of exceedance per 50 years in Montreal are illustrated in Figure 2.3.

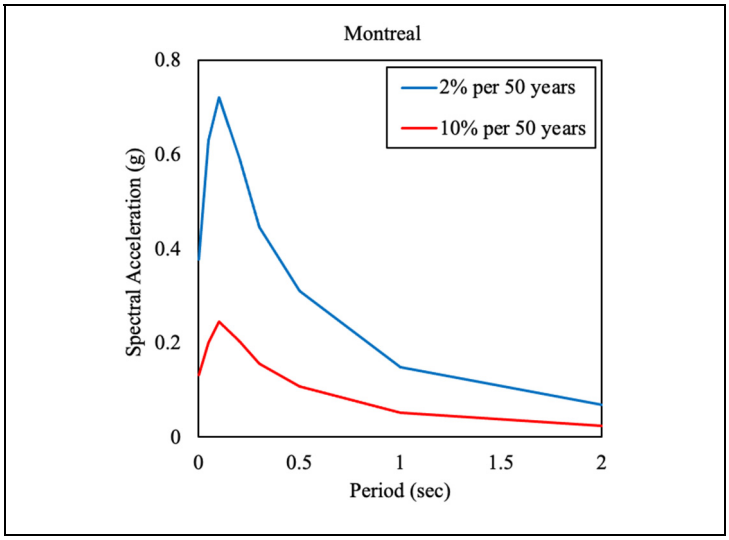

Figure 2.3 UHS with 2% and 10% probabilities
of exceedance per 50 years in Montreal

According to the method A, the selected ground motion records could be scaled in the specified range of period (T_R), proposed by NBC 2015. The lower (T_{min}) and the upper (T_{max}) bounds of the period can be calculated using Equations 2.1, and 2.2, respectively.

$$T_{min} = \min\left[0.2\,T_{Bldng}, T_{90\%}\right] \tag{2.1}$$

$$T_{max} = \max\left[2.0\,T_{Bldng}, 1.5\,sec\right] \tag{2.2}$$

Where; $T_{90\%}$ is the modal period of building without considering cracking in the sections, in which at least 90% of the mass participation is achieved. The ground motion records are selected such that each ground motion covers a proper segment of the specified period range (T_R). Based on the earthquake magnitude-distance combo, the synthetic ground motion records (Atkinson, 2009) are generated for different scenarios in which the scenario-based period ranges (T_{RS}) should be determined such way they may overlap at some periods; however, they altogether should cover the whole range of the specified period (T_R).

In this case and by presuming Montreal as the source of the hazard, two scenarios have been considered for the Atkinson synthetic ground motion records. The first scenario consists of

ground motion records with the moment magnitude of $M = 6.0$ and the fault distance varying from 10 to 30-Km. The second scenario includes ground motion records with the moment magnitude of $M = 7.0$, with the fault distance ranging from 20 to 100-Km. The period range of the first scenario (T_{R1}) varies from T_{min} determined by Equation 2.1, to 1.0 sec. Also, the period range of the second scenario (T_{R2}) varies from 0.5 sec to T_{max} determined by Equation 2.2. The values of T_{Bldng}, $T_{90\%}$, and the different scenario-specific period ranges for various buildings are summarized in Table 2.2.

Table 2.2 Modal periods and scenario-specific period ranges for the studied buildings

Case-study Buildings	T_{Bldng}	$T_{90\%}$	T_{R1}	T_{R2}
3 Storey	0.691	0.2	0.1382 – 1.0	0.5 – 1.5
6 Storey	0.739	0.229	0.1478 – 1.0	0.5 – 1.5
9 Storey	0.934	0.297	0.1868 – 1.0	0.5 – 1.868
12 Storey	1.0	0.325	0.2 – 1.0	0.5 – 2.0

Units are second. The values are obtained without considering the effect of cracking.

Based on NBC 2015, at least 11 ground motion records should be utilized to perform time-history analysis, in which for each scenario-specific period range, at least five ground motion records should be selected. In this case, a set of 12 synthetic ground motion records considering six ground motions for each scenario were selected and scaled for the studied buildings.

Different parameters related to the selected and scaled ground motion records for each scenario including moment magnitude, fault distance, duration of the ground motion records, time step, and the scale factor required for each record to match the uniform hazard spectrum with 2% and 10% probabilities of exceedance in 50 years in Montreal are tabulated for all buildings. Tables 2.3 and 2.4 show the values corresponding to the 3-storey frame building. The spectral accelerations of the selected ground motion records scaled within the scenario-specific period ranges (T_{R1} and T_{R2}), considering the UHS with 2% and 10% probabilities of exceedance in 50 years, are illustrated in Figure 2.4 and 2.5, respectively.

Table 2.3 Parameters of the selected and scaled ground motion records considering UHS with 2% probability of exceedance for the 3-storey frame in Montreal

Scenario	M	R	Record	Duration	Time step	Scale factor	PGA
1	6.0	15	E6c1_31	43.598	0.002	0.761	0.323
			E6c1_4			0.524	0.361
			E6c1_28			0.924	0.455
		30	E6c2_34	47.530		1.964	0.401
			E6c2_3			1.659	0.522
			E6c2_15			1.293	0.329
2	7.0	25	E7c1_18	51.126	0.002	0.564	0.395
			E7c1_30			0.538	0.285
			E7c1_40			0.873	0.538
		100	E7c2_12	57.352		1.638	0.213
			E7c2_4			2.041	0.329
			E7c2_36			1.956	0.178

Table 2.4 Parameters of the selected and scaled ground motion records considering UHS with 10% probability of exceedance for the 3-storey frame in Montreal

Scenario	M	R	Record	Duration	Time step	Scale factor	PGA
1	6.0	15	E6c1_28	43.598	0.002	0.331	0.163
			E6c1_37			0.334	0.171
			E6c1_14			0.322	0.211
		30	E6c2_19	47.530		0.645	0.117
			E6c2_33			0.599	0.101
			E6c2_3			0.595	0.187
2	7.0	25	E7c1_38	51.126	0.002	0.311	0.157
			E7c1_41			0.364	0.162
			E7c1_31			0.329	0.139
		100	E7c2_26	57.352		0.768	0.088
			E7c2_4			0.662	0.106
			E7c2_12			0.53	0.069

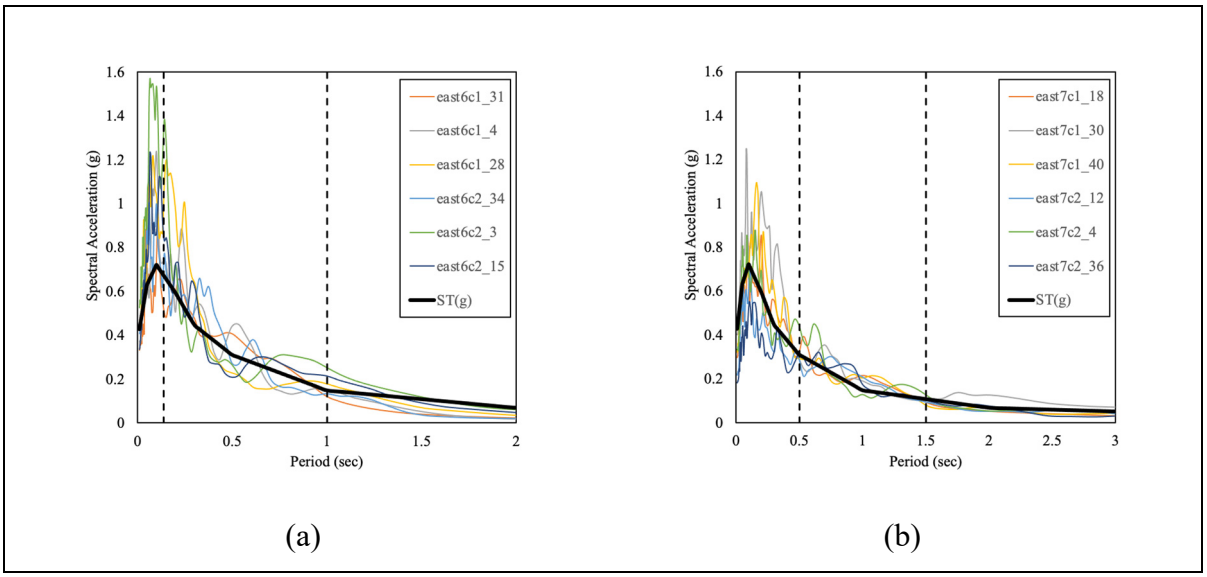

Figure 2.4 Spectral accelerations of the selected ground motion records of 3-storey moderately ductile frame scaled to the UHS with 2% probability of exceedance per 50 years in Montreal, a) TR1, b) TR2

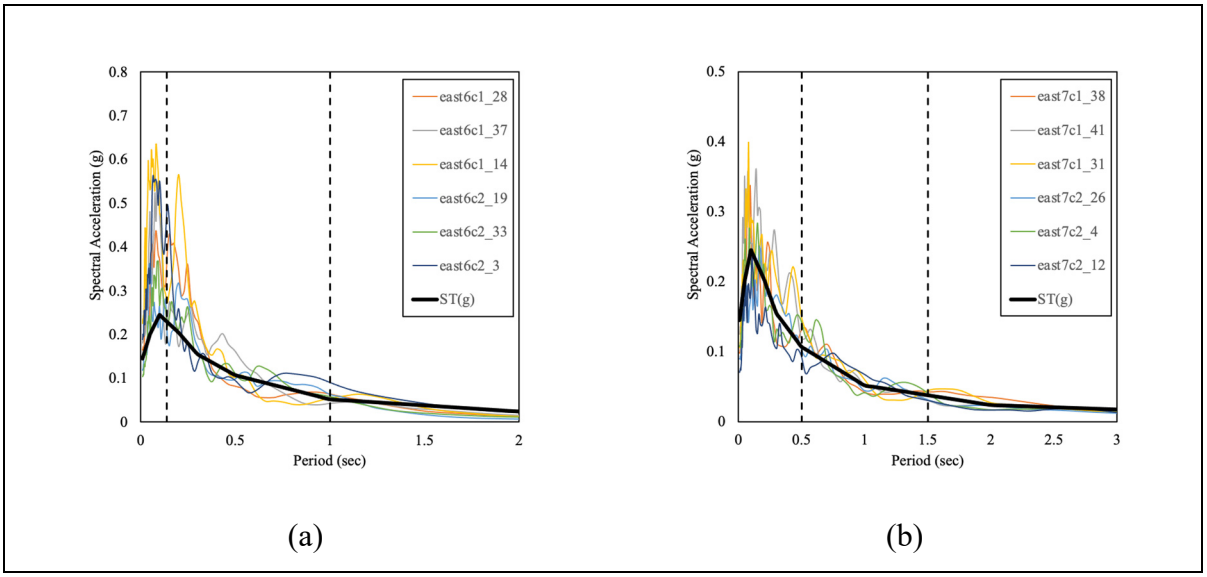

Figure 2.5 Spectral accelerations of the selected ground motion records of 3-storey moderately ductile frame scaled to the UHS with 10% probability of exceedance per 50 years in Montreal, a) TR1, b) TR2

The selected ground motions are scaled to the target spectrum such that the mean spectral acceleration of the ground motion record does not exceed 10% below the target spectrum to

satisfy the NBC 2015 scaling requirements. For those ground motion records with more than 10% difference below the target spectrum, a second scale factor is applied.

Figure 2.6 illustrates the difference between the mean spectral acceleration of the selected and scaled ground motion records for both scenarios of the 3-storey frame building and the target spectrum and the need for applying a second scale factor. As is depicted in Figure 2.6, the difference between the mean spectral acceleration of the selected and scaled ground motion records of the first and the second scenarios and the target spectrum after the first scaling exceeded 10% below the target spectrum for both scenarios at the period of 0.43 sec and 1.5 sec, respectively. Therefore, a second scale factor has been applied to limit the maximum difference between the mean spectral acceleration and the target spectrum to 10 percent below the target spectrum.

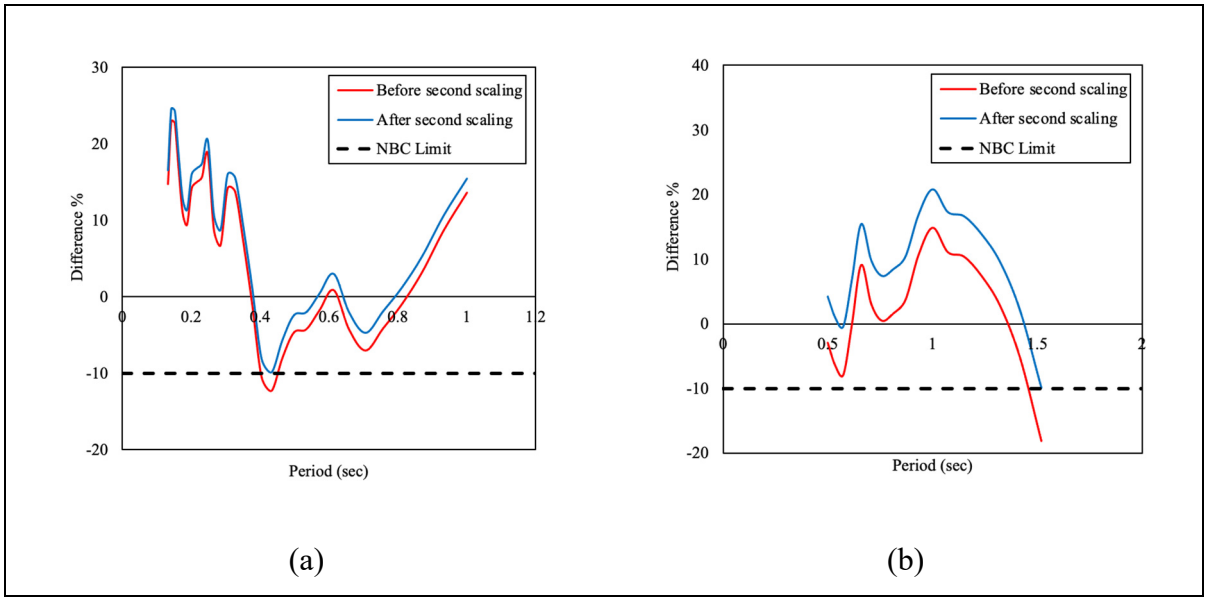

Figure 2.6 The difference between the mean spectral acceleration of the selected and scaled ground motion records with the target spectrum with 2% probability of exceedance per 50 years for a) Scenario 1, and b) Scenario 2

Figure 2.7 shows the mean spectral acceleration of the selected ground motions after second scaling compared to the target spectrum with 2% probability of exceedance per 50 years, and the difference between the mean spectral acceleration after the second scaling and the target

spectrum. The same parameters corresponding the UHS at 10% probability of exceedance in 50 years, are illustrated in Figure 2.8.

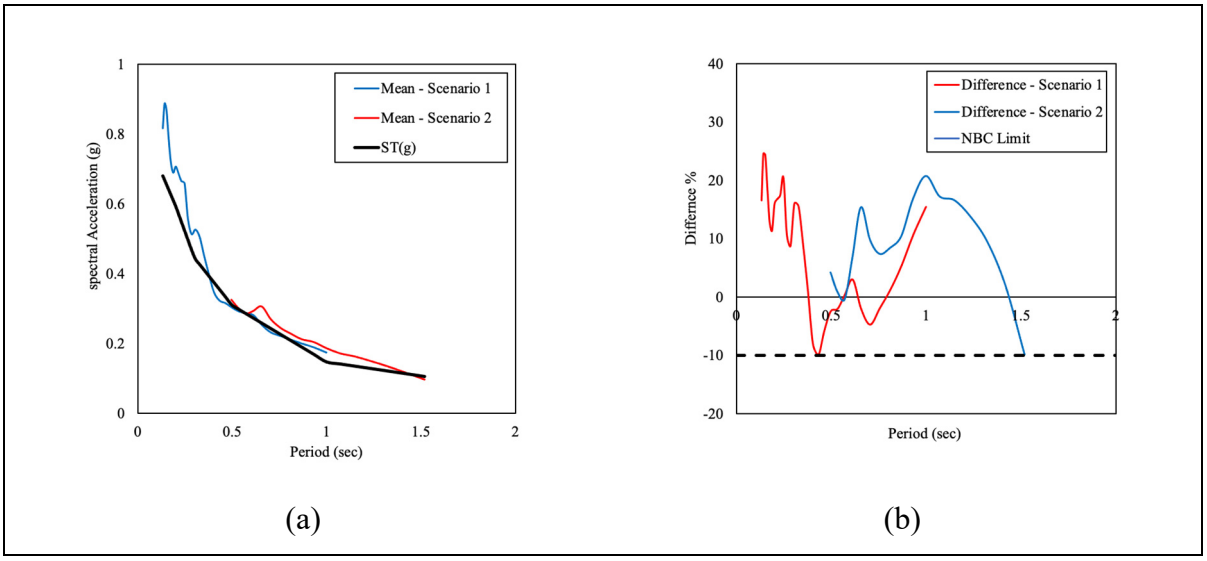

Figure 2.7 a) Mean spectral acceleration for scenarios 1 and 2 for 3-storey frame compared with target spectrum, b) Difference of the mean spectral acceleration with the target spectrum at 2% probability of exceedance per 50 years, within TR1 and TR2

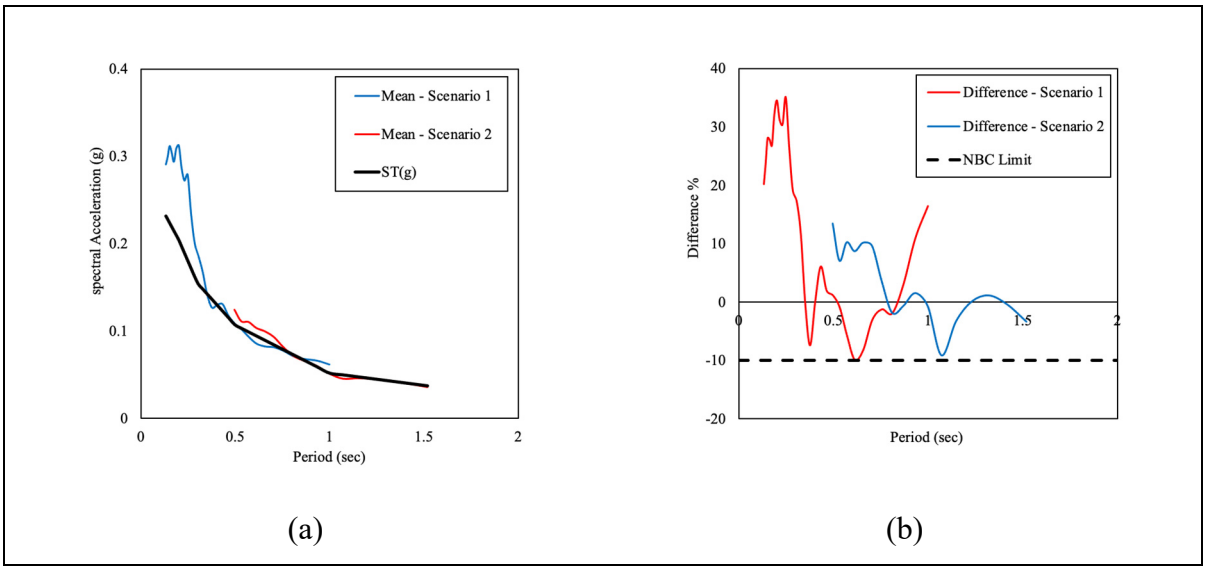

Figure 2.8 a) Mean spectral acceleration for scenarios 1 and 2 for 3-storey frame compared with target spectrum, b) Difference of the mean spectral acceleration with the target spectrum at 10% probability of exceedance per 50 years, within TR1 and TR2

The scenario-specific parameters for other buildings are shown in Tables 2.5 to 2.10. Also, the parameters corresponding to the UHS at 2% and 10% probability of exceedance per 50 years in Montreal, for other buildings are presented in Appendix II.

Table 2.5 Parameters of the selected and scaled ground motion records considering UHS with 2% probability of exceedance for the 6-storey frame in Montreal

Scenario	M	R	Record	Duration	Time step	Scale factor	PGA
1	6.0	15	E6c1_43	43.598	0.002	1.441	0.607
			E6c1_4			0.534	0.368
			E6c1_21			0.883	0.493
		30	E6c2_17	47.530		1.522	0.522
			E6c2_37			1.613	0.419
			E6c2_15			1.328	0.338
2	7.0	25	E7c1_18	51.126	0.002	0.564	0.395
			E7c1_30			0.538	0.285
			E7c1_40			0.873	0.538
		100	E7c2_12	57.352		1.638	0.213
			E7c2_4			2.041	0.329
			E7c2_36			1.956	0.178

Table 2.6 Parameters of the selected and scaled ground motion records considering UHS with 10% probability of exceedance for the 6-storey frame in Montreal

Scenario	M	R	Record	Duration	Time step	Scale factor	PGA
1	6.0	15	E6c1_43	43.598	0.002	0.527	0.222
			E6c1_10			0.337	0.155
			E6c1_14			0.336	0.22
		30	E6c2_17	47.530		0.557	0.191
			E6c2_37			0.589	0.153
			E6c2_36			0.655	0.107
2	7.0	25	E7c1_18	51.126	0.002	0.311	0.218
			E7c1_41			0.364	0.162
			E7c1_31			0.329	0.139
		100	E7c2_26	57.352		0.768	0.088
			E7c2_4			0.662	0.106
			E7c2_12			0.53	0.069

Table 2.7 Parameters of the selected and scaled ground motion records considering UHS with 2% probability of exceedance for the 9-storey frame in Montreal

Scenario	M	R	Record	Duration	Time step	Scale factor	PGA
1	6.0	15	E6c1_30	43.598	0.002	0.431	0.607
			E6c1_33			0.326	0.368
			E6c1_31			0.333	0.493
		30	E6c2_33	47.530		0.306	0.522
			E6c2_13			0.418	0.419
			E6c2_36			0.302	0.338
2	7.0	25	E7c1_27	51.126	0.002	0.564	0.382
			E7c1_28			0.538	0.306
			E7c1_14			0.873	0.336
		100	E7c2_3	57.352		1.638	0.279
			E7c2_15			2.041	0.268
			E7c2_1			1.956	0.276

Table 2.8 Parameters of the selected and scaled ground motion records considering UHS with 10% probability of exceedance for the 9-storey frame in Montreal

Scenario	M	R	Record	Duration	Time step	Scale factor	PGA
1	6.0	15	E6c1_33	43.598	0.002	0.391	0.106
			E6c1_26			0.337	0.173
			E6c1_10			0.317	0.146
		30	E6c2_44	47.530		0.868	0.151
			E6c2_33			0.591	0.099
			E6c2_43			0.728	0.142
2	7.0	25	E7c1_31	51.126	0.002	0.327	0.138
			E7c1_38			0.312	0.157
			E7c1_34			0.368	0.171
		100	E7c2_15	57.352		0.715	0.096
			E7c2_40			0.827	0.092
			E7c2_38			0.967	0.103

Table 2.9 Parameters of the selected and scaled ground motion records considering UHS with 2% probability of exceedance for the 12-storey frame in Montreal

Scenario	M	R	Record	Duration	Time step	Scale factor	PGA
1	6.0	15	E6c1_4	43.598	0.002	0.582	0.607
			E6c1_30			0.819	0.368
			E6c1_21			0.925	0.493
		30	E6c2_10	47.530		1.263	0.522
			E6c2_33			1.841	0.419
			E6c2_34			2.121	0.338
2	7.0	25	E7c1_34	51.126	0.002	1.045	0.382
			E7c1_31			0.917	0.306
			E7c1_28			0.629	0.336
		100	E7c2_6	57.352		1.837	0.279
			E7c2_36			1.927	0.268
			E7c2_10			2.015	0.276

Table 2.10 Parameters of the selected and scaled ground motion records considering UHS with 10% probability of exceedance for the 12-storey frame in Montreal

Scenario	M	R	Record	Duration	Time step	Scale factor	PGA
1	6.0	15	E6c1_26	43.598	0.002	0.322	0.165
			E6c1_37			0.313	0.16
			E6c1_28			0.337	0.166
		30	E6c2_33	47.530		0.57	0.096
			E6c2_36			0.577	0.092
			E6c2_29			0.592	0.107
2	7.0	25	E7c1_34	51.126	0.002	0.356	0.166
			E7c1_31			0.312	0.132
			E7c1_40			0.313	0.193
		100	E7c2_24	57.352		0.812	0.083
			E7c2_6			0.626	0.081
			E7c2_40			0.804	0.09

CHAPITRE 3

NONLINEAR MODELLING AND ANALYSIS OF THE SELECTED BUILDINGS

This chapter presents the concept and method used to define and implement material nonlinearity in numerical modelling and analysis. The extension of the inelasticity in the supporting structures is discussed by performing the nonlinear static analysis. Also, the nonlinear time-history analysis is explained in detail.

3.1 Modeling of nonlinearity in the concrete components

In this study, plastic hinges are defined and assigned to the components since hinges are more suitable and are commonly utilized for nonlinear analysis. Different types of plastic hinges, including the uncoupled moment (M), axial (P), torsion (T), shear (V), and coupled axial with moment interaction (PMM), and any combination of the different types of plastic hinges can be considered for a plastic hinge in a single location. Also, any number of plastic hinges can be assigned to a member; however, this may end up with a much longer analysis run-time in analyzing large-scale frames. So, by considering frame buildings with considerable sectional dimensions, two-moment plastic hinges are assigned to the ends of the beam elements.

The location of the plastic hinges assigned to the frames is also of great importance and can be determined as the relative distance along the length of the component. The location of the plastic hinges should represent the maximum moment demand in a member such that the hinge can be adequately activated; thus, the performance of the entire structure would be reasonable. This location is typically considered at the 5 percent of relative distance from the rigid zones of the beams and columns so that the plastic hinges can be formed close enough to the face of the joints. The location of the plastic hinges assigned to the members of the 6-storey frame building is illustrated in Figure 3.1.

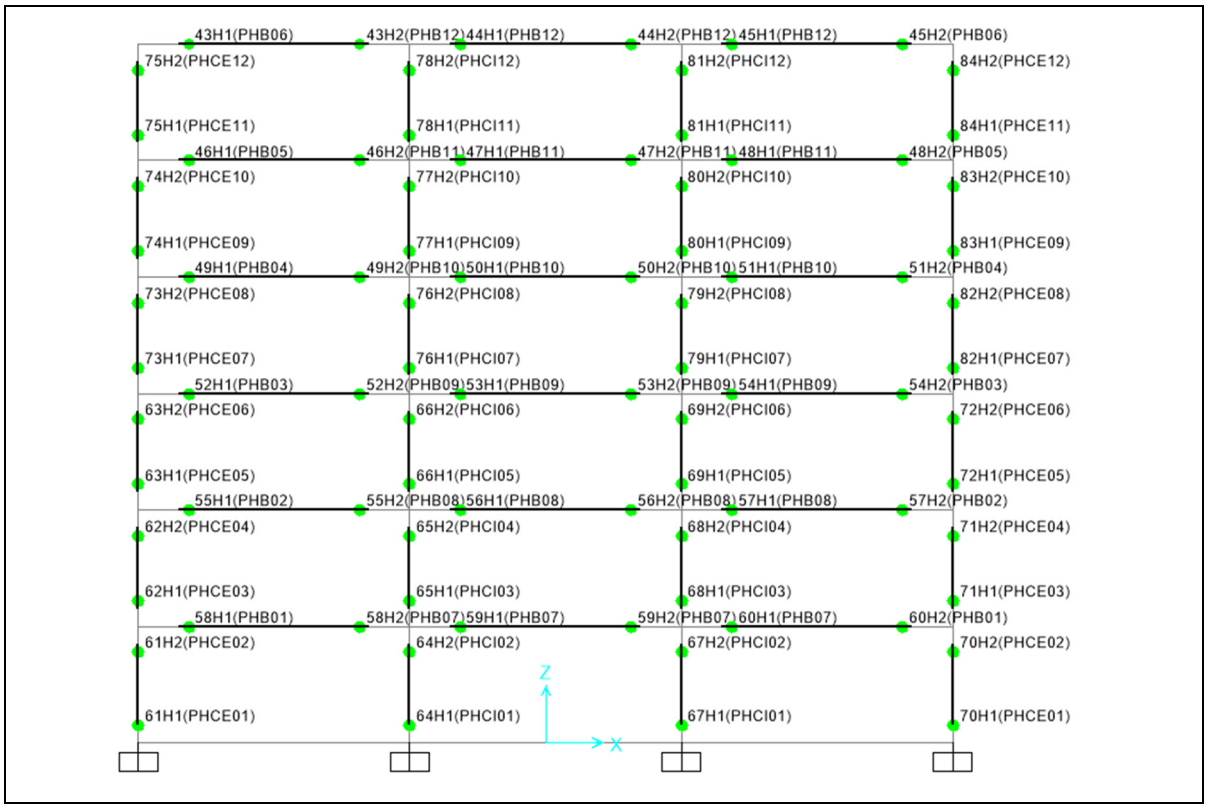

Figure 3.1 Configuration of concentrated hinges for the 6-storey frame building

The plastic hinges considered in this study are characterized by the force-deformation or moment-rotation relations for concrete elements and acceptance criteria, using the backbone curve and specified quantities introduced by ASCE 41-17 (2017). As it is shown in Figure 3.2 (a), at point A, the component is unloaded, and from point A to point B, the deformation is linear; thus, point B represents the yield strength of the component and the corresponding amount in the horizontal axis is yield displacement. The behavior of the hinges in SAP2000 is rigid plastic; hence, as is shown in Figure 3.2 (b), no displacement is exhibited in the linear section. Therefore, the displacement at point B is zero, and the plastic deformation only occurred beyond the yield point. From the yield point to point C, referred to as the ultimate capacity, the effect of strength hardening has been shown.

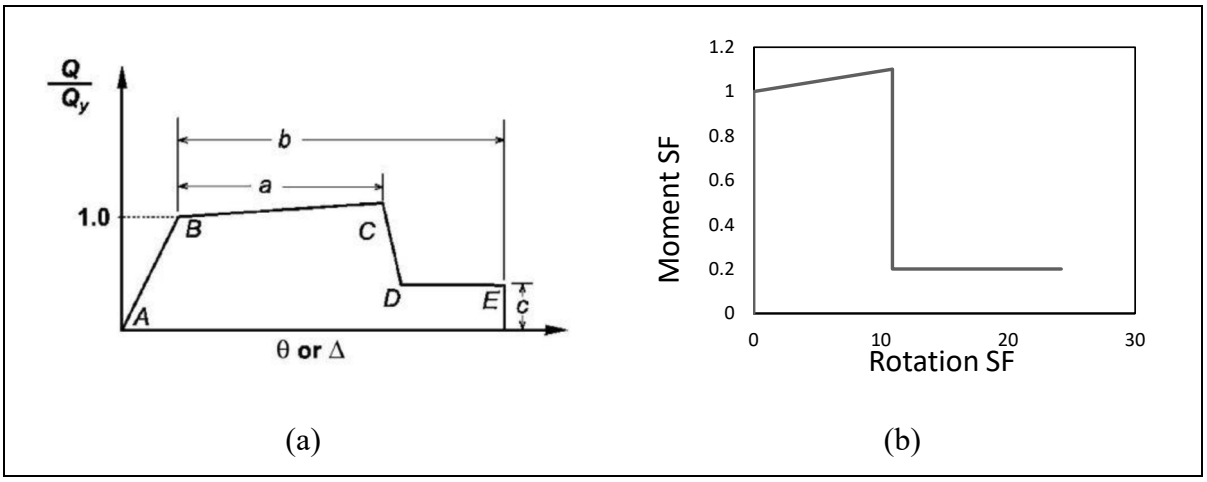

Figure 3.2 Force-deformation relation defined as per (a) ASCE41-17 (b) SAP2000

By reaching the ultimate capacity, since the system is experiencing a progressive failure, there is a significant reduction in seismic force resistance with a positive slope toward point D. It can be seen in Figure 3.2 (b), that for simplicity the residual strength branch of backbone curve defined in SAP 2000 is occurred with a sudden drop from point C to point D. The plastic hinge is then followed toward point E, which represents the total loss of the resistance.

Aside from the different points of hinge deformation which are defined in the backbone curve, different performance-based limit-states including Immediate occupancy (IO), Life Safety (LS), and Collapse Prevention (CP) levels can also be defined. These modelling parameters and acceptance criteria are defined based on the sectional properties, the flexural capacity of the components, and the parameters considered for nonlinear procedures given by Tables 10-7 and 10-8 of ASCE 41-17 which describe the modeling parameters and numerical acceptance criteria for nonlinear procedures in reinforced beams and columns, respectively. The moment capacity of one section can be obtained using Response 2000 which is a sectional analysis software introduced by Bentz (1999). One example of determining the moment capacity of a 400mm x 600mm concrete beam is presented in Appendix III.

Once the yield moment (M_y) of a section is obtained, the yield rotation (θ_y) of the section which depends on the section dimensions can be calculated for beam and column sections, using Equations 3.1 and 3.2, respectively, introduced by Priestley et al. (2007).

$$\theta_y = 0.283\varepsilon_y L_b/h_b \tag{3.1}$$

$$\theta_y = 0.283\varepsilon_y L_b/h_b \tag{3.2}$$

Where: ε_y is the yield strain of the section, L_b is the length of the beam span, and h_b is the depth of the section. The yield moment determined by Response 2000, and the yield rotation calculated by Equations 3.1 and 3.2 are utilized as the moment scale factor (SF) and rotation scale factor in SAP2000, respectively. Moreover, the moment and rotation of the hinge at different points in the backbone curve can be calculated as a ratio of a yield moment and yield rotation and can be assigned to the SAP 2000 software.

The moment at point C is considered as $1.1M_y$ which is suggested by NIST GCR 17-917 (2017). Also, the rotation at point C, and the moments and rotations at point D and E can be calculated using Equations 3.3 to 3.5 (NIST, 2017).

$$\frac{\theta_C}{\theta_y} = 1 + \frac{a}{\theta_y} \tag{3.3}$$

$$\frac{M_D}{M_y} = \frac{M_E}{M_y} = c \tag{3.4}$$

$$\frac{\theta_E}{\theta_y} = 1 + \frac{b}{\theta_y} \tag{3.5}$$

Where: a and b, are the parameters that describe the deformation capacity of the section and c, describes the residual strength of the section. These parameters and the acceptance criteria are discussed and tabulated in ASCE 41-17.

The abovementioned parameters are calculated for all the beams and columns to be able to define the plastic hinges and their properties in SAP 2000 and are presented in Appendix IV.

3.2 Hysteretic model

It is also essential to account for the cyclic deterioration of the structural components by defining a proper hysteretic model. In this study, Takeda's trilinear degrading hysteretic model (Takeda et al., 1970) is employed to represent the cyclic response of individual RC frames since it captures the strength and stiffness degradation of the concrete components. Takeda's hysteretic model was introduced based on the experimental observation and performance assessment of reinforced concrete components subjected to lateral load reversals with axial loads. In the Takeda model illustrated in Figure 3.3, the hysteretic loop crosses the horizontal axis upon unloading, following a path that intersects the backbone curve and forms the internal loops. Thus, the stiffness gradually degrades from cycle to cycle at the yield point.

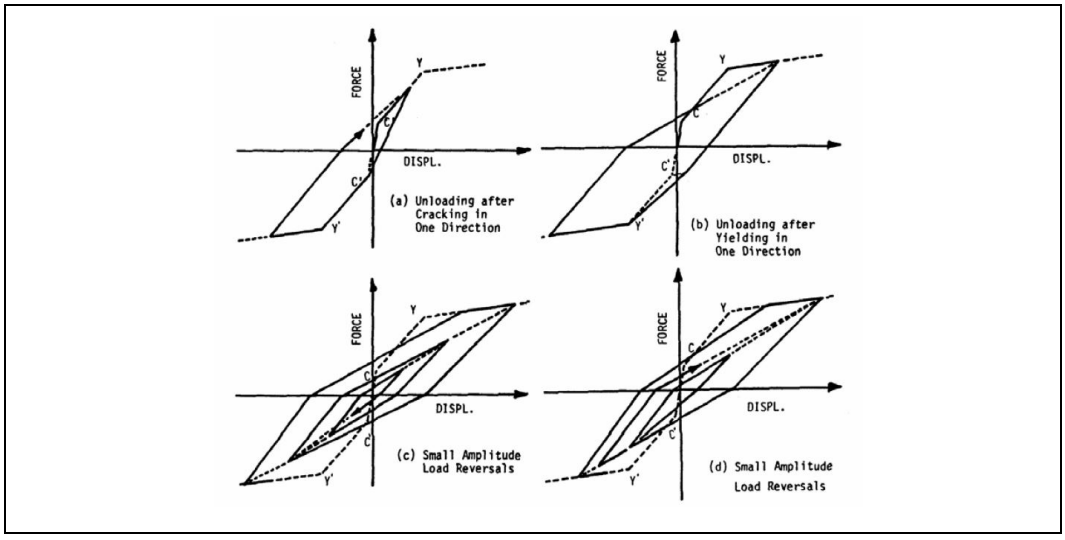

Figure 3.3 Takeda hysteresis model

3.3 Nonlinear static analysis

Nonlinear static analysis, commonly referred to as a pushover analysis, is a typical and fast track analysis procedure to evaluate the nonlinear capacity of the structures subjected to the seismic loads. In static pushover analysis, lateral loads applied to the structure are monotonically increased such that the structure reaches a certain level of displacement, so-called target displacement. In this analysis stage, the rotation of all the columns located at the lowest floor level reaches the ultimate value, and the plastic hinges are formed in most beam elements. The objective of a static pushover analysis is to obtain the seismic base shear value and its corresponding lateral roof displacement range at each step of the analysis. This results in plotting the capacity curve of one structure which provides valuable information on the ductility capacity and overstrength of the lateral load resisting system. Although the static pushover analysis is advantageous since it is computationally less time-consuming, it does not correspond to the acceleration response of the structure and other helpful information compared to the time-history analysis.

After defining the plastic hinges with appropriate properties discussed in section 3.1, and assigning them to the frame members, three analysis load cases including Modal, Gravity, and Pushover are defined. The gravity load case type is static, and the analysis type is nonlinear. Zero initial condition is selected and the load combination of dead load plus 25 percent of live load plus snow load is considered. In the next step, another load case called pushover is then defined. The type of this load case is also static, and the analysis type is nonlinear. The initial condition of this load case is the gravity load case which is defined in the former step. For the load application, the displacement control option is selected and 10 percent of the total height of the building is applied to the monitored degree of freedom located at the roof of the building (CSA, 2014a). The results of nonlinear static analysis of the studied buildings are illustrated in Figure 3.4.

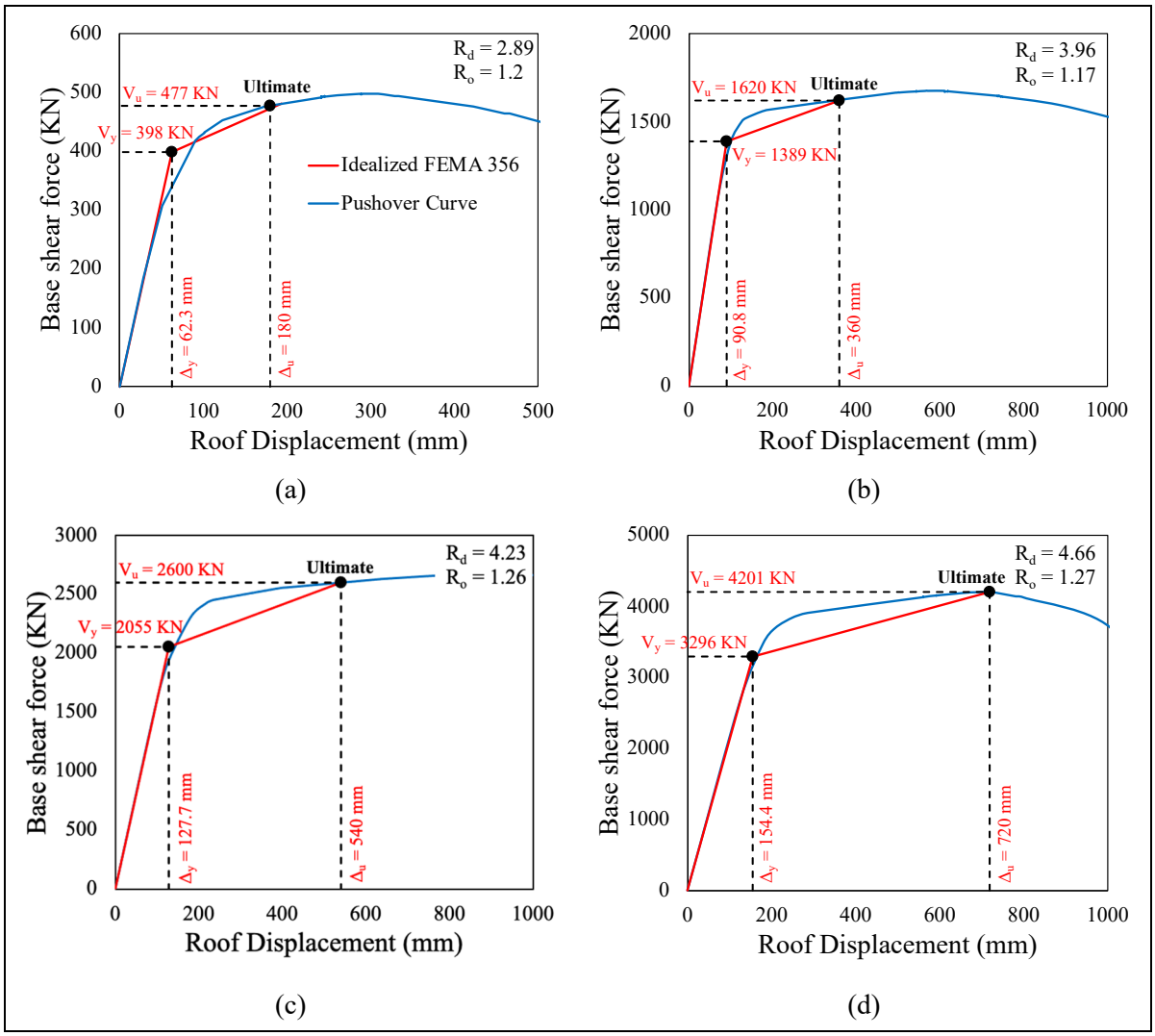

Figure 3.4 Pushover and idealized bilinear curves according to FEMA 356 for the: a) 3, b) 6, c) 9, and d) 12-storey buildings

From the idealized bilinear force-deformation curve based on FEMA-356 (2000) curve, the yield point is where the slope of the curve changes. This point refers to the yield strength V_y (i.e., 398 KN in the 3-storey building) and the corresponding amount in the horizontal axis which is yield displacement Δ_y (i.e., 62.3 mm in the 3-storey building). The slope of the first segment of the idealized curve is the stiffness of the structure before cracking ($K_i = V_y/\Delta_y$) that is 6398 KN/m in the 3-storey building. Following the pushover curve, the ultimate performance limit state of the structures (Δ_u) equal to 2% of the total height of the building (i.e., 180 mm in the 3-storey building) is determined and illustrated in the pushover curves.

The extension of inelastic action in the studied structures can be determined by evaluating the force modification factor which is the product of ductility-related force modification factor (R_d) that accounts for the capability of the structure to dissipate energy and the overstrength-related force modification factor (R_O) that reflects the portion of reserve strength in the structure. R_d factor can be determined by dividing the corresponding displacement at the ultimate performance level Δ_u by the yielding displacement Δ_y. Also, R_O factor can be calculated by dividing the corresponding base shear at the ultimate performance level V_u by the yielding base shear V_y (i.e., $R_d R_O = 3.47$ for the 3-storey building). By comparing the values of $R_d R_O$ factor of each structure with the corresponding factor assumed in the design phase ($R_d = 2.5,\ R_O = 1.4$), it can be concluded that except for the 3-storey building, the actual ductility capacity of all the structures is greater than the system ductility assumed in the design phase. Therefore, the higher the ductility capacity, the lower the seismic acceleration demands on NSCs are expected in the inelastic phase (Anajafi et al., 2021).

3.4 Nonlinear dynamic analysis

In this case, modal, gravity, and nonlinear dynamic analysis cases are defined to perform the nonlinear time-history analysis. The loads applied in the gravity analysis case include the dead load, 25% of the live load, and the snow load. Also, the direct integration nonlinear time-history analysis was performed utilizing the synthetic ground motion records with 2% and 10% probabilities of exceedance per 50 years and matched to the UHS of Montreal site class C, as discussed in section 2.2. In the following, the results obtained from the elastic and inelastic time-history analyses are discussed in the form of FRS and other forms, i.e., the height factor, component dynamic amplification factor, and the component force factor, are presented in Chapter 4. Also, the obtained results are compared with various seismic provisions. Median values of 5% damped FRS illustrated in Figures 3.5 to 3.8 are only presented for the roof of the buildings in addition to some intermediate floors. Also, the numerical results are compared with the proposed FRS by Petrone et al. (2016), discussed in section 1.4.2.

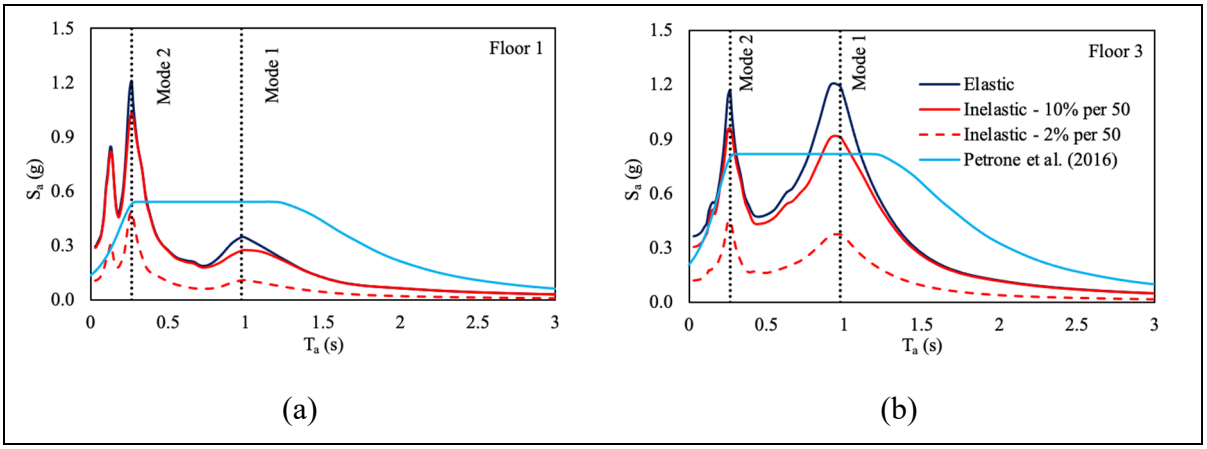

Figure 3.5 Elastic and inelastic FRS of 3-storey building, a) Floor 1, b) Floor 3

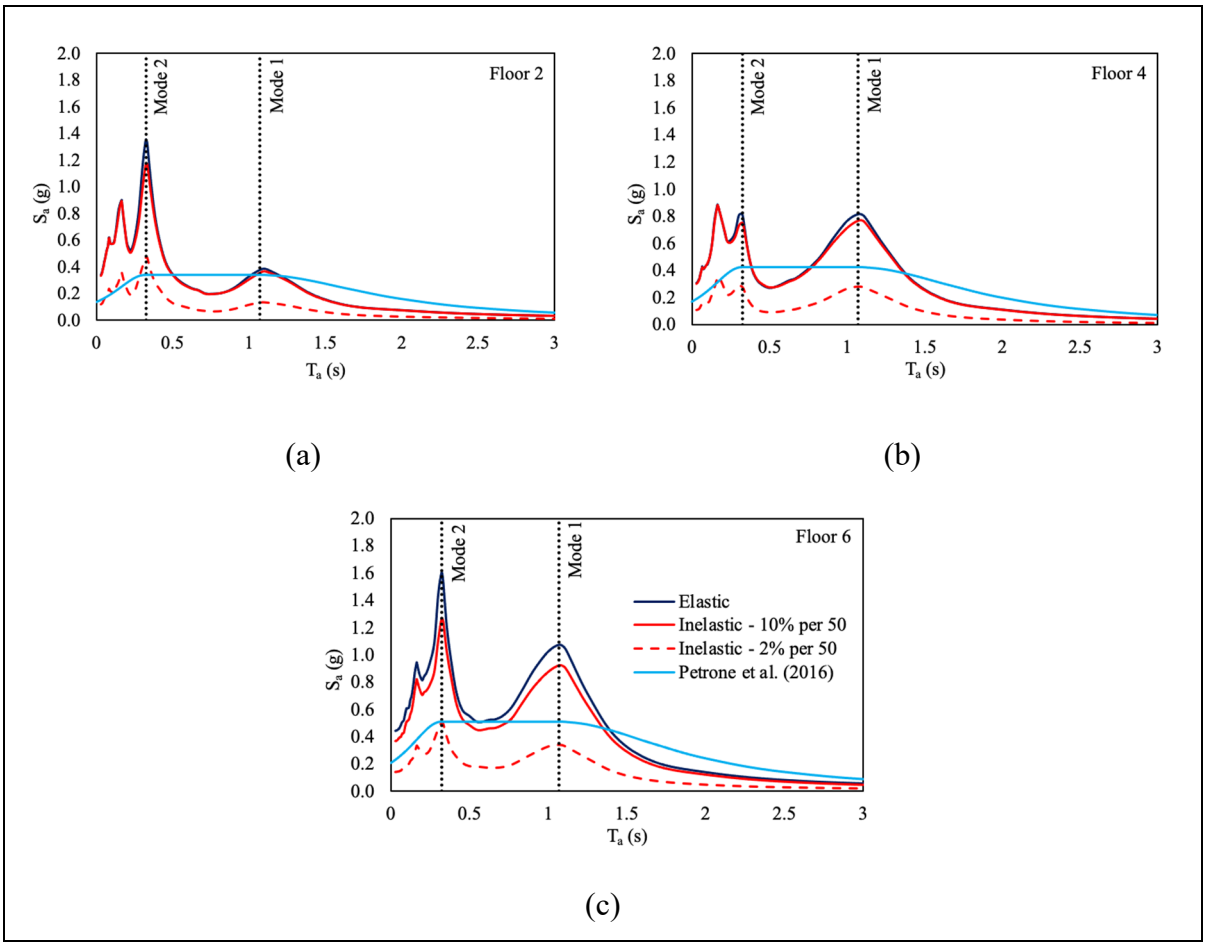

Figure 3.6 Elastic and inelastic FRS of 6-storey building, a) Floor 2, b) Floor 4, c) Floor 6

The inelastic FRS is following the same pattern as the elastic ones; however, there is a reduction in the values due to considering nonlinearity in the supporting structure, which is in accordance with the observation of Petrone et al. (2016). In all cases, the elastic FRS around the peaks of the second modal period of the building is significantly greater than those in the vicinity of the first modal period, except for the roof of the 3-storey building in which the elastic spectral acceleration of the first modal period is slightly greater than those of the second modal period. The same result is also reported from Berto et al. (2020).

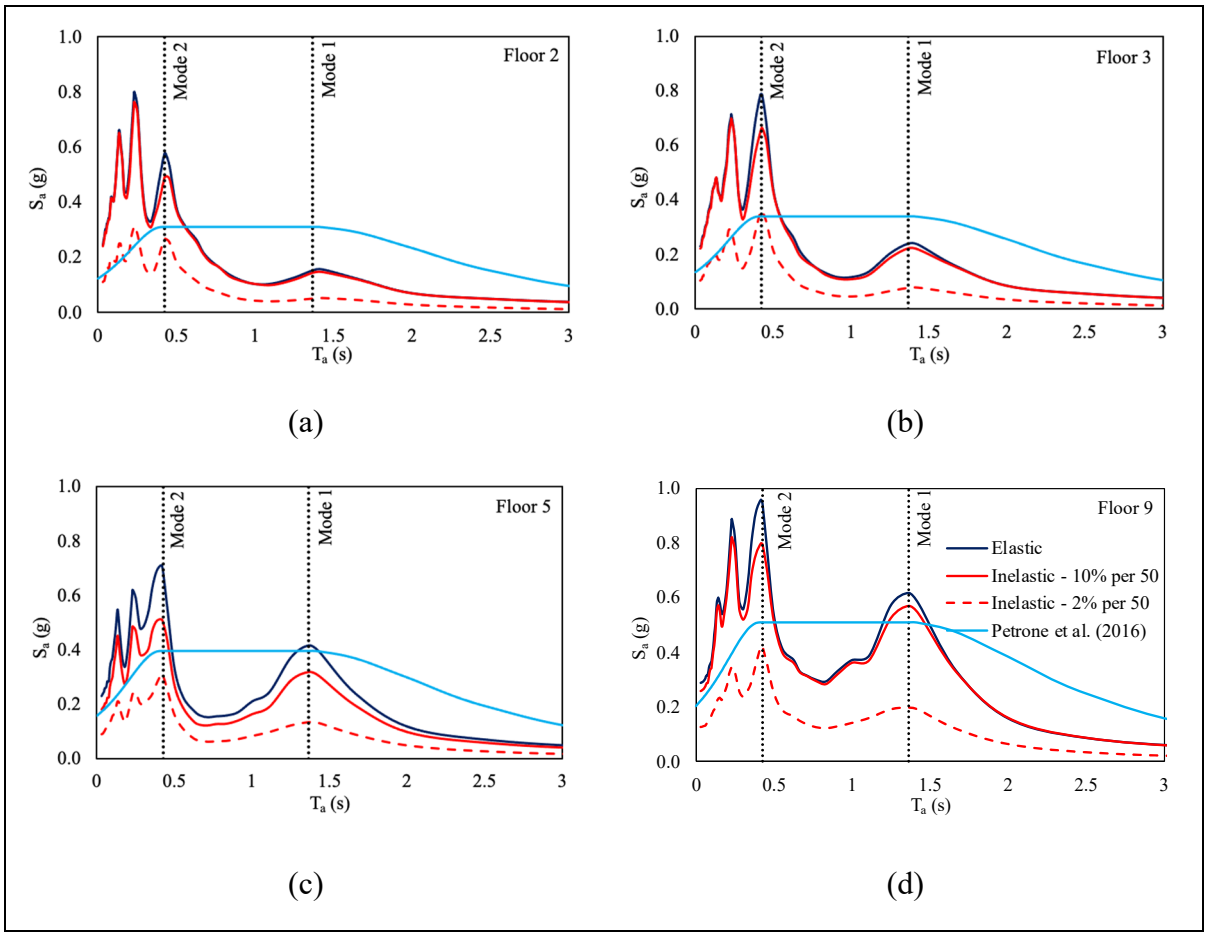

Figure 3.7 Elastic and inelastic FRS of 9-storey building, a) Floor 2, b) Floor 3, c) Floor 5, d) Floor 9

Generally, by increasing the height of the building, the difference between the FRS of the first and the second modal periods of the building is increased. Moreover, the FRS at the higher modes recorded from the lower floors is significantly greater than those of the first modal

period of the building, compared to upper floors in which the FRS at the higher modes is slightly greater than those at the first mode. Hence, the contribution of the higher modes is more pronounced on the lower floors.

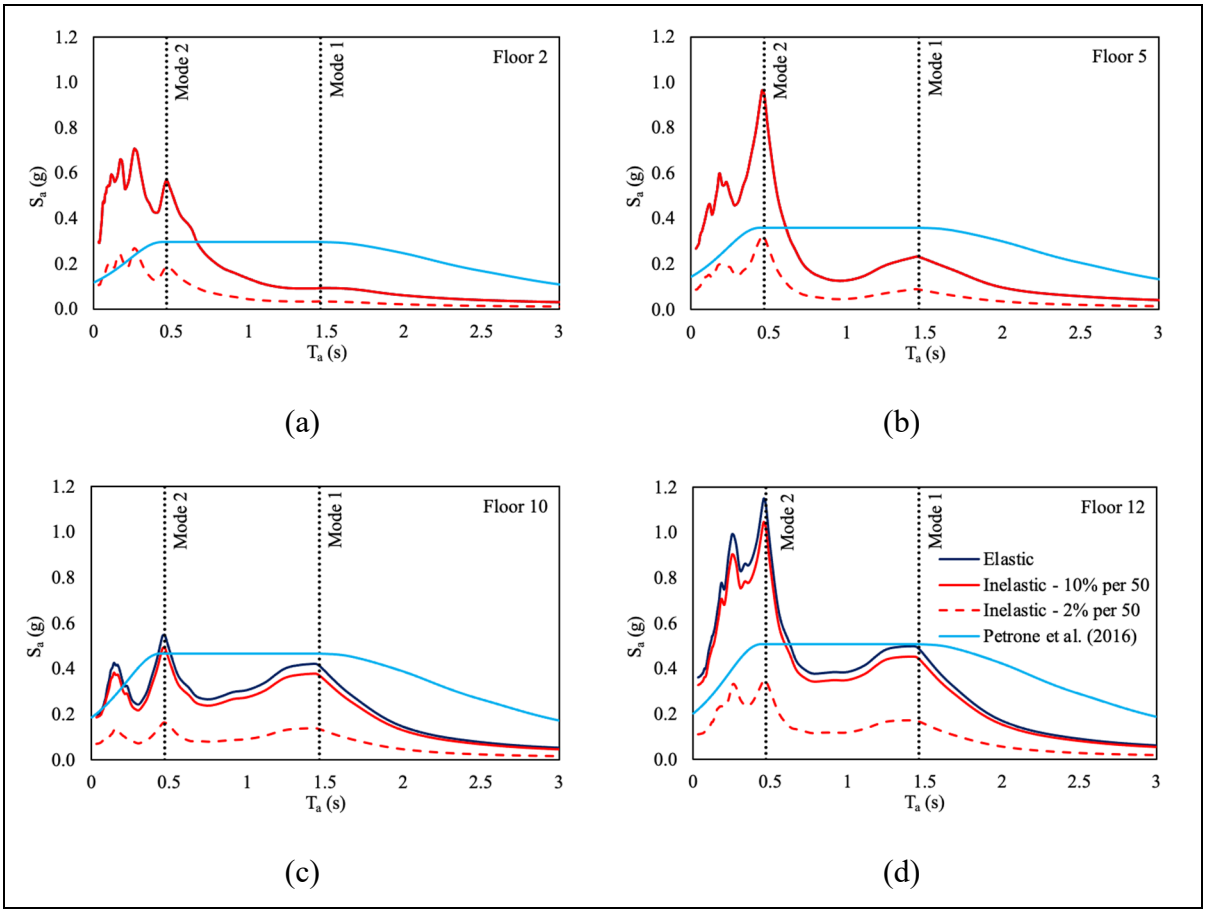

Figure 3.8 Elastic and inelastic FRS of 12-storey building, a) Floor 2, b) Floor 5, c) Floor 10, d) Floor 12

The effect of nonlinearity in the supporting structure is more evident at the higher modes, as the reduction of the peak floor response spectra is more significant at the second modal period. For instance, inelastic FRS of the roof of the 12-storey building at the second modal period shows a 71% reduction compared to the elastic FRS, while a 61% reduction was observed at the first mode. Thus, the contribution of the higher modes is more significant in the inelastic range. This observation conforms to the obtained height factor discussed in section 4.1 and the previous research studies (Petrone et al., 2016; Berto et al., 2020).

Furthermore, a comparison of the inelastic FRS recorded at the roof, and intermediate floors with the formulation suggested by Petrone et al. (2016) indicates a proper estimation of the seismic acceleration demands on NSCs by the proposed method. It is worth noting that employing the suggested formulation would result in a reasonable estimation of the floor spectral acceleration in a wide range of periods as it accounts for the uncertainty in estimating the fundamental period of the structure.

CHAPITRE 4

ASSESSMENT OF SEISMIC ACCELERATION DEMANDS ON NONSTRUCTURAL ELEMENTS IN MODERATELY DUCTILE FRAME BUILDINGS DESIGNED ACCORDING TO NBC 2015

Reza Sheikhzadeh Shayan, Rola Assi

École de Technologie Supérieure, Montreal, QC H3C 1K3, Canada

Paper submitted to the Canadian Journal of Civil Engineering, May 21, 2022

4.1 Abstract

This paper presents an extensive investigation of the seismic demands on acceleration-sensitive NSCs attached to the RC moment-resisting frame buildings with limited ductility and designed according to the National Building Code of Canada (NBC, 2015). A total of four benchmark structures with varying heights are considered in this study. Linear and nonlinear time-history analyses have been performed using artificial ground motions compatible with the Montreal site Class C uniform hazard spectra corresponding to 2% and 10% probabilities of being exceeded in 50 years. Seismic acceleration demands on NSCs were evaluated by assessing the horizontal height factor and the component dynamic amplification factor, compared to various building code provisions. The overall acceleration demands of NSCs were discussed by evaluating the force factor, and a corresponding optimized profile is proposed to improve the estimation of the seismic force demands of NSCs in moderate seismic zones.

KEYWORDS: Non-structural components; Seismic acceleration demand; Component force factor; Uniform hazard spectra; Height factor; Component amplification factor

4.2 Introduction

Non-structural components (NSCs) generally do not contribute to the load-bearing systems but are still required for the building to function. In fact, their failure during seismic events may lead to a long-term disruption of the building's serviceability, resulting in extensive direct and indirect monetary loss (Gupta & McDonald, 2008; Bradley et al., 2009; Anajafi et al., 2020; Rashid et al., 2021). This condition can be critical, specifically for the buildings of high importance, such as hospitals (Achour et al., 2011; Filiatrault & Sullivan, 2014; Hur et al., 2017; Shang et al., 2019). Therefore, it becomes vital to precisely estimate the floor acceleration demands imposed on NSCs in each story level in order to meet the overall seismic performance objectives of a building (Taghavi & Miranda, 2005b; Vukobratović & Fajfar, 2017; Welch & Sullivan, 2017; González et al., 2019).

When a seismic motion strikes a structure, vertical and horizontal floor accelerations trigger inertia forces that govern the seismic design of acceleration-sensitive NSCs located on the floor, e.g., anchored and free-standing mechanical and electrical systems for fire protection, heating-ventilation-air conditioning (HVAC), piping systems, and ceiling systems. One of the standard methods to determine the seismic acceleration demands on NSCs is using the simplified formulations suggested by the current code provisions, including ASCE/SEI 7-16 (American Society of Civil Engineers, 2017), NBC (NRCC, 2015), Eurocode 8 (CEN, 2005), NZS 1170.5 (Standards Association of New Zealand & Standards New Zealand, 2016), and Applied Technology Council (ATC, 2018). The horizontal seismic force demand of acceleration-sensitive components and their corresponding force factors in the various design standards are summarized in Table 4.1.

Although these formulations are mainly based on engineering judgment rather than the analytical or experimental results (Filiatrault & Sullivan, 2014), they are commonly utilized as a convenient tool when scant information about NSCs and supporting structures is available during the design phase.

Table 4.1 Seismic force demand for acceleration-sensitive components in the building codes discussed herein

Code	Seismic force demand	Design PGA	Component importance factor	Component amplification factor	Component response modification factor	Height factor	Component weight
NBC 2015	$V_P = 0.3F_aS_a(0.2)I_ES_PW_P$ $S_P = C_PA_rA_x/R_P$	$0.3F_aS_a(0.2)I_E$	C_P	A_r	R_P	$A_x = 1 + 2\,h_x/h_n$	W_P
ASCE 7-16	$F_P = \frac{0.4a_PS_{DS}W_P}{R_P/I_P}\left(1 + 2\frac{z}{h}\right)$ $0.3S_{DS}I_PW_P \le F_P \le 1.6S_{DS}I_PW_P$	$0.4S_{DS}$	I_P	a_P	R_P	$\left(1 + 2\frac{z}{h}\right)$	W_P
Eurocode 8	$F_a = \frac{S_a.\gamma_a}{q_a}W_a$ $S_a = \frac{a_g}{g}S\left[\frac{3(1+z/H)}{1+(1-T_P/T_1)^2} - 0.5\right] \ge \frac{a_g}{g}S$	$\frac{a_g}{g}S$	γ_a	$\left[\frac{3(1+z/H)-0.5}{1.5(1+z/H)-0.5}\right]$	q_a	$1.5\left(1+\frac{z}{H}\right)-0.5$	W_a
ATC	$\frac{F_P}{W_P} = PGA\left[\frac{(\mathrm{PFA/PGA})}{R_{\mu bldg}}\right]\left[\frac{(PCA/PFA)}{R_{Pocomp}}\right]I_P$ $a_1 = (1/T_{abldg}) \le 2.5$ $a_2 = \left[1 - (0.4/T_{abldg})^2\right] > 0$	PGA	I_P	$(\frac{PCA}{PFA})$	R_{Pocomp}	$\frac{PFA}{PGA} = 1 + a_1\left[\frac{z}{h}\right] + a_2\left[\frac{z}{h}\right]^{10}$	W_P
NZS 1170.5	$F_{Ph} = C_P(T_P)C_{Ph}R_PW_P \le 3.6W_P$ $C_P(T_P) = C(0)C_{Hi}C_i(T_P)$ $C(0) = C_h(0)ZRN(T,D)$	$C(0)$	R_P	$C_i(T_P)$	C_{Ph}	$\begin{cases} h < 12m, & C_{Hi} = 1 + h/6 \\ h \ge 12m, & C_{Hi} = 3.0 \end{cases}$	W_P

In the code formulations, the component force amplification factor denoted by A_r in NBC represents the dynamic amplification of the component relative to the position of its attachment. It can be computed as the floor response spectrum (FRS) normalized by the peak floor acceleration (PFA) at a given building level (Medina et al., 2006). In the Canadian and US building codes, it is equal to 1.0 for the rigid NSCs ($T_{NSC} < 0.06s$) and 2.5 for the flexible ones ($T_{NSC} \geq 0.06\ s$) and remains constant along the height of the building. Similarly, the component amplification factor in NZS 1170.5 does not account for the building period, while EC8 proposes a profile that is a function of the periods of the NSC and the supporting structure. It has been observed that the component amplification factor is strongly affected by several parameters associated with the primary structure and NSCs characteristics, including the nonlinearity in the supporting structure (Wieser et al., 2013; Anajafi & Medina, 2018b, 2019a; Surana, 2019), the nonlinearity in the NSCs (Vukobratović & Fajfar, 2017; Obando & Lopez-Garcia, 2018; Kazantzi et al., 2018; Anajafi et al., 2020), the location of the NSCs in the supporting structure (Petrone et al., 2016; Anajafi & Medina, 2018b), the ratio of the NSCs period to the fundamental period of the supporting structure (Medina et al., 2006; Anajafi & Medina, 2019a), and the damping ratio of both NSC and supporting structure (Clayton & Medina, 2012; Sullivan et al., 2013; Obando & Lopez-Garcia, 2018; Anajafi & Medina, 2019b).

Likewise, the height factor denoted by A_x in NBC represents the amplification of the acceleration from the base of the structure to the height at which the component is attached and is determined as the ratio of PFA to peak ground acceleration (PGA). Unlike NBC 2015, ASCE 7 and EC8 with floor amplification linearly increasing along the height of the building, ATC suggests a nonlinear equation for the floor amplification. In the NZS 1170.5, the PFA/PGA ratio is determined based on the building height using the floor height coefficient (C_{Hi}).

Moreover, the NBC 2015 and NZS 1170.5 consider the importance level of the host building; therefore, one NSC might be designed for different design forces. In this case, different seismic

performance levels are expected for one NSC located in similar buildings with different importance levels.

It is worth noting that NBC 2015, ASCE 7, and EC8 formulations do not account for the effect of the building higher modes, effect of torsion, and NSC internal damping, which might result in over-or-underestimating the seismic acceleration demands on NSCs, as pointed out by several researchers (Sullivan et al., 2013; Petrone et al., 2016; Anajafi & Medina, 2019a). Therefore, several studies attempted to improve the various seismic regulations related to NSCs, specifically ASCE 7 and EC8. Some recent studies will be summarized, with special emphasis on the height and dynamic amplification factors.

Petrone et al. (2016) performed a time-history analysis on elastic and inelastic RC frame buildings designed according to EC8. They concluded that EC8 and ASCE 7 overestimated the floor acceleration amplification envelope for the inelastic structures. Berto et al. (2020) performed linear and nonlinear time-history analysis on slender cantilever wall (CW) and moment-resisting frame (MRF) buildings with varying height levels. They noticed that the ASCE 7 overestimated the floor amplification in both building types, even in the elastic case; however, the EC8 has proposed a safe-sided floor acceleration amplification.

By evaluating the component dynamic amplification factor, Anajafi et al. (2020) observed that the maximum amplification has occurred in the range of component period tuned to the period of the translational mode of the supporting structure, with a maximum value of 10 for components mounted on elastic buildings. A value of 4.5 was obtained based on the work of Kazantzi et al. (2020), which complied with the computed amplification factor by Taghavi and Miranda (2005b).

On the other hand, very few studies have been conducted to evaluate the accuracy of the Canadian seismic provisions related to NSCs. Shooshtari et al. (2010) evaluated floor design spectra by conducting nonlinear analyses on reinforced concrete buildings with different seismic force-resisting systems and building heights. It was observed that the floor response

spectra are significantly amplified, specifically for the buildings with shorter periods. Moreover, Asgarian and McClure (2020a, 2020b) proposed a practical approach for generating NSC floor design spectra, considering different damping ratios for NSCs. In this case, the dynamic characteristics of buildings were determined based on the ambient vibration measures. The obtained results showed that NBC 2015 and ASCE 7 significantly underestimated the component amplification factor in the low and medium-rise buildings. It was also observed that the NSC damping ratio considerably affects the component acceleration response.

The present paper investigates the effect of building height, nonlinearity, and the severity of ground motions on the seismic acceleration demands of NSCs in RC moment-resisting frame buildings with limited ductility designed according to NBC 2015 and located in Montreal that has a moderate level of seismicity. In particular, the component dynamic amplification factor and the height factor were assessed and compared to the various seismic provisions, including ASCE 7, NBC 2015, Eurocode 8, NZS 1170.5, and Applied Technology Council. Also, the overall seismic force factor equivalent to the product of A_r and A_x for ductile NSCs ($R_P = 2.5$) was discussed and compared to the aforementioned code provisions. Finally, an optimized force factor profile is proposed to improve the estimation of the seismic force demands of acceleration-sensitive NSCs.

4.3 Description of the studied buildings

Low to medium-rise reinforced concrete (RC) moment-resisting frame (MRF) archetype regular buildings with limited ductility and designed according to NBC 2015 have been selected for this study (Mazloom & Assi, 2022). The building plans consist of three 7-meters bays in North-South (N-S) and East-West (E-W) directions. Also, each floor has 3-meters of typical height. Elevation views of the buildings, dimensions of the sections, and the fundamental period obtained from modal analysis of the structures performed in SAP2000 (CSI, 2019) are shown in Figure 4.1.

Material nonlinearity was implemented using discrete lumped plastic hinges in the beams and columns based on acceptance criteria specified by ASCE 41-17 (2017). In this case, two-moment plastic hinges are assigned close to the rigid zones at the ends of the elements so that the plastic hinges can be formed close enough to the face of the joints. The yield moment and rotation were determined by performing sectional analysis using Response-2000 (E. Bentz, 1999), and the ultimate moment capacity is considered equal to $1.1M_y$, as suggested by NIST GCR 17-917-44 (2017).

Moreover, Takeda's trilinear degrading hysteretic model (Takeda et al., 1970) is employed to represent the cyclic response of individual RC frames since it captures the strength and stiffness degradation of the concrete components.

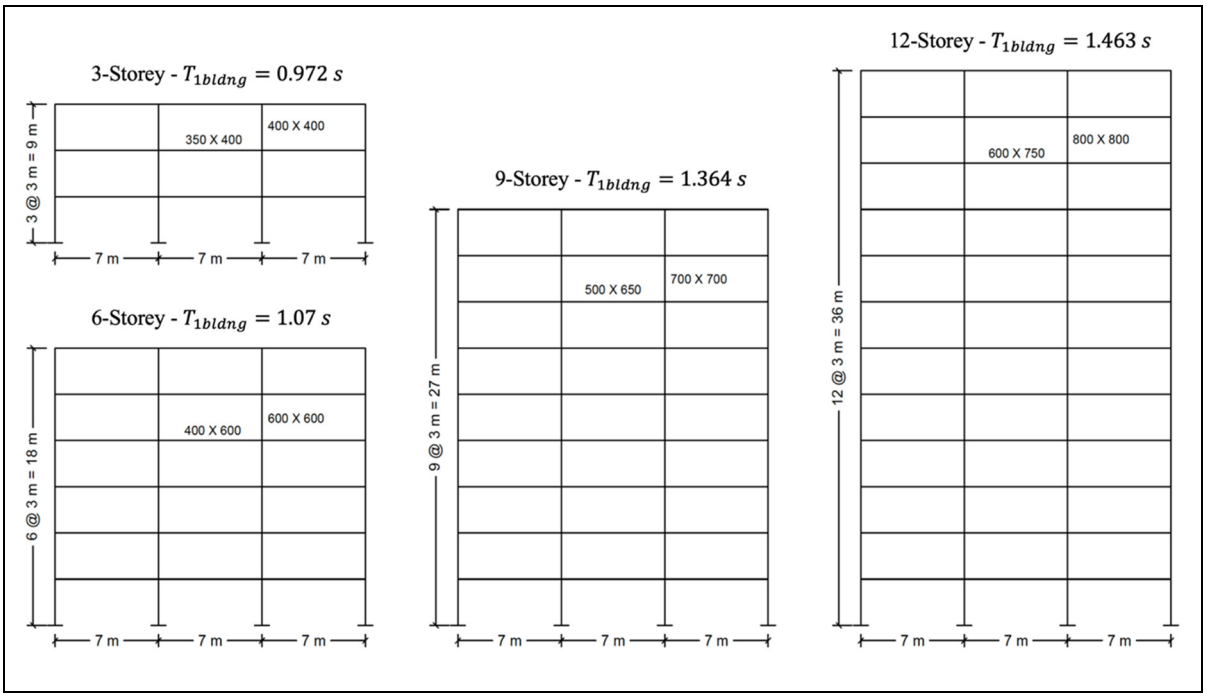

Figure 4.1 Elevation views, with fundamental period and cross-sectional dimensions in mm of the selected structures

4.4 Selection and scaling of the ground motion records

Due to insufficient recorded ground motions from historic events in Eastern Canada, synthetic ground motion records (GMRs) (Atkinson, 2009) compatible with Montreal uniform hazard spectra (UHS) for firm ground known as site class C in NBC were used. GMRs were selected and scaled based on method A proposed in NBC commentary (2017) and explained by Tremblay et al. (2015). In this case, scenario-specific period ranges (T_R) and two target spectra with 2% and 10% probabilities of exceedance per 50 years are defined based on the location and soil type, according to NBC 2015. Two M-R scenarios were considered, including six GMRs with the magnitude of M6.0 and a fault distance varying from 10 to 30-Km, and six GMRs with the magnitude of M7.0 and a fault distance ranging from 15 to 75-Km. Parameters of the selected and scaled GMRs are presented in Table 4.2.

Table 4.2 Parameters of the synthetic GMRs used in this study

Building	Scenario	Magnitude	Period range TR	Number of GMRs and fault distance
3-storey	1	M 6.0	0.14 - 1.0	6 @ 10-30 Km
	2	M 7.0	0.5 - 1.5	6 @ 15-75 Km
6-storey	1	M 6.0	0.15 - 1.0	6 @ 10-15 Km
	2	M 7.0	0.5 - 1.5	6 @ 15-25 Km
9-storey	1	M 6.0	0.19 - 1.0	6 @ 10-15 Km
	2	M 7.0	0.5 - 1.8	6 @ 15-25 Km
12-storey	1	M 6.0	0.2 - 1.0	6 @ 10-15 Km
	2	M 7.0	0.5 - 2.0	6 @ 15-25 Km

4.5 Preliminary nonlinear static analysis of the archetype frames

Numerous studies have rigorously argued that the level of inelasticity in one structure could result in mitigating the large seismic acceleration demands on NSCs in the buildings exhibiting an elastic behavior, specifically those tuned to one of the resonant periods of the supporting structure (Chaudhuri & Villaverde, 2008; Adam et al., 2013; Surana et al., 2018; Anajafi et al., 2020, 2021). The extension of inelastic action in the host structure can be determined based on the ductility-related force modification factor (R_d) that accounts for the capability of the

structure to dissipate energy and the overstrength-related force modification factor (R_O) that reflects the portion of reserve strength in the structure. In this regard, pushover analysis was performed on the buildings to evaluate their actual ductility and overstrength, using the equivalent static seismic force applied along the frame height in the shape of an inverted triangle. The computed pushover curve and bilinear force-deformation curve based on FEMA-356 (2000) for frame buildings are illustrated in Figure 4.2.

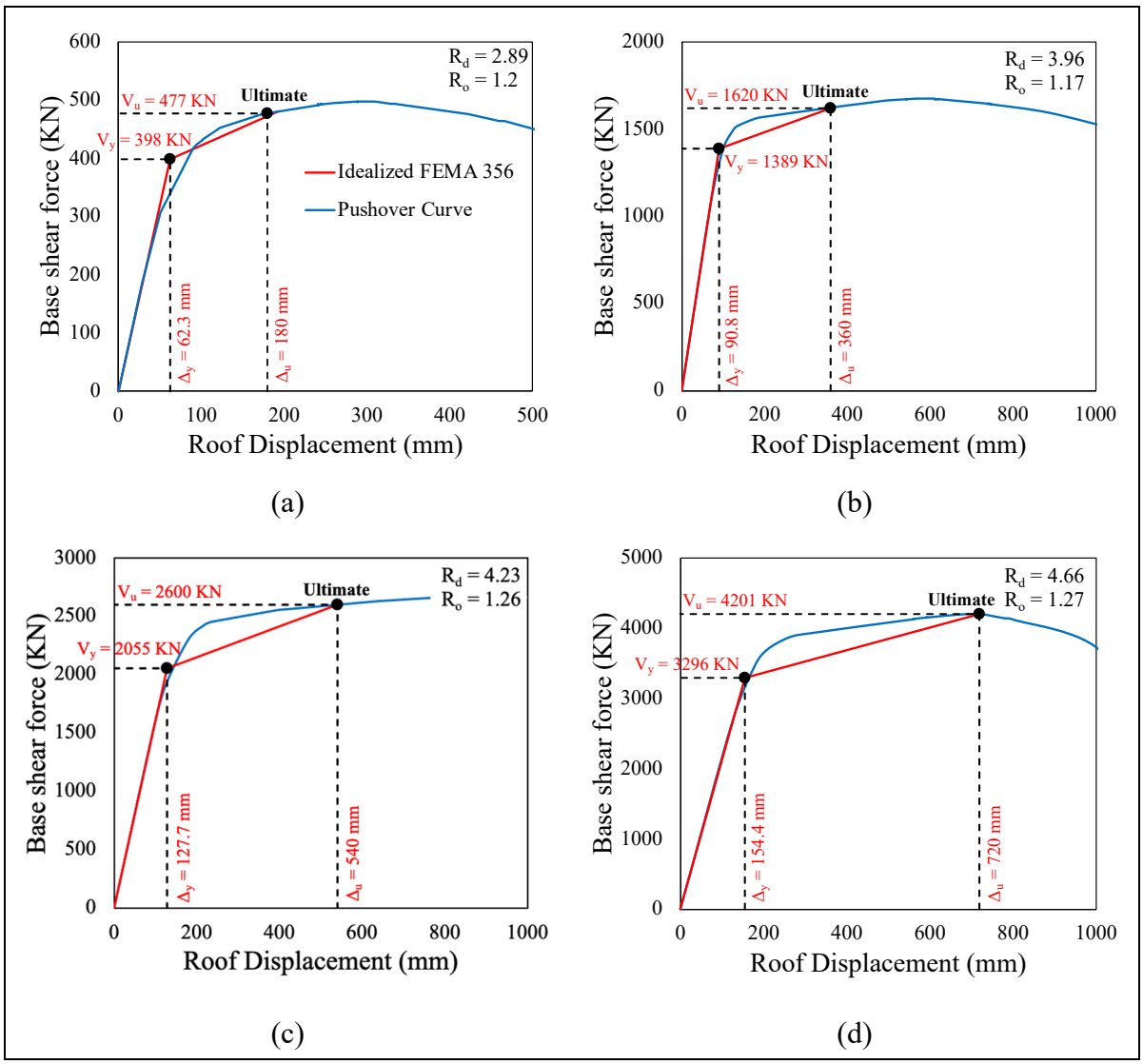

Figure 4.2 Pushover and idealized bilinear curves according to FEMA 356 for the: a) 3, b) 6, c) 9, and d) 12-storey buildings

The obtained modification factors reveal that, generally, the actual ductility capacity of all the structures is greater than the system ductility assumed in the design phase ($R_d = 2.5,\ R_O = 1.4$). Therefore, the higher the ductility capacity, the lower the seismic acceleration demands on NSCs are expected in the inelastic phase (Petrone et al., 2016; Anajafi et al., 2021).

4.6 Time-history results and discussion

4.6.1 Evaluation of the height factor, A_x

Median values of PFA/PGA profiles of the elastic buildings considering GMRs with a 10% probability of exceedance per 50 years (referred to as elastic) are calculated as a lower seismic activity is deemed adequate for elastic behavior. The height factor for elastic buildings and inelastic cases considering GMRs with 2% and 10% chances of being exceeded per 50 years (referred to as 2% inelastic and 10% inelastic, respectively) and the height factors proposed by the various building codes are illustrated in Figure 4.3.

In the elastic range, the PFA/PGA ratio tends to linearly increase from 1.0 at the structure's base to 1.24 at the top level of the 3-storey building since the response is dominated only by the first vibrational mode. There was no amplification along the height in other medium-rise buildings except at the rooftop levels with the PFA/PGA ratio of 1.32, 1.29, and 1.16 for the 6, 9, and 12-storey buildings, respectively.

Similar profiles were obtained in the nonlinear range; as almost no PGA amplification over the building height was observed; this can be explained by the fact that the effective ductility of the buildings is greater than the ductility assumed in the design phase, as discussed in section 4.5. Moreover, the swinging shape of the PFA profiles, referred to as the whiplash effect, was formed around the top floors, manifesting the dominance of the second mode of the buildings over the structural response, as highlighted in several research studies (Taghavi & Miranda, 2005b; Petrone et al., 2016; Berto et al., 2020).

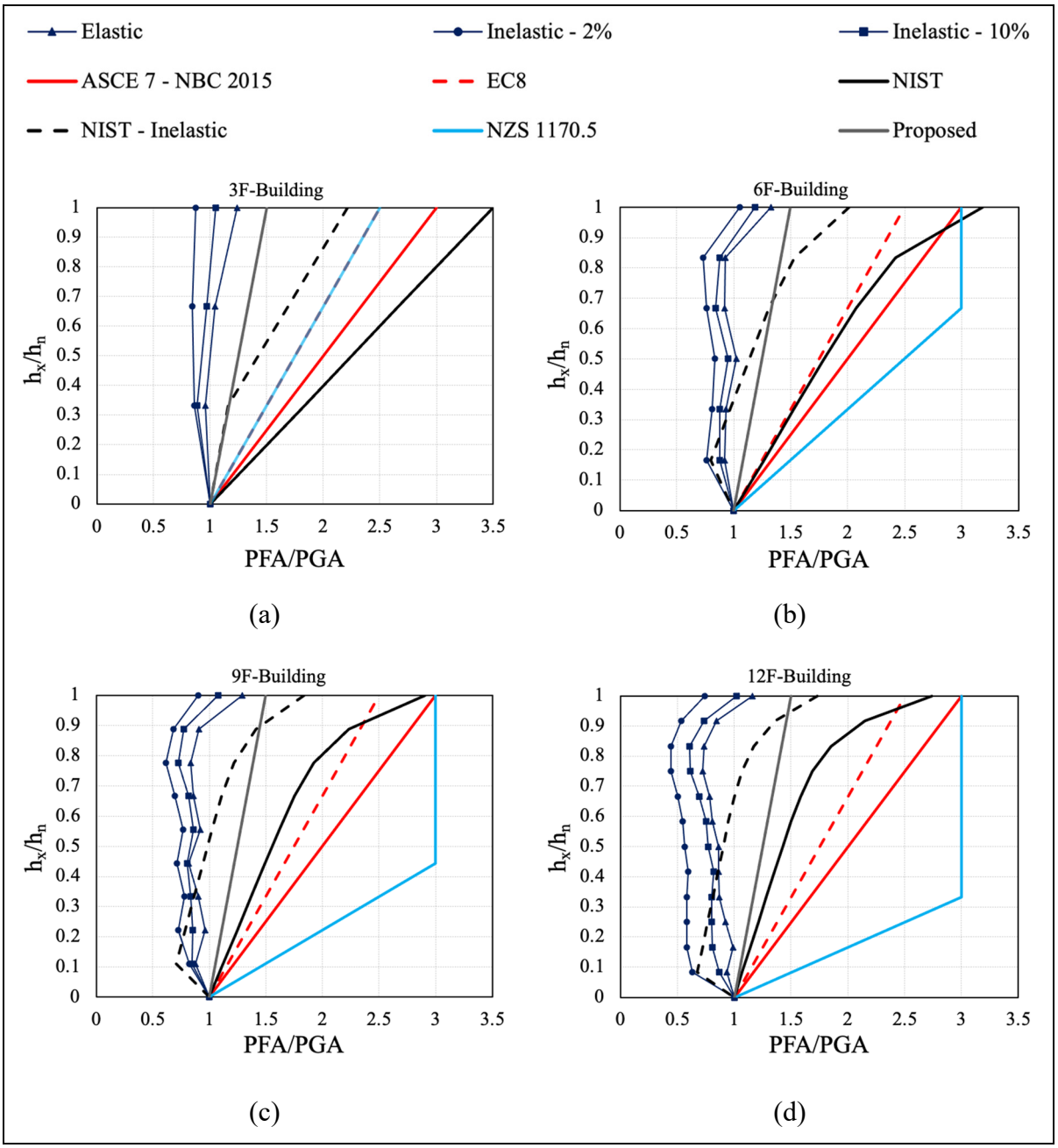

Figure 4.3 Median values of PFA/PGA ratio along the building height obtained from elastic and inelastic analysis, a) 3-storey, b) 6-storey, c) 9-storey, d) 12-storey

It can be noted that the ASCE 7, NBC 2015, NZS 1170.5, and EC8 formulations are conservative considering the elastic and inelastic models. The ATC profile for the elastic cases is conservative for all the buildings. However, the inelastic ATC profile is closer to the PFA/PGA ratio of the 2% inelastic case on the lower floors except for the 3-storey building

while overestimating the acceleration demands on NSCs on the upper floors. Also, the inelastic ATC profile underestimates the inelastic PFA/PGA ratio for the first three floors of all buildings except for the 10% inelastic 3-storey building, while it yields a relatively proper estimation for the intermediate floors. Furthermore, it is observed that the reduction in PFA/PGA ratio along the building height due to inelasticity is more significant when using a higher seismic intensity.

In light of the obtained results, it is concluded that the height factor proposed by NBC 2015 is overly conservative for NSCs attached to the frame buildings with limited ductility, which are located in the moderate seismic zone. Therefore, it is suggested that considering the value of 1.0 for the PFA/PGA ratio at the base of the structure increasing to 1.5 at the topmost level adequately estimates the floor acceleration amplification in such buildings.

4.6.2 Dynamic amplification factor, A_r

The median values of the ratio of FRS over the PFA denoted by A_r in NBC are shown in Figures 4.4 to 4.7 on selected floors of the elastic and inelastic buildings.

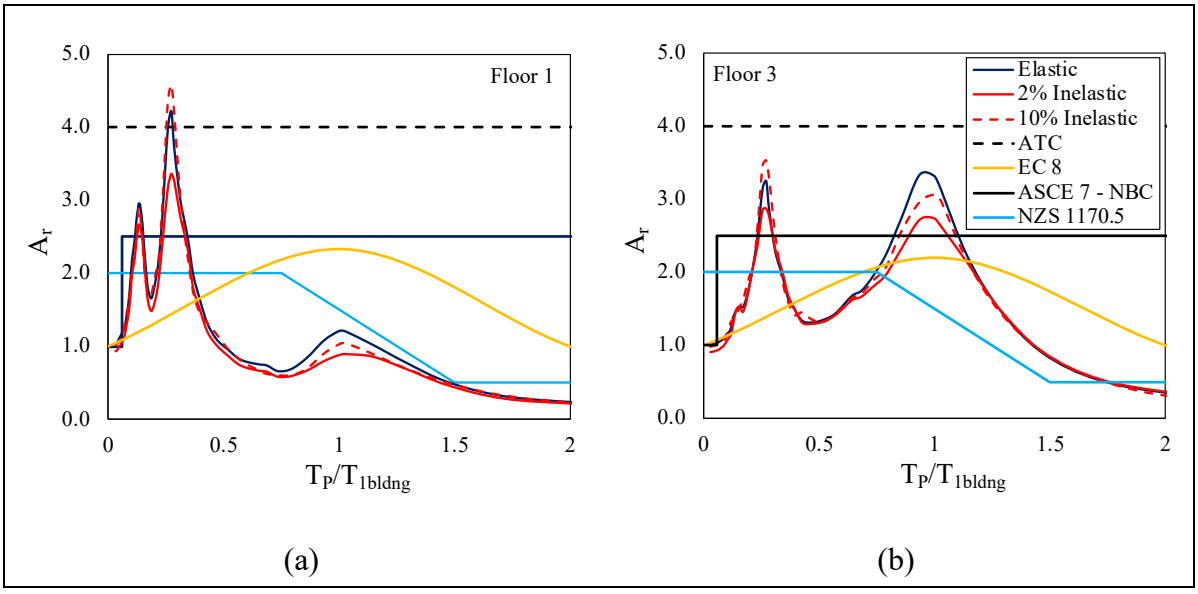

Figure 4.4 The median values of the component amplification factor in the 3-storey building, a) Floor 1, b) Floor 3

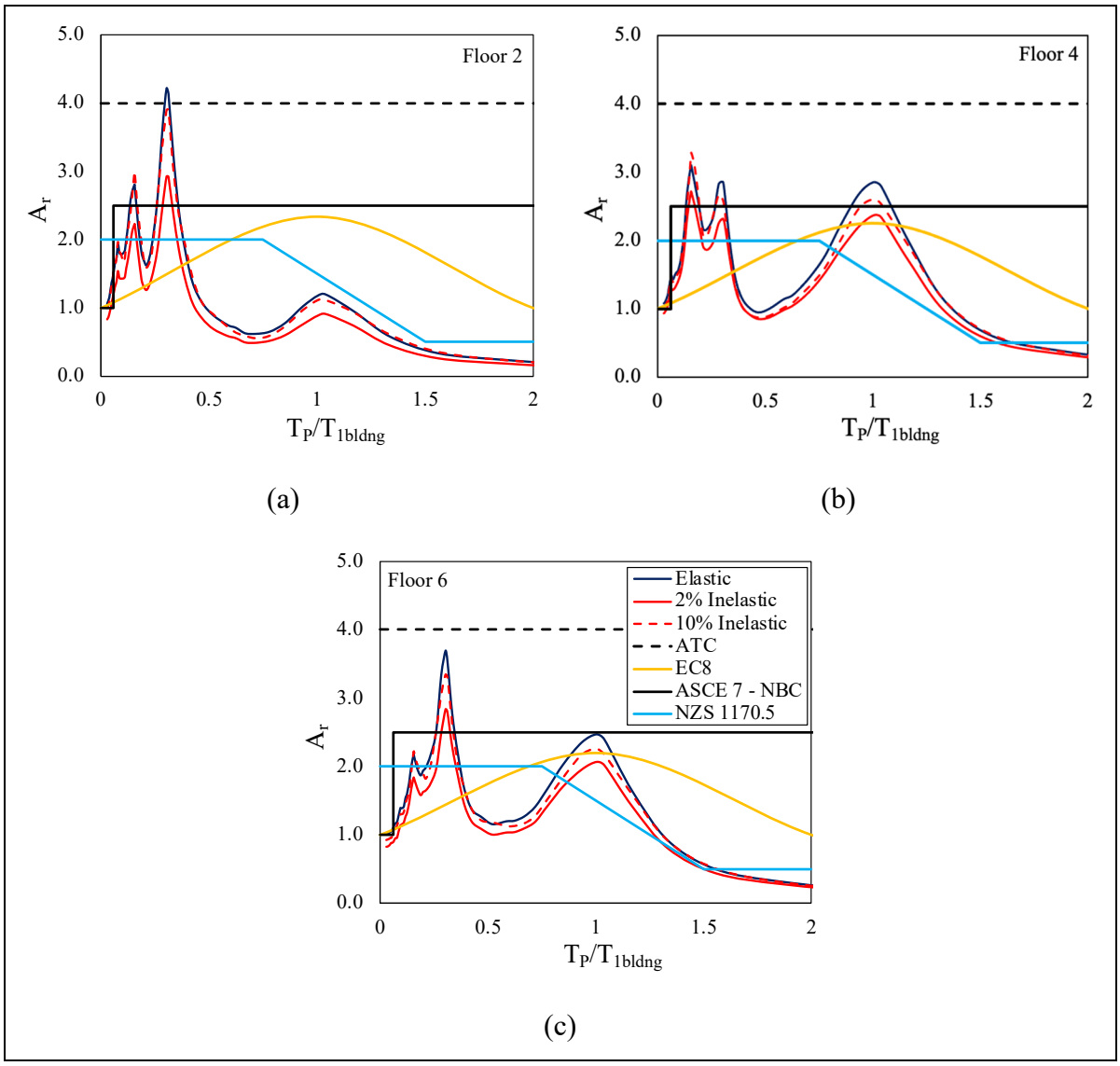

Figure 4.5 The median component amplification factor in the 6-storey building, a) Floor 2, b) Floor 4, c) Floor 6

The horizontal axis corresponds to the NSC period (T_P) normalized by the first modal period of the supporting structure (T_{1bldng}) for a more precise estimation of the acceleration demands on NSCs, as recommended by Kazantzi et al. (2020).

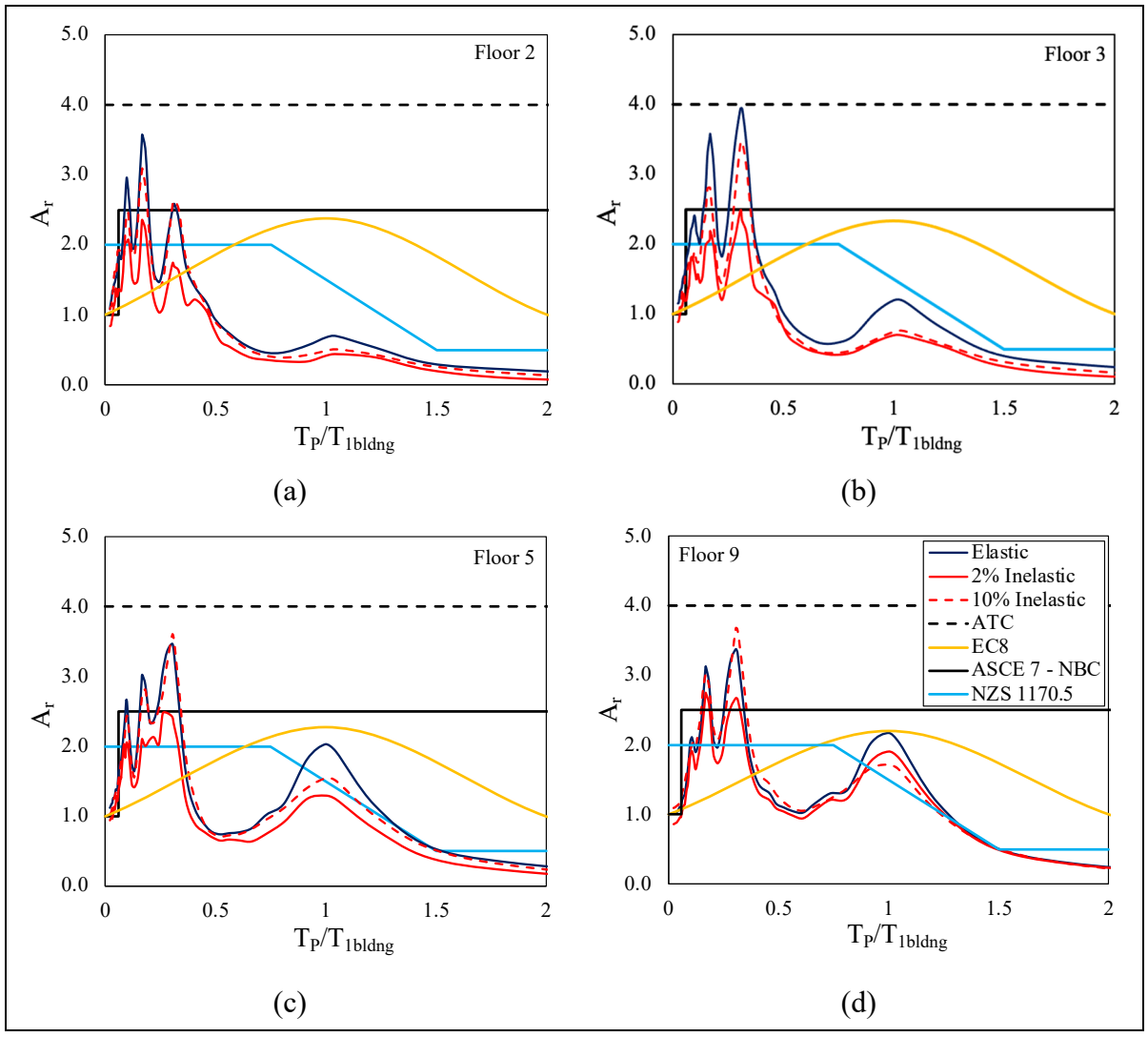

Figure 4.6 The median values of the component amplification factor in the 9-storey building, a) Floor 2, b) Floor 3, c) Floor 5, d) Floor 9

4.6.2.1 Effect of period range

It is observed that the component amplification factor is nearly equal to 1.0 for the components with a period range below one-tenth of the modal period of the supporting building ($T_P/T_{1bldng} \leq 0.1$), meaning that the component is experiencing the identical maximum acceleration as the corresponding building floor. The peak component amplification factor for all the buildings is observed in the period range of $0.1 < T_P/T_{1bldng} < 0.5$, which implies that the spectral ordinates are dominated by the higher modes of the structure. As expected,

another peak spectral ordinate with a relatively smaller amplitude is located around the resonant period range of $T_P/T_{1bldng} = 1.0$. Thereafter, a deamplification ($A_r < 1.0$) was observed in the period range of $T_P/T_{1bldng} \geq 1.5$. for highly flexible components with a period larger than the fundamental period of the supporting structure.

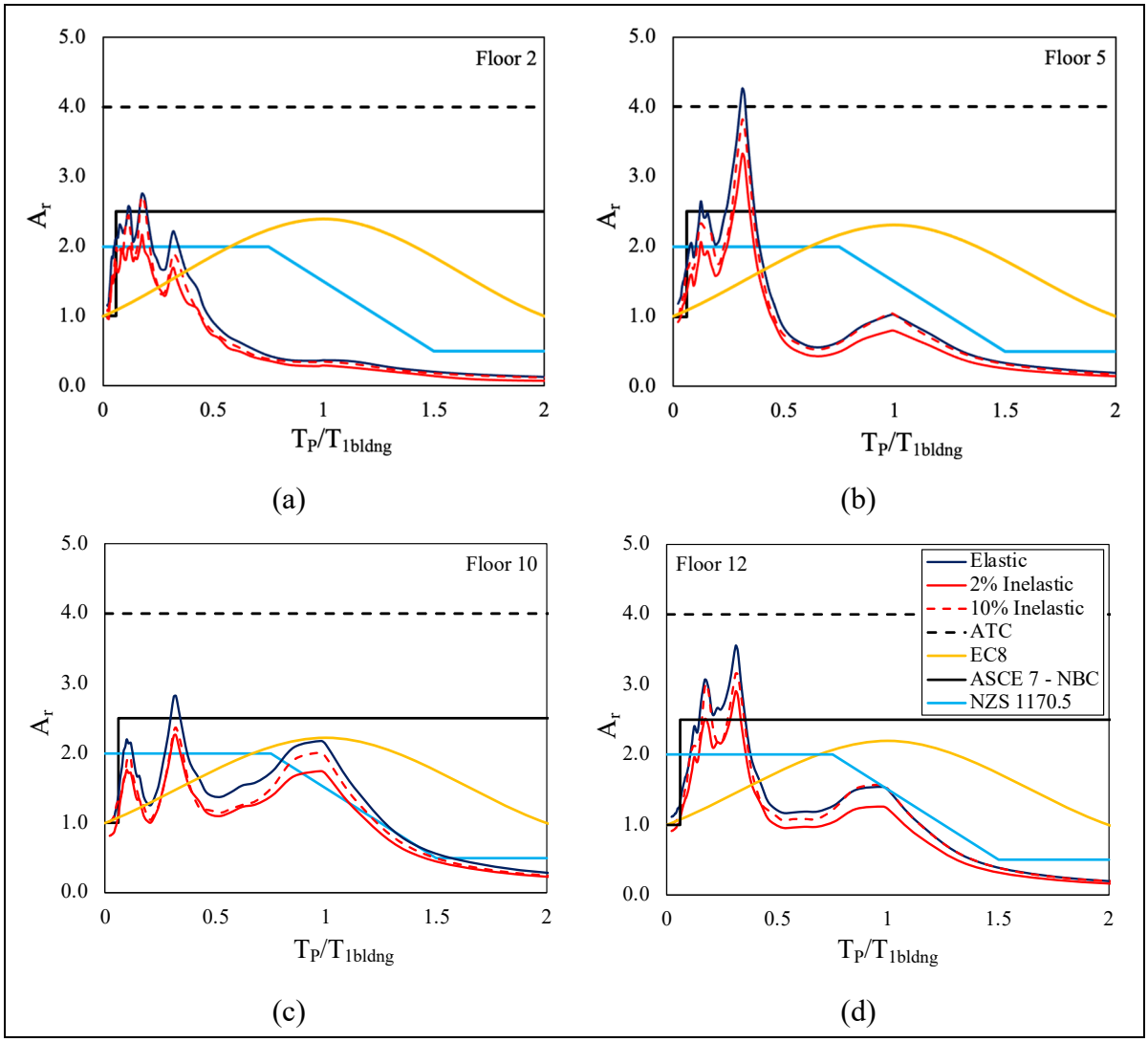

Figure 4.7 The median values of the component amplification factor in the 12-storey building, a) Floor 2, b) Floor 5, c) Floor 10, d) Floor 12

4.6.2.2 Effect of building nonlinearity

As is illustrated in Figures 4.4 to 4.7, a decrease in component amplification factor resulted, owing to the nonlinear characteristics of the supporting structure. The effect of nonlinearity in the supporting structure is significant around the modal periods of the buildings, and it is less tangible for NSCs with periods away from the resonant periods of the supporting structure. It is also noticed that the extension of nonlinearity in the supporting structure is more pronounced in inelastic buildings subjected to higher intensity earthquakes (2475 years return period). It is worth noting that the obtained peak values of the component amplification of NSCs on 2% inelastic buildings, i.e., 2.87, 2.55, 2.75, and 2.91 for the rooftop of the 3, 6, 9, and 12 storey buildings, respectively, are relatively smaller than those reported in some research on MRF buildings (Petrone et al., 2016; Berto et al., 2020; Kazantzi A. K. et al., 2020; Anajafi et al., 2021), which can be due to the higher actual ductility of the structures as discussed in section 4.5.

4.6.2.3 Comparison with code provisions

A comparison between the analysis results and the different provisions has been made. The NBC 2015 and ATC have suggested period-independent component amplification factors that do not account for the local amplification for the components with a period close to the modal period of the supporting structure; therefore, the values remain constant along the building height. Moreover, NBC 2015 and ASCE 7 considerably underestimate the peak component amplification factor for NSCs tuned to the higher modes of the supporting structure. On the other hand, for NSCs with periods around the fundamental period of the host structure, NBC 2015 and ASCE 7 overestimate the acceleration demands of the components located on the lower floors of all the buildings, while underestimating the A_r factor for components located on the higher floor levels of the elastic 3 and 6-storey buildings.

The ATC proposal overestimates the component amplification factor for the NSCs nearly in the entire NSC period range. However, in some cases, the A_r factor is close to the ATC

proposal for the components tuned to the higher modes of the elastic buildings. The NZS 1170.5 considerably underestimates the seismic acceleration demands on NSCs with a period range of $T_P/T_{1bldng} < 0.5$. Also, NZS 1170.5 tends to significantly overestimate the A_r factor in a wide range of NSCs periods, especially for those tuned to the fundamental period of the supporting structure and located on the lower floors. However, the A_r factor for the NSCs tuned to the fundamental period of the supporting structures located on the higher floors of the buildings exceeds the NZS 1170.5 provisions.

It is also observed that the values of the A_r factor obtained from the analysis remarkably exceeded the EC8 proposal for NSCs tuned to the higher modes of the supporting structure. Generally, EC8 conservatively predicts the values of the component amplification factor for the NSCs with a period close to the fundamental period of the supporting structure ($T_P/T_{1bldng} \approx 1.0$) and located on the lower floors. However, EC8 underestimates the A_r factor for the NSCs tuned or nearly tuned to the fundamental period of the supporting structure located on the higher floors, especially for the 3 and 6-storey buildings. Considering the EC8 suggestion for the A_r factor leads to a significant overestimation of the results for the NSCs with a period longer than the fundamental period of the supporting structure in all the buildings. Unlike EC8, other provisions, including ASCE 7, NBC 2015, ATC, and NZS 1170.5, generally extend the maximum value of the component amplification factor to the component period range $T_P/T_{1bldng} < 1.0$ so that they implicitly account for the effect of the higher modes of the supporting structure.

4.6.3 Effect of building height

In order to gain insight into the variation of peak component amplification along the height, the maximum A_r values resulting from the elastic and inelastic time-history analysis of the buildings were computed on each floor, as illustrated in Figure 4.8. It can be noted that values of A_r are relatively larger in the shorter buildings than that in the taller buildings. Also, the A_r factor varies nonlinearly along the height of the building, with the maximum values obtained on the intermediate floors. It is also apparent that the NBC 2015, suggesting the component

amplification with the constant value of 2.5 along the building's height, underestimates the peak component amplification values, especially in the elastic low-rise buildings with the values of 3.69 and 4.46 for the 3 and 6-storey buildings, respectively. The obtained values and results are consistent with the Petrone et al. (2016) observations.

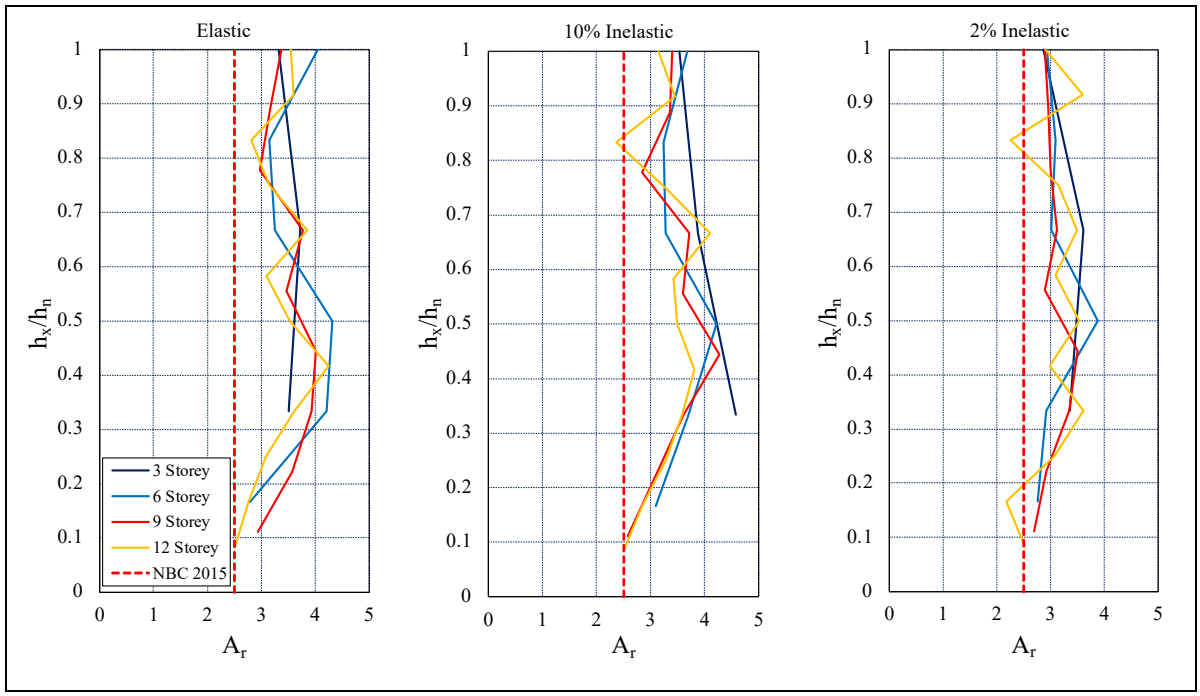

Figure 4.8 Component amplification along the building height for elastic and inelastic buildings, compared to the suggested value of NBC 2015

4.7 Evaluation of the component force factor, S_P

For an overall assessment of the seismic acceleration demands of acceleration sensitive NSCs, the ratio of $FRS/(PGA \times R_P)$ equivalent to the component force factor $A_r.A_x/R_P$ and denoted by S_P in NBC was evaluated at the rooftop of the studied buildings. In fact, it was highlighted in reconnaissance reports that rooftop equipment was more heavily damaged than equipment located elsewhere in buildings (NIST GCR 17-917-44, 2017). The elastic and inelastic force factors versus the component period normalized by the fundamental period of the supporting structure are shown in Figure 4.9. Values are obtained by considering a response modification

factor (R_P) equal to 2.5, corresponding to a ductile attachment since NSCs are expected to exhibit a ductile and dissipative behavior.

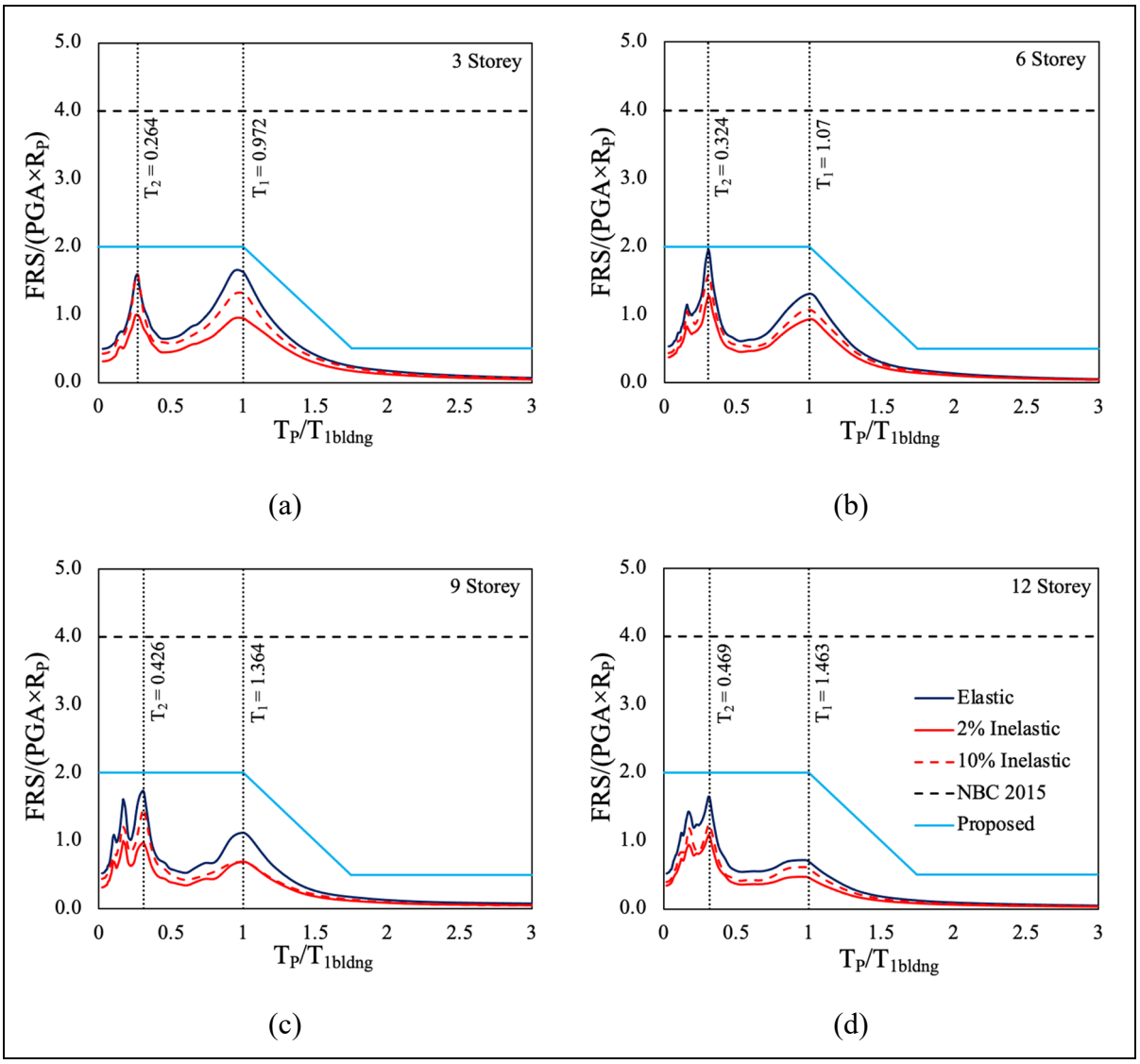

Figure 4.9 Computed and proposed rooftop component force factors versus T_P/T_{1bldng}, compared to the NBC profile

We can note that the maximum value of the S_P factor occurs in the vicinity of the fundamental period of the 3-story building, equal to 1.64. In contrast, the extremum values for the other buildings, e.g., 1.96, 1.74, and 1.65 for the 6, 9, and 12-storey buildings, respectively, occur close to the T_P/T_{1bldng} ratio of 0.3, which covers higher modes. A considerable reduction in

the values of the component force factor, up to 43% in the 9-storey building, considering GMRs with the higher return period, unfolds the prominent effect of inelasticity in the supporting structure. Moreover, the extreme values of the S_P factor in the 10% inelastic buildings vary from 1.23 to 1.59.

Furthermore, an optimized profile of the S_P factor versus T_P/T_{1bldng} has been proposed to assess the overall seismic acceleration demand of NSCs, presuming RC moment-resisting frame building with limited ductility as the reference structure. The proposed profile is suggested based on the obtained results from the elastic buildings in compliance with NBC philosophy. As is illustrated in Figure 10, the proposed profile with a peak value of $FRS/(PGA \times R_P) = 2.0$ would give a reasonable estimation of the seismic demands on NSCs in the vicinity of the higher modes ($S_P = 2.0, 0 < T_P/T_{1bldng} \leq 1.0$). Moreover, the peak value of the suggested profile is extended to T_P/T_{1bldng} equal to 1.0 to account for the resonance around the fundamental period of the primary structure. Thereafter, the suggested profile is decreased for the NSCs with a period larger than the fundamental period of the host structure ($S_P = 0.5,\ T_P/T_{1bldng} \geq 1.75$), demanding a lesser amount of the component force factor.

Also, comparing the maximum proposed value of the S_P factor with the NBC provisions ($S_{P,max} = 4.0$) reveals the need to revise the overly conservative code-based component force factor in NBC provisions.

4.8 Conclusion

This study has extensively investigated the effect of building height and nonlinearity on seismic demands of acceleration sensitive NSCs. Elastic and inelastic time-history analyses were performed on four code compliant RC moment-resisting frame buildings with limited ductility. Synthetic ground motion records compatible with Montreal site Class C uniform hazard spectra corresponding to 475 and 2475 return periods were used in this study.

Considering the nonlinearity of the benchmark structure led to a reduction in PFA/PGA ratio along the building height. This reduction is more pronounced when using ground motions with a higher return period. In the inelastic cases, almost no PGA amplification was observed along the height of the building, except for the rooftop of the buildings, with maximum amplification of 1.32 for the 3-storey building. This is primarily due to the buildings' relatively higher ductility capacity than the ductility assumed in the design phase. Therefore, the linearly increasing acceleration profile along the building height as proposed in NBC 2015 turns out to be overly conservative. On the other hand, the ATC profile that accounts for the building inelasticity is unconservative in the lower half and adequate in the upper half of the buildings. Furthermore, it was observed that the peak component amplification factor occurred either around the fundamental period of the low-rise buildings (3-storey) or in the vicinity of the higher modes for the medium-rise buildings (6 to 12 stories) with maximum values ranging from 4.27 in the elastic range to 3.89 in the 2% inelastic buildings. Therefore, it was deemed that a considerable alleviation in the component amplification factor was attributed to the nonlinearity in the supporting structures. This reduction is more pronounced for the components with periods tuned around the modal periods of the supporting structure. In addition, the effect of nonlinearity is less tangible for components with periods away from the resonating periods of the host structures.

Comparison between the numerical results and the various code provisions has shown that except for EC8, all the provisions have extended the peak component amplification value to $T_P/T_{1bldng} = 1.0$. However, almost all the building codes underestimate the component amplification factor for NSCs tuned to the higher modes of the supporting structure except for ATC, which generally overestimates the acceleration demands on NSCs nearly over the entire component period range. As for the components with a period close to the fundamental period of the supporting structure, the code formulations overestimate the component amplification factor on the lower floors while remarkably underestimating it on the higher floor levels of the 3 and 6-storey buildings.

The overall seismic acceleration demands on NSCs were evaluated by estimating the force factor while assuming a ductile NSC attachment. The maximum values occur in the higher modes tuning region, especially for the medium rise buildings. Also, the inelasticity of the supporting building is highly impactful on decreasing the amplitude of the component force factor. Furthermore, an optimized profile of the S_P factor has been proposed based on the numerical results obtained from the elastic and inelastic buildings, considering the ductility of the components.

CONCLUSION

The main objective of this study is to evaluate the seismic acceleration demands on NSCs in RC moment-resisting frame buildings designed according to NBC 2015. Four benchmark structures with varying heights and limited ductility are selected. Also, a set of 24 synthetic ground motion records with 2% and 10% probabilities of exceedance are selected for each structure and scaled based on the methodology proposed by NBC 2015. Elastic and inelastic time-history analyses are performed, and the results are discussed in the forms of height factor, FRS, the component dynamic amplification factor, and the component force factor.

A moderate reduction in the seismic demands on NSCs is observed using synthetic ground motion records with 10% probability of exceedance per 50 years, owing to the nonlinearity in the reference structure. However, the reduction in the seismic response of NSCs is more remarkable considering ground motions with a 2% probability of exceedance per 50 years. Moreover, due to considering ground motions with PGA range between 0.1g to 0.3g, no significant amplification is observed in the PFA/PGA ratio which is in compliance with the observations of Berto et al. (2020).

The comparison between the numerical results and the various code provisions shows that for the NSCs with period around the higher modes, specifically the second mode of the supporting structure, selected provisions underestimated the component dynamic amplification factor. However, provisions overestimated the A_r factor for the NSCs with period tuned to the fundamental period of the host structure and attached to the lower floor levels.

The overall seismic acceleration demand on NSCs is investigated through estimating the component force factor (S_P) equal to the product of height factor and component amplification factor divided by the component force modification factor. The maximum values occur in the vicinity of the higher modes of the supporting structures. Also, a significant reduction in the values of S_P factor is resulted owing to the nonlinearity of the supporting structure. Finally, an optimized profile of the component force factor with a peak value of 2.0 extended to $T_P/T_{1bldng} = 1.0$ was deemed adequate for evaluating the seismic acceleration demands on

NSCs on the rooftop level of the frame buildings with limited ductility and located in the moderate seismic zones.

RECOMMENDATIONS

Considering the limitations of this research, following attempts are recommended for further investigations:

1. Investigating the effect of considering various lateral force-resisting systems or any combination of them, since this research only investigated the seismic acceleration demands on NSCs in RC-MRF buildings.
2. Considering the effect of ductility levels of the different buildings on seismic acceleration demands on NSCs.
3. Investigating the seismic demands on displacement-sensitive NSCs.
4. Investigating the effect of considering various NSC damping ratio on the component dynamic amplification factor.
5. Evaluating the effect of considering different parameters on the nonlinear behavior of the concrete structures, specifically considering various hysteretic models to implement material nonlinearity to the concrete sections.
6. Investigating the effect of utilizing historical ground motion record to perform dynamic analysis.
7. Investigating the effect of considering Method B proposed in the commentary J of NBC 2015, for the selection and scaling the ground motions.

ANNEX I

DETERMINATION OF MODAL PERIODS AND SEISMIC BASE-SHEAR OF THE FRAME BUILDINGS

The gravity loading considered for both design and analysis procedures includes the dead, live, and mechanical loads for roofs and typical floors. The loads due to partitions, exterior walls, snow load, and self-weight of beams, columns, and slabs are also considered in calculating gravity loads. The gravity loads are listed in Table A-I.1.

Modal analysis has been performed utilizing SAP2000 to obtain the modal periods of the structures, considering a 2D model of the studied buildings in which the 6-storey building model has been illustrated in Figure A-I.1. Concrete material with compressive strength of 35 MPa is considered for all elements. The modulus of elasticity of the concrete material is determined as per CSA A23.3-14, equal to 26622 MPa. Since the self-weight of elements is considered in calculating applied gravity loads, the weight per unit volume of the concrete is neglected in the modeling to avoid duplication in considering the self-weight of the components. Moreover, steel material with a yield stress of 400 MPa and modulus of elasticity of 200 GPa is used for the reinforcing material.

Table A I.1 The gravity loads considered in the design and analysis

Dead (KPa)				Live (KPa)		Snow (KPa)	Self-weight (KN)		
Roof		Floors		Roof	Floors	Roof	Beam	Column	Slab
W-finishing	0.7	W-finishing	0.5	1.0	2.4	2.48	28.26	24.71	29.03
Mechanical	0.5	Mechanical	0.5						
		Partitions	1.0						
		Exterior Walls	1.2						

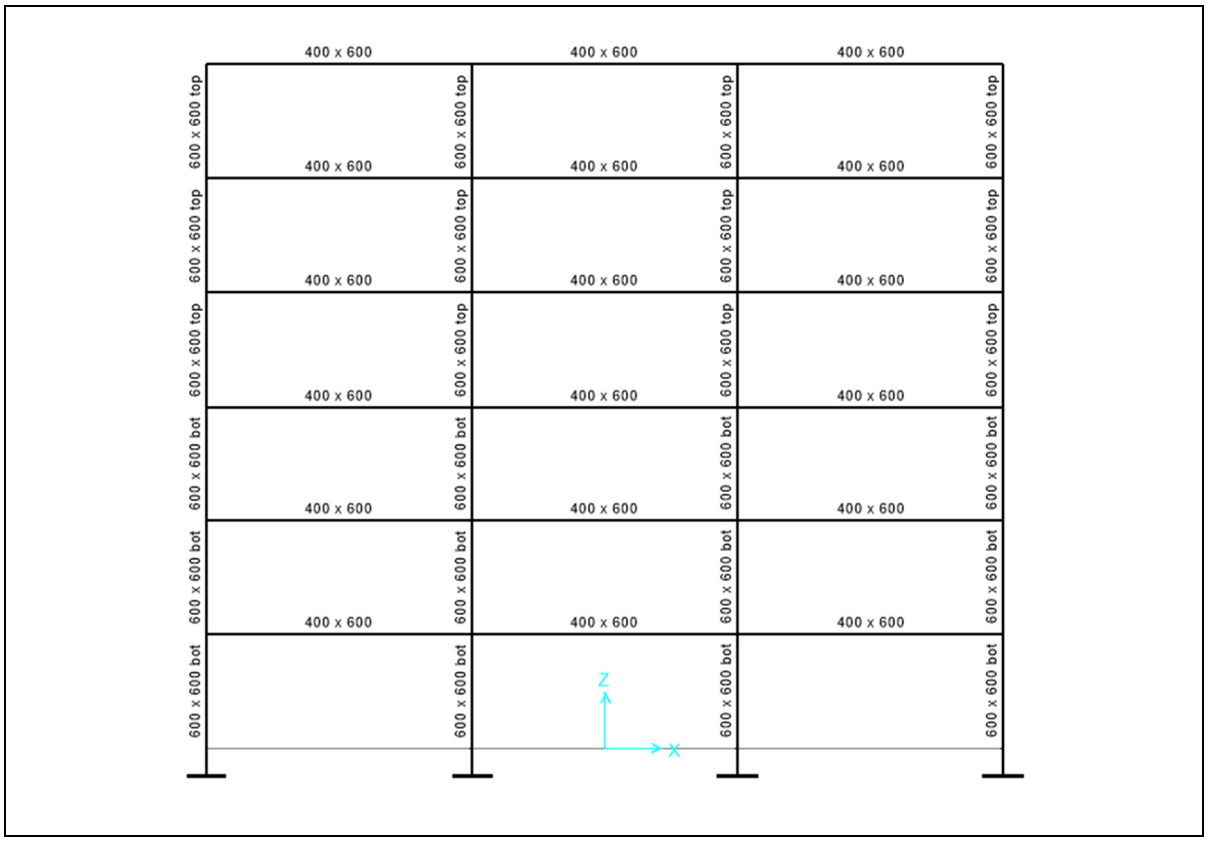

Figure A I.1 2D model of the 6-storey building with sections

The gravity loads, including dead load, live load, and snow load, considered for the analysis of the 6-storey building are calculated and applied to the structure as shown in Figure A-I.2. Columns at the structure's base are considered fixed support, and diaphragm constraints are defined and assigned to each floor level. Diaphragm constraint can link all the joints located within a plane, so they can move together and are rigid against in-plane deformation. Therefore, by assigning diaphragm constraints to each floor, all elements are deforming monotonically.

The seismic weight of the structure is calculated as the dead load plus 25 percent of the snow load and is assigned to the frame at each floor level. The effect of cracking in the concrete sections is also taken into account by considering the reduced gross moment of inertia of the beams and columns.

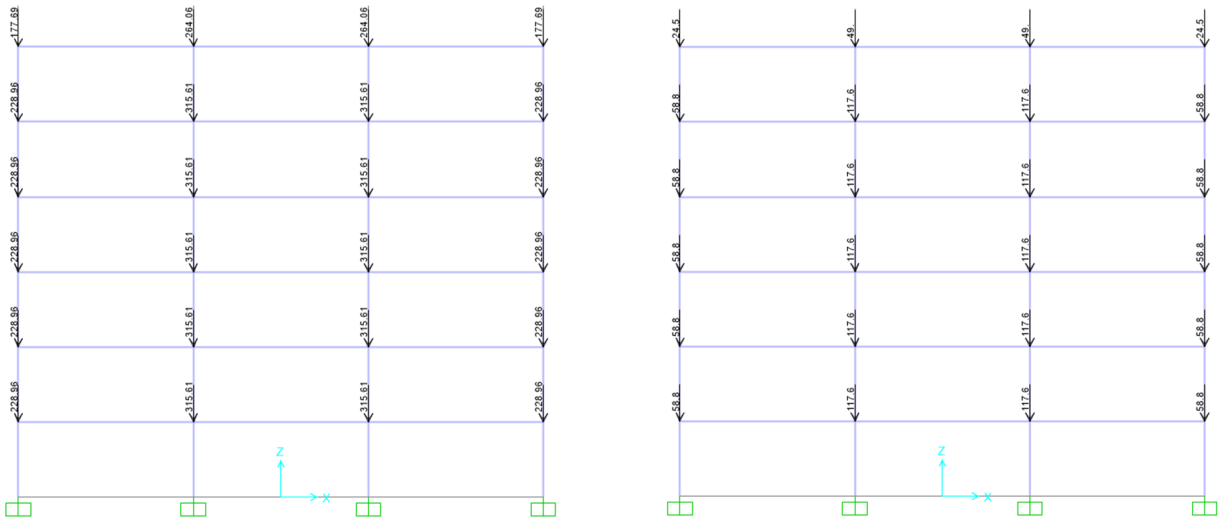

(a)

(b)

(c)

Figure A I.2 Gravity loads considering in the analysis of the building including (a) Dead load, (b) Live load, and (c) Snow load

In modeling, all the sectional properties of the members are assigned to the line objects. However, in reality, the dimensions are cross-sectional finite, such that beams, and columns may have an overlap of the cross-sections at joints. To account for the finite dimensions of members, the end offset along the length of the members is assigned with a rigid zone factor of 0.5, which is recommended for the reinforced concrete structures. The first three fundamental periods of the buildings are obtained and shown in Table A-I.2. Also, the fundamental periods of the 6-storey frame building are shown in Figure A-I.3.

Table A I.2 Fundamental periods of the studied buildings

Number of Storeys	T_1	T_2	T_3
3	0.972	0.264	0.128
6	1.07	0.324	0.165
9	1.364	0.426	0.229
12	1.463	0.469	0.260

Units are in Second

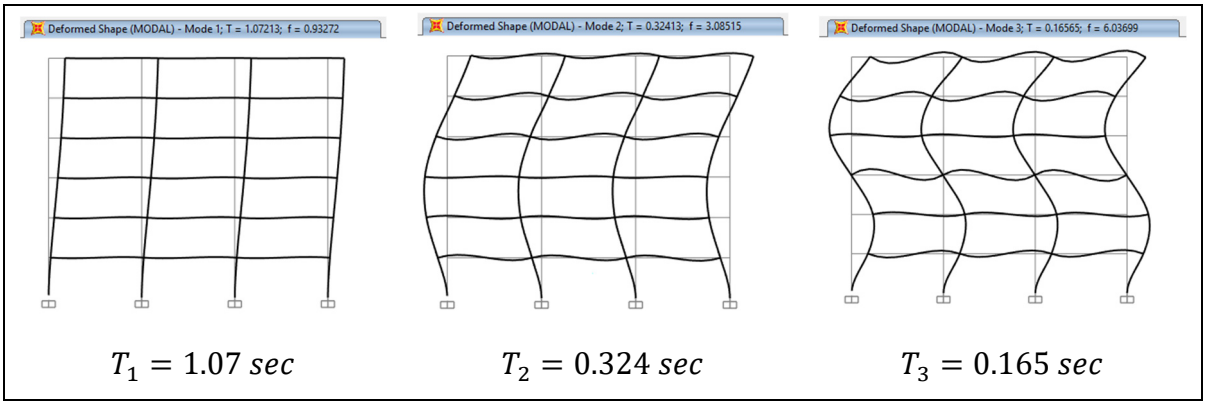

Figure A I.3 Fundamental periods of the first three modes of the 6-storey building

From the modal analysis, the fundamental period of the first mode of the 6-storey building is 1.07 sec. However, the empirical equation of the fundamental period of the reinforced concrete moment-resisting frame is proposed by NBC 2015, as follows:

$$T_n = 0.075(h_n)^{3/4} \quad \text{(A-I.1)}$$

Where: h_n, is the total height of the building. For the studied building T_n is:

$$T_n = 0.075(18)^{3/4} = 0.6554\ sec$$

However, as per NBC 2015, the fundamental period of the building used in seismic design purposes shall not be taken greater than $1.5T_{n,empirical}$. Therefore, the fundamental lateral period of the studied building can be calculated as follows:

$$\begin{cases} 1.5T_{n,empirical} = 1.5 \times 0.655 = 0.983\ \text{sec} \\ T_{a,SAP2000} = 1.07\ \text{sec} \end{cases} \quad \rightarrow \quad T_n = 0.983\ \text{sec}$$

As per NBC 2015, the seismic shear force can be calculated as follows:

$$V = \frac{S(T_a)M_v I_E}{R_d R_O} W \quad \text{(A-I.2)}$$

Where: V is the minimum lateral earthquake load, $S(T_a)$ is the design spectral acceleration value, M_v is to account for the higher modes of the structure, I_E is the importance factor of the structure which is considered 1 for the building with normal importance category, W is the seismic weight of the building, R_d is the ductility related force modification factor and, R_O is the overstrength factor. For the moderately ductile reinforced concrete moment-resisting frame, the ductility and overstrength factors are 2.5 and 1.4, respectively. The studied buildings are located in Montreal, QC, founded on soil class "C". The acceleration-based (F_a) and velocity-based (F_v) site coefficients are 1.0, and the reference peak ground acceleration is 0.3016 g.

The site-specific Uniform hazard spectrum (UHS) with a two percent probability of exceedance in 50 years is adopted from the website of the Natural Resources of Canada. Also,

the design spectral acceleration is calculated considering the site coefficient values (F_T) for different spectral acceleration as per NBC 2015 and by using linear interpolation as is shown in Table A-I.3. The 5% damped spectral acceleration responses at different periods are obtained and plotted within the UHS curve versus the design spectral acceleration shown in Figure A-I.4. The higher mode factor (M_v) can also be calculated as per NBC2015. The spectral accelerations at the periods of 0.2 and 5.0 sec are 0.594 and 0.018, respectively. In this case, the higher mode factor is 1.0 as the calculation is shown in Table A-I.4.

The fundamental period of the structure is equal to 0.983 sec so that by using linear interpolation the corresponding spectral acceleration can be calculated as 0.1535. Also, the seismic weight of the structure is equal to 22031.31 KN. So, by considering the different parameters and using Equation A-I.2, the seismic base shear can be calculated as follows:

$$V = \frac{S(T_a)M_v I_E}{R_d R_O} W \qquad \rightarrow \qquad V = \frac{1535 \times 1.0 \times 1.0}{2.5 \times 1.4} \times 22031.31 = 966.08\ KN$$

Two thresholds for the seismic base shear force are defined in NBC2015, in which the base shear of the structures located on a site other than Class F and having a seismic force-resisting system (SFRS) with an R_d equal to or greater than 1.5, should not exceed the larger of the product of Equation A-I.3 and need not be less than the product of Equation A-I.4:

$$V_{\max} = \text{Max}\begin{cases} \frac{2}{3} S(0.2)\text{I}_\text{E}\, W/(\text{R}_\text{d}\text{R}_\text{O}) \\ S(0.5)\text{I}_\text{E}\, W/(\text{R}_\text{d}\text{R}_\text{O}) \end{cases} \qquad \text{(A-I.3)}$$

$$V_{min} = \frac{S(2.0)M_V I_E}{(R_d R_O)} W \qquad \text{(A-I.4)}$$

$$V_{max} = max\begin{cases} 2492\ KN \\ 1951\ KN \end{cases} \rightarrow\ V_{max} = 2492\ KN \quad , \quad V_{min} = 428\ KN$$

$$V_{min} = 428\ KN\ <\ V = 966\ KN\ <\ V_{max} = 2492\ KN$$

Table A I.3 Calculation of the design spectral acceleration

T (sec)	$S_a(T)$	F(T) for PGA_{ref}			$S_d(T)$
		0.3	0.3016	0.4	
0.00	0.377	1.000	1.000	1.000	0.594
0.05	0.631	1.000	1.000	1.000	0.594
0.10	0.722	1.000	1.000	1.000	0.594
0.20	0.594	1.000	1.000	1.000	0.594
0.30	0.446	1.000	1.000	1.000	0.446
0.50	0.310	1.000	1.000	1.000	0.310
0.983	0.153	1.000	1.000	1.000	0.153
1.00	0.148	1.000	1.000	1.000	0.148
2.00	0.068	1.000	1.000	1.000	0.068
4.00	0.035	1.000	1.000	1.000	0.035
5.00	0.018	1.000	1.000	1.000	0.018
10.00	0.0061	1.000	1.000	1.000	0.0061

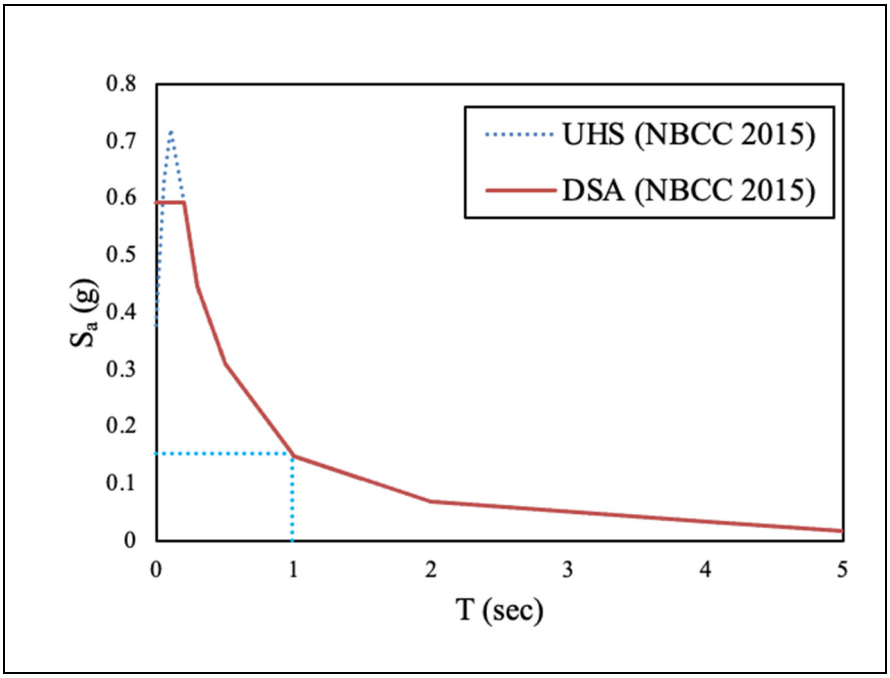

Figure A I.4 Uniform hazard spectrum and the design spectral acceleration curves for Montreal site class C

Table A I.4 Calculation of the higher mode factor

S (0.2) / S (5.0)	M_v		
	$T_a \leq 0.5$	$T_a = 1.0$	$T_a = 2.0$
5	1	1	1
20	1	1	1
33	1	1	1
40	1	1	1
65	1	1	1.03

The seismic base shear for one frame obtained from SAP2000 is 240 KN as is shown in Figure A-I.5, in which by dividing the calculated seismic base shear by the number of frames the same value has resulted.

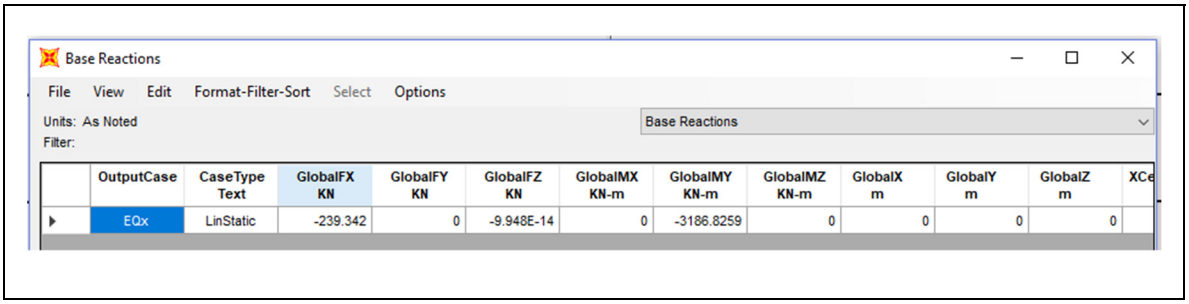

Figure A I.5 The base reaction of the 6-storey building model obtained from SAP2000

For one frame: $$V = \frac{966}{4} = 241\ KN \approx 240\ KN$$

The calculated seismic lateral force is distributed along with the building height and the portion of each floor can be calculated using Equation A-I.5:

$$F_x = (V - F_t)\frac{W_x . h_x}{\sum_{i=1}^{n} W_i h_i} \qquad \text{(A-I.5)}$$

Where, F_t is the concentrated force at the top of the structure, which is calculated using Equation A-I.6, h_x is the floor height relative to the ground, and W_x is the seismic weight of the floor.

$$F_t = \begin{cases} 0.07TV \leq 0.25V, & T > 0.7\ s \\ 0, & T \leq 0.7\ s \end{cases} \quad \text{(A-I.6)}$$

The calculated seismic base shear and seismic lateral loads applied at each floor level are presented in Table A-I.5.

Table A I-5 Distribution of lateral load at each floor level

Floor	h_i (m)	W_i (kN)	$W_i h_i$ (kN.m)	F_i (kN)	V_i (kN)	M_i (kN.m)	T_i (kN.m)
6 (roof)	18	3 572.70	64 308.56	319.49	0.00	5750.80	690.10
5	15	3 652.19	54 782.78	215.53	319.49	3232.94	465.54
4	12	3 652.19	43 826.23	172.42	535.02	2069.08	372.43
3	9	3 652.19	32 869.67	129.32	707.44	1163.86	279.33
2	6	3 652.19	21 913.11	86.21	836.76	517.27	186.22
1	3	3 652.19	10 956.56	43.11	922.97	129.32	93.11
0	0	197.68	0.00	0.00	966.08	0.00	0.00
Total	-	22 031.31	228 656.91	966.08	-	12 863.26	2 086.73

ANNEX II

SELECTION AND SCALING OF GROUND MOTION RECORDS

In this section, the parameters corresponding to the UHS at 2% and 10% probability of exceedance per 50 years in Montreal, for 6, 9, and 12-storey buildings are presented.

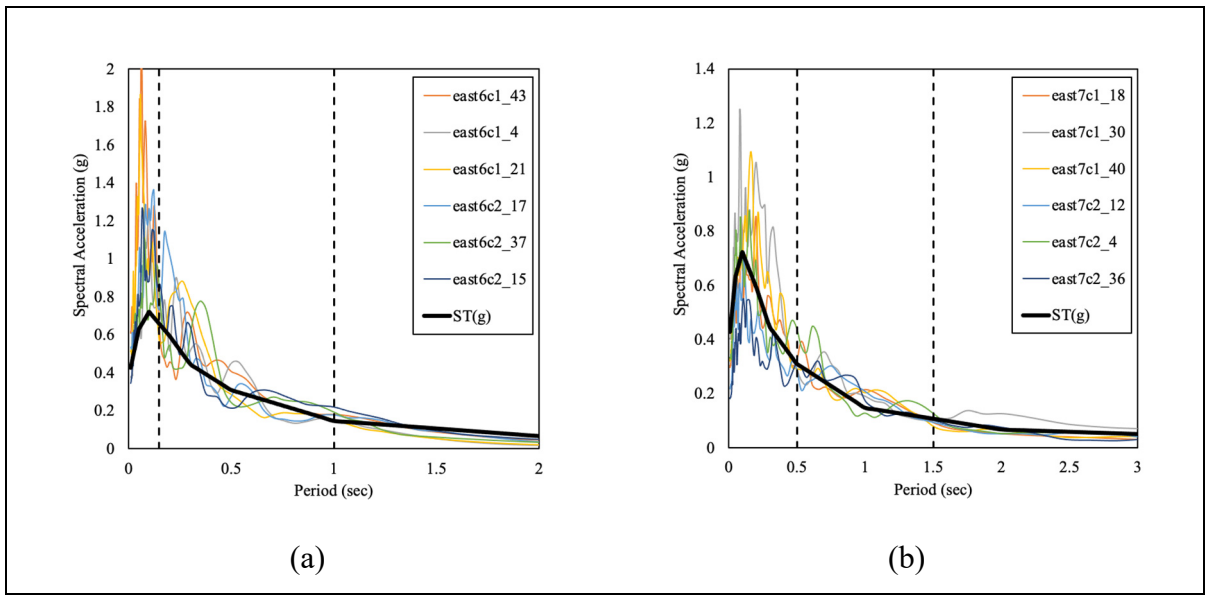

Figure A II.1 Spectral accelerations of the selected GMRs of 6-storey building scaled to the UHS with 2% probability of exceedance per 50 years in Montreal, a) TR1, b) TR2

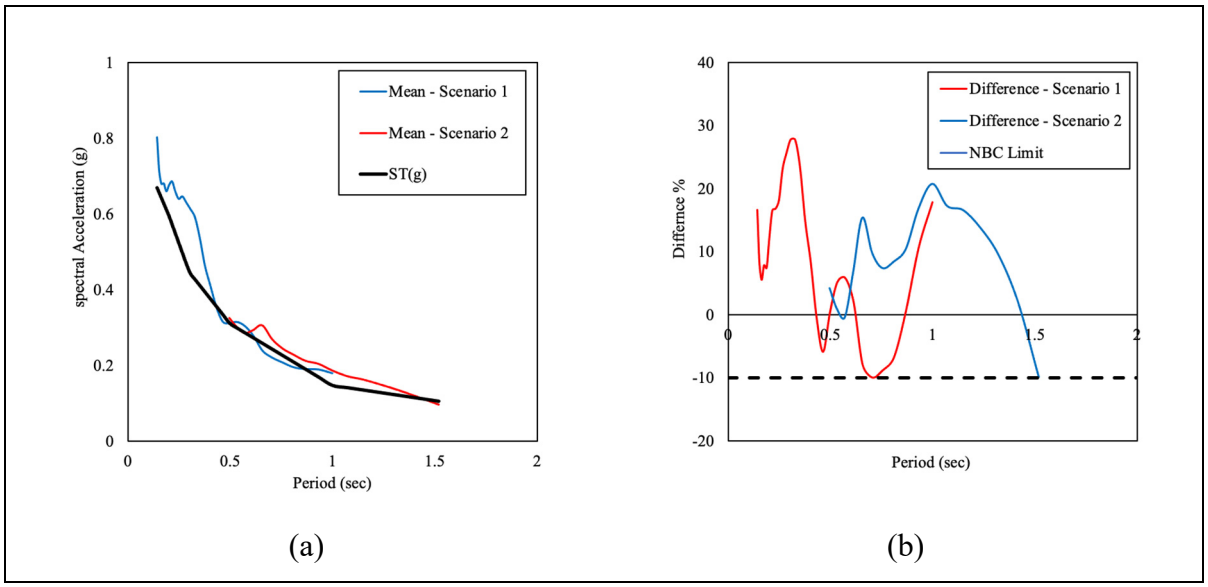

Figure A II.2 a) Mean spectral acceleration for scenarios 1 and 2 for 6-storey frame compared with target spectrum, b) Difference of the mean spectral acceleration with the target spectrum at 2% probability of exceedance per 50 years, within TR1 and TR2

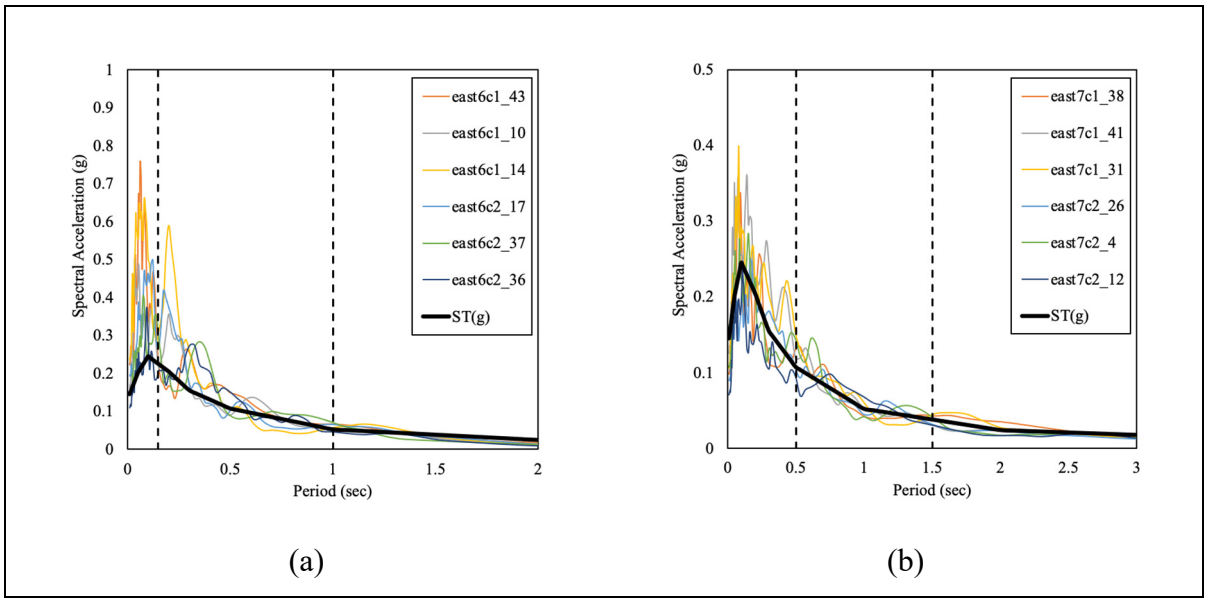

Figure A II.3 Spectral accelerations of the selected ground motion records of 6-storey moderately ductile frame scaled to the UHS with 10% probabiliy of exceedence per 50 years in Montreal, a) TR1, b) TR2

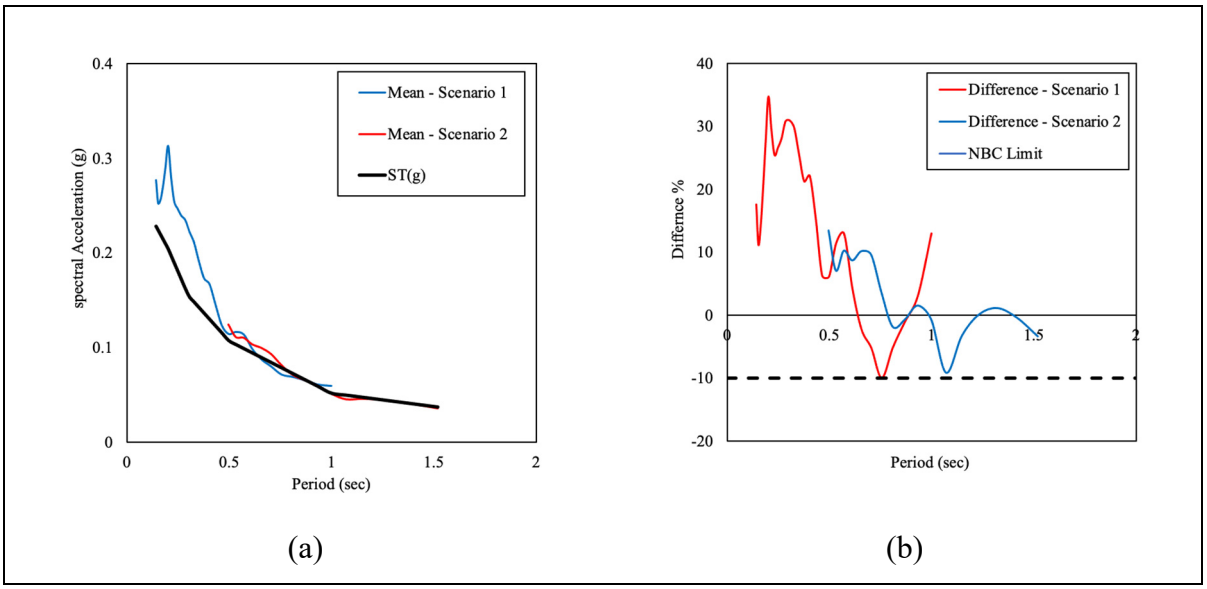

Figure A II.4 a) Mean spectral acceleration for scenarios 1 and 2 for 6-storey frame compared with target spectrum, b) Difference of the mean spectral acceleration with the target spectrum at 10% probablity of exceedence per 50 years, within TR1 and TR2

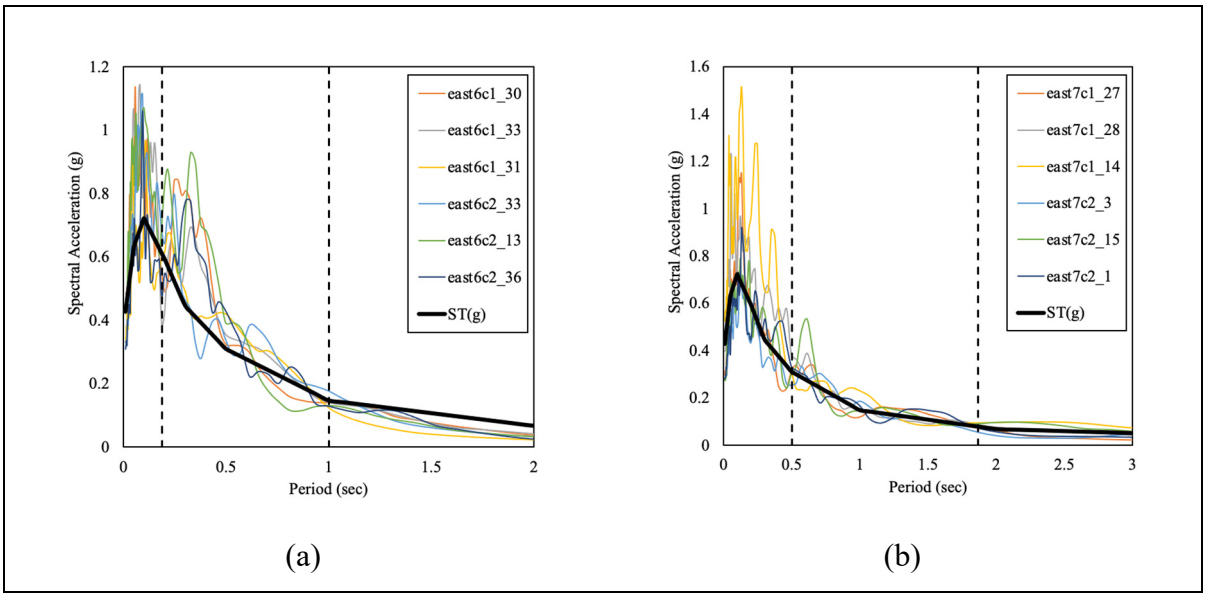

Figure A II.5 Spectral accelerations of the selected ground motion records of 9-storey moderately ductile frame scaled to the UHS with 2% probabiliy of exceedence per 50 years in Montreal, a) TR1, b) TR2

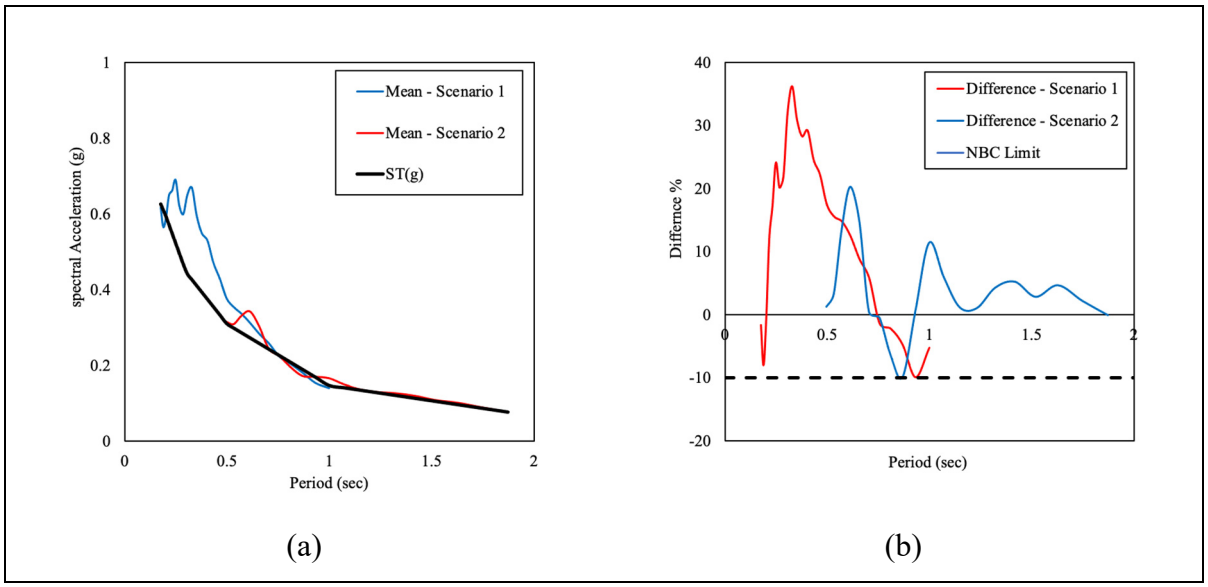

Figure A II.6 a) Mean spectral acceleration for scenarios 1 and 2 for 9-storey frame compared with target spectrum, b) Difference of the mean spectral acceleration with the target spectrum at 2% probablity of exceedence per 50 years, within TR1 and TR2

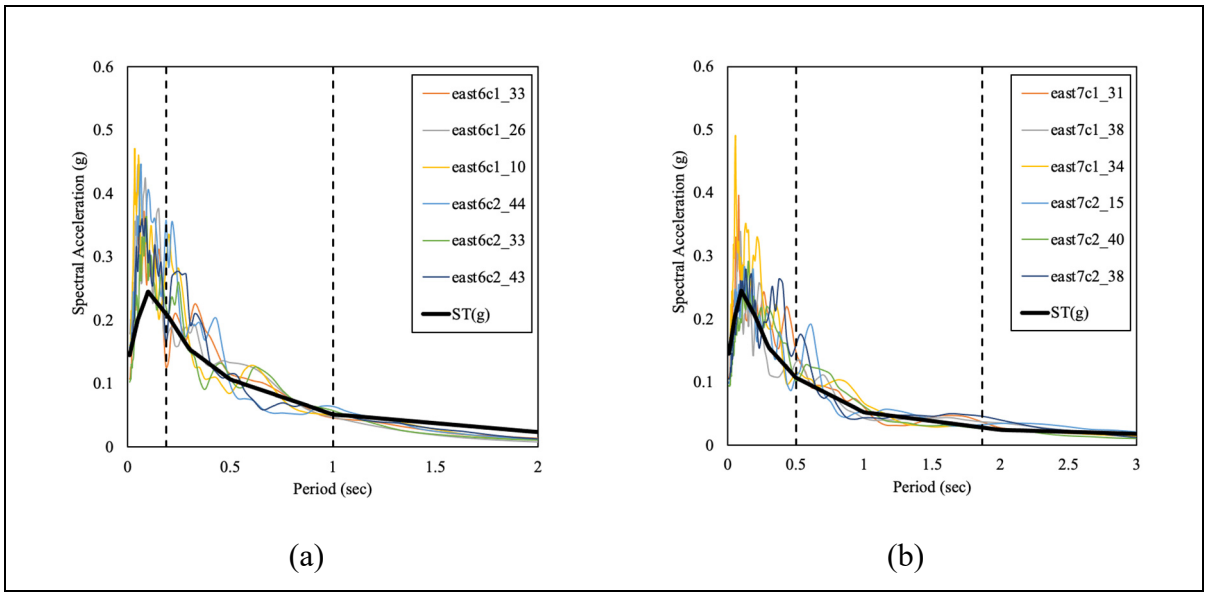

Figure A II.7 Spectral accelerations of the selected ground motion records of 9-storey moderately ductile frame scaled to the UHS with 10% probabiliy of exceedence per 50 years in Montreal, a) TR1, b) TR2

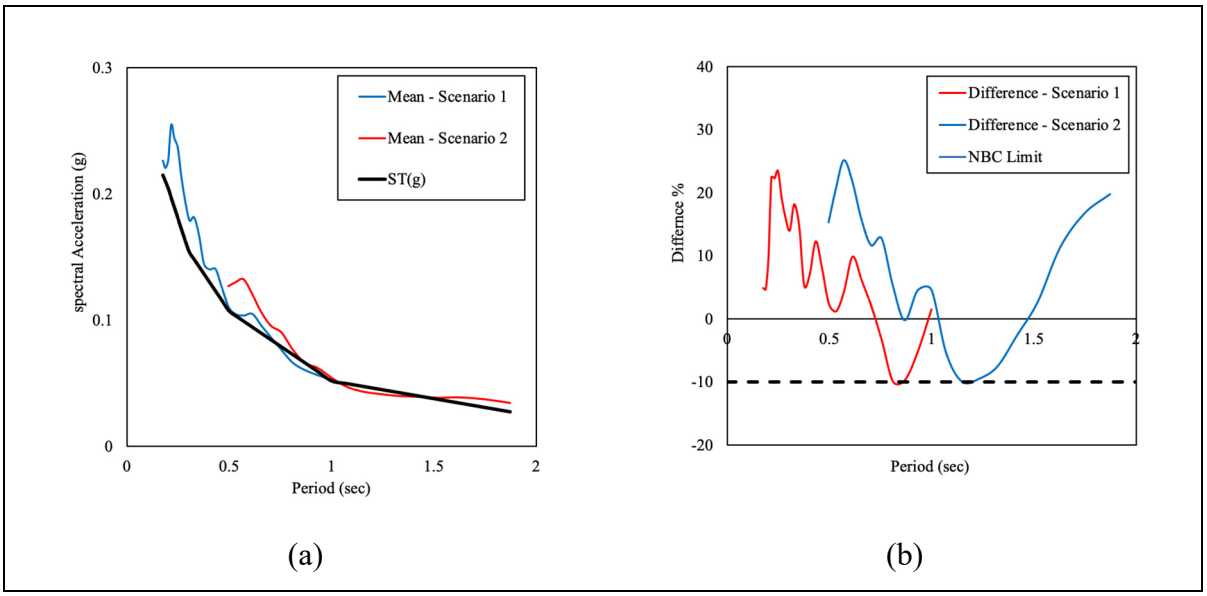

Figure A II.8 a) Mean spectral acceleration for scenarios 1 and 2 for 9-storey frame compared with target spectrum, b) Difference of the mean spectral acceleration with the target spectrum at 10% probablity of exceedence per 50 years, within TR1 and TR2

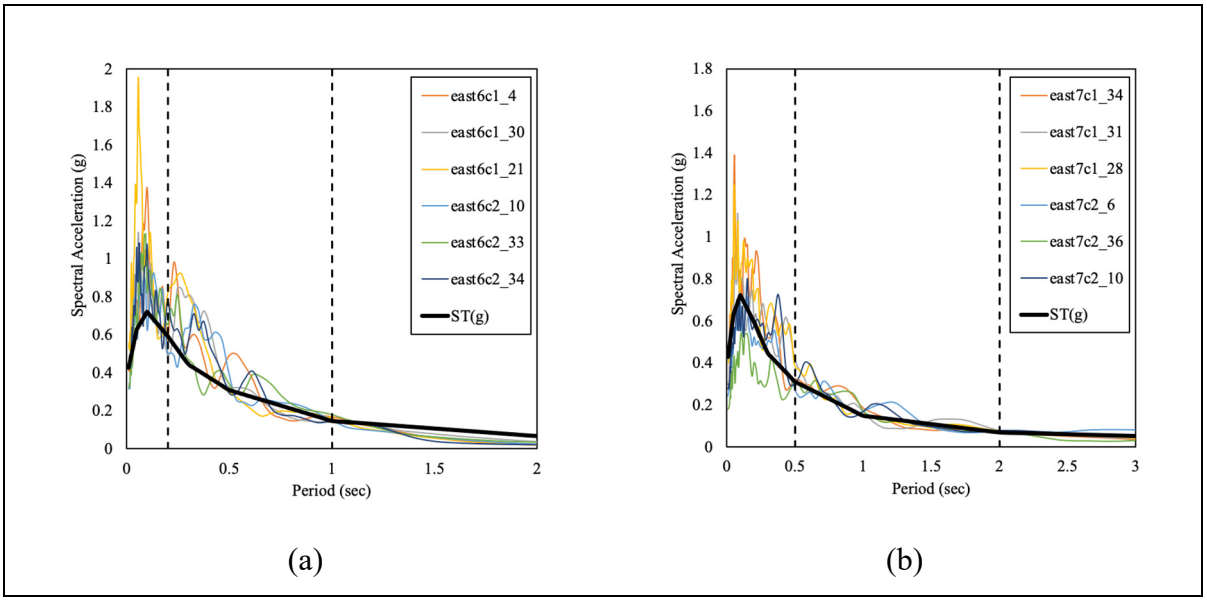

Figure A II.9 Spectral accelerations of the selected ground motion records of 12-storey moderately ductile frame scaled to the UHS with 2% probabiliy of exceedence per 50 years in Montreal, a) TR1, b) TR2

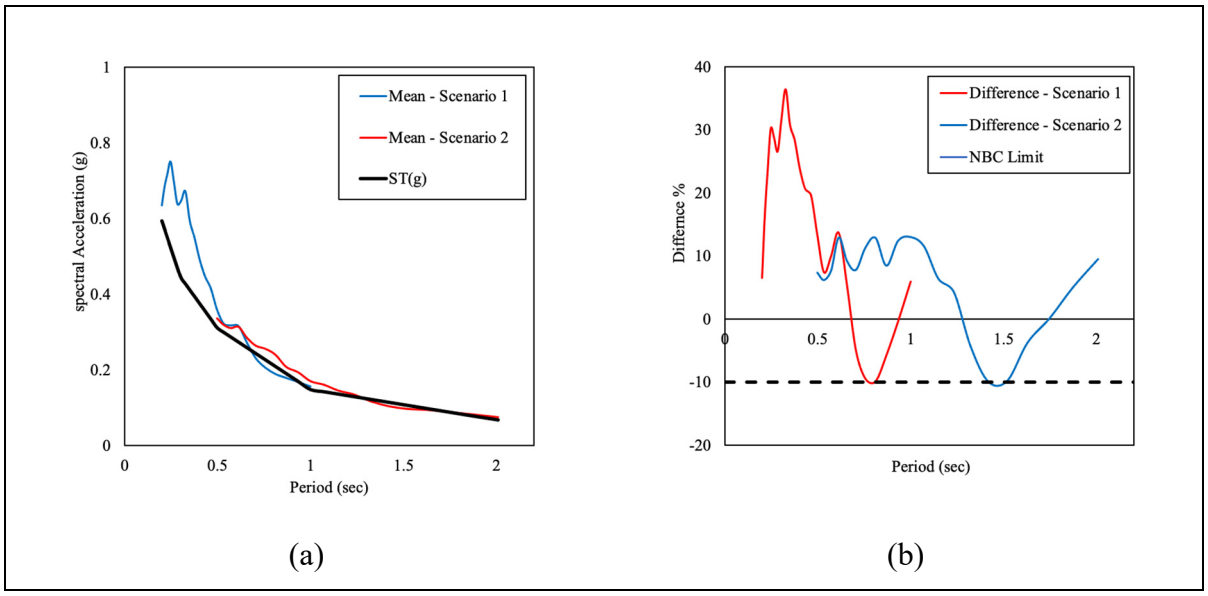

Figure A II.10 a) Mean spectral acceleration for scenarios 1 and 2 for 12-storey frame compared with target spectrum, b) Difference of the mean spectral acceleration with the target spectrum at 2% probability of exceedance per 50 years, within TR1 and TR2

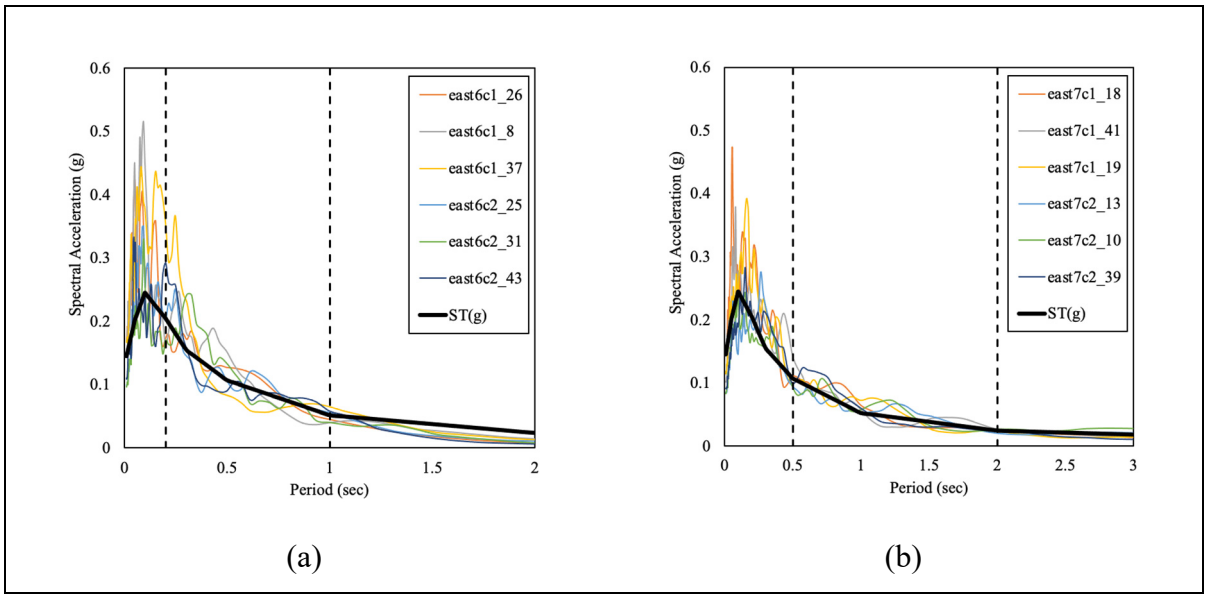

Figure A II.11 Spectral accelerations of the selected ground motion records of 12-storey moderately ductile frame scaled to the UHS with 10% probability of exceedance per 50 years in Montreal, a) TR1, b) TR2

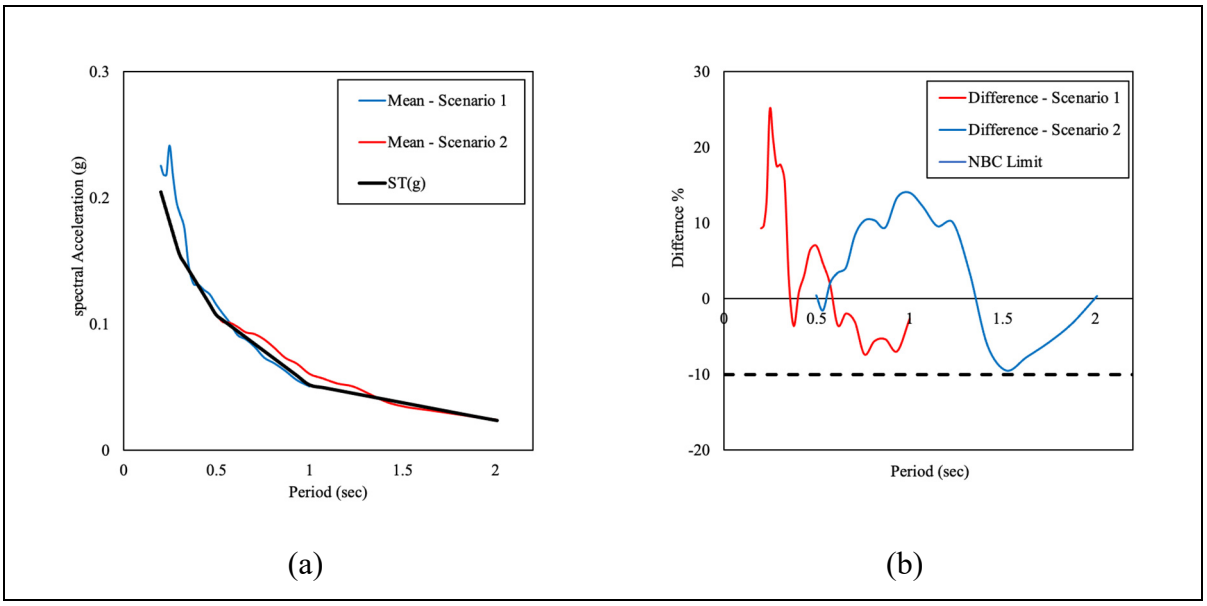

Figure A II.12 a) Mean spectral acceleration for scenarios 1 and 2 for 12-storey frame compared with target spectrum, b) Difference of the mean spectral acceleration with the target spectrum at 10% probability of exceedance per 50 years, within TR1 and TR

ANNEX III

SECTION ANALYSIS USING RESPONSE2000

Following details have been utilized for the sectional analysis (Frame B):

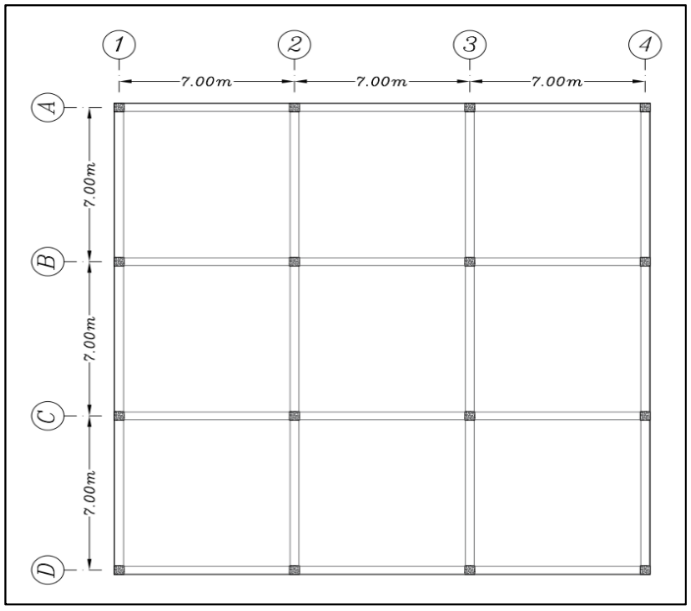

Figure A III.1 Typical plan view of the selected buildings

Table A III-1 Flexural design of the beams – 3-storey frame

Storey	Dim. (mm)	Bars loc.	1-2	2-1	2-3	3-2
3rd	350 × 400	Top Bars	2 15M	2 15M	2 15M	2 15M
		Bottom Bars	3 20M	3 15M	3 15M	3 15M
2nd	350 × 400	Top Bars	3 25M	3 25M	3 25M	3 25M
		Bottom Bars	3 25M	3 25M	3 25M	3 25M
1st	350 × 400	Top Bars	4 25M	4 25M	3 25M	3 25M
		Bottom Bars	4 25M	3 25M	3 25M	3 25M

Table A III-2 Shear design of the beams – 3-storey frame

Beam 1-2											
Beam's end				Middle				Beam's end			
#	Bar	s (mm)	L (mm)	#	Bar	s (mm)	L (mm)	#	Bar	s (mm)	L (mm)
1	10M	75	800	1	10M	200	5000	1	10M	75	800
1	10M	75	800	1	10M	200	5000	1	10M	75	800
1	10M	75	800	1	10M	200	5000	1	10M	75	800
Beam 2-3											
Beam's end				Middle				Beam's end			
#	Bar	s (mm)	L (mm)	#	Bar	s (mm)	L (mm)	#	Bar	s (mm)	L (mm)
1	10M	75	800	1	10M	200	5000	1	10M	75	800
1	10M	75	800	1	10M	200	5000	1	10M	75	800
1	10M	75	800	1	10M	200	5000	1	10M	75	800

Table A III-3 Column’s reinforcement details – 3-storey frame

Storey	Dim. (mm)	B1 - B4		B2 - B3	
3rd	400 × 400	8	20M	8	20M
2nd	400 × 400	8	20M	8	20M
1st	400 × 400	8	20M	8	20M

Table A III-4 Shear design of the columns – 3-storey frame

Storey	Location	Stirrup Type	B1 - B4				B2 - B3			
			Num.	Bar	s (mm)	L (mm)	Num.	Bar	s (mm)	L (mm)
3rd	top end	squared	1	10M	135	450	1	10M	135	450
		lozenge	1	10M			1	10M		
	middle	squared	1	10M	135	1700	1	10M	135	1700
		lozenge	1	10M			1	10M		
	bot. end	squared	1	10M	135	450	1	10M	135	450
		lozenge	1	10M			1	10M		
2nd	top end	squared	1	10M	135	450	1	10M	135	450
		lozenge	1	10M			1	10M		
	middle	squared	1	10M	135	1700	1	10M	135	1700
		lozenge	1	10M			1	10M		
	bot. end	squared	1	10M	135	450	1	10M	135	450
		lozenge	1	10M			1	10M		
1st	top end	squared	1	10M	135	450	1	10M	135	450
		lozenge	1	10M			1	10M		
	middle	squared	1	10M	135	1700	1	10M	135	1700
		lozenge	1	10M			1	10M		
	bot. end	squared	1	10M	135	450	1	10M	135	450
		lozenge	1	10M			1	10M		

Table A III-5 Flexural design of the beams – 6-storey frame

Storey	Dim. (mm)	Bars loc.	1-2	2-1	2-3	3-2
6th	400 × 600	Top Bars	2 15M	2 15M	2 15M	2 15M
		Bottom Bars	3 20M	3 20M	3 20M	3 20M
5th	400 × 600	Top Bars	3 20M	3 20M	3 20M	3 20M
		Bottom Bars	4 20M	4 20M	4 20M	4 20M
4th	400 × 600	Top Bars	4 25M	3 25M	3 25M	3 25M
		Bottom Bars	4 25M	4 25M	4 25M	4 25M
3rd	400 × 600	Top Bars	5 25M	8 20M	5 25M	5 25M
		Bottom Bars	5 25M	5 25M	5 25M	5 25M
2nd	400 × 600	Top Bars	6 25M	6 25M	6 25M	6 25M
		Bottom Bars	6 25M	6 25M	6 25M	6 25M
1st	400 × 600	Top Bars	5 25M	5 25M	5 25M	5 25M
		Bottom Bars	5 25M	5 25M	5 25M	5 25M

Table A III-6 Shear design of the beams – 6-storey frame

Beam 1-2											
Beam's end				Middle				Beam's end			
#	Bar	s (mm)	L (mm)	#	Bar	s (mm)	L (mm)	#	Bar	s (mm)	L (mm)
1	10M	125	1200	1	10M	250	4000	1	10M	125	1200
1	10M	125	1200	1	10M	250	4000	1	10M	125	1200
1	10M	125	1200	1	10M	250	4000	1	10M	125	1200
1	10M	125	1200	1	10M	250	4000	1	10M	125	1200
1	10M	125	1200	1	10M	250	4000	1	10M	125	1200
1	10M	125	1200	1	10M	250	4000	1	10M	125	1200
Beam 2-3											
Beam's end				Middle				Beam's end			
#	Bar	s (mm)	L (mm)	#	Bar	s (mm)	L (mm)	#	Bar	s (mm)	L (mm)
1	10M	125	1200	1	10M	250	4000	1	10M	125	1200
1	10M	125	1200	1	10M	250	4000	1	10M	125	1200
1	10M	125	1200	1	10M	250	4000	1	10M	125	1200
1	10M	125	1200	1	10M	250	4000	1	10M	125	1200
1	10M	125	1200	1	10M	250	4000	1	10M	125	1200
1	10M	125	1200	1	10M	250	4000	1	10M	125	1200

Table A III-7 Column's reinforcement details – 6-storey frame

Storey	Dim. (mm)	B1 - B4		B2 - B3	
6th	600 × 600	16	20M	16	20M
5th	600 × 600	16	20M	16	20M
4th	600 × 600	16	20M	16	25M
3rd	600 × 600	16	20M	16	25M
2nd	600 × 600	16	20M	16	25M
1st	600 × 600	16	20M	16	25M

Table A III-8 Shear design of the columns – 6-storey frame

Storey	Location	Stirrup Type	B1 - B4				B2 - B3			
			Num.	Bar	s (mm)	L (mm)	Num.	Bar	s (mm)	L (mm)
6th	top end	squared	1	10M	100	600	1	10M	100	600
		lozenge	1	10M			1	10M		
	middle	squared	1	10M	100	1200	1	10M	100	1200
		lozenge	1	10M			1	10M		
	bot. end	squared	1	10M	100	600	1	10M	100	600
		lozenge	1	10M			1	10M		
5th	top end	squared	1	10M	100	600	1	10M	100	600
		lozenge	1	10M			1	10M		
	middle	squared	1	10M	100	1200	1	10M	100	1200
		lozenge	1	10M			1	10M		
	bot. end	squared	1	10M	100	600	1	10M	100	600
		lozenge	1	10M			1	10M		
4th	top end	squared	1	10M	100	600	1	10M	100	600
		lozenge	1	10M			1	10M		
	middle	squared	1	10M	100	1200	1	10M	100	1200
		lozenge	1	10M			1	10M		
	bot. end	squared	1	10M	100	600	1	10M	100	600
		lozenge	1	10M			1	10M		
3rd	top end	squared	1	10M	100	600	1	10M	100	600
		lozenge	1	10M			1	10M		
	middle	squared	1	10M	100	1200	1	10M	100	1200
		lozenge	1	10M			1	10M		
	bot. end	squared	1	10M	100	600	1	10M	100	600
		lozenge	1	10M			1	10M		
2nd	top end	squared	1	10M	100	600	1	10M	100	600
		lozenge	1	10M			1	10M		
	middle	squared	1	10M	100	1200	1	10M	100	1200
		lozenge	1	10M			1	10M		
	bot. end	squared	1	10M	100	600	1	10M	100	600
		lozenge	1	10M			1	10M		
1st	top end	squared	1	10M	100	600	1	10M	100	600
		lozenge	1	10M			1	10M		
	middle	squared	1	10M	100	1200	1	10M	100	1200
		lozenge	1	10M			1	10M		
	bot. end	squared	1	10M	100	600	1	10M	100	600
		lozenge	1	10M			1	10M		

Table A III-9 Flexural design of the beams – 9-storey frame

Storey	Dim. (mm)	Bars loc.	1-2		2-1		2-3		3-2	
9th	500 × 650	Top Bars	4	20M	4	20M	4	20M	4	20M
		Bottom Bars	4	20M	4	20M	4	20M	4	20M
8th	500 × 650	Top Bars	4	20M	4	20M	4	20M	4	20M
		Bottom Bars	4	20M	4	20M	4	20M	4	20M
7th	500 × 650	Top Bars	4	20M	4	20M	4	20M	4	20M
		Bottom Bars	6	20M	6	20M	6	20M	6	20M
6th	500 × 650	Top Bars	5	20M	5	20M	5	20M	5	20M
		Bottom Bars	5	25M	5	25M	5	25M	5	25M
5th	500 × 650	Top Bars	5	25M	5	25M	5	25M	5	25M
		Bottom Bars	7	25M	7	25M	7	25M	7	25M
4th	500 × 650	Top Bars	5	30M	5	30M	5	30M	5	30M
		Bottom Bars	6	30M	6	30M	6	30M	6	30M
3rd	500 × 650	Top Bars	6	30M	6	30M	6	30M	6	30M
		Bottom Bars	7	30M	7	30M	7	30M	7	30M
2nd	500 × 650	Top Bars	7	30M	6	30M	6	30M	6	30M
		Bottom Bars	8	30M	8	30M	7	30M	7	30M
1st	500 × 650	Top Bars	6	25M	6	25M	6	25M	6	25M
		Bottom Bars	6	30M	6	30M	6	30M	6	30M

Table A III-10 Shear design of the beams – 9-storey frame (a)

Beam 1-2											
Beam's end				Middle				Beam's end			
#	Bar	s (mm)	L (mm)	#	Bar	s (mm)	L (mm)	#	Bar	s (mm)	L (mm)
1	10M	145	1300	1	10M	350	3700	1	10M	145	1300
1	10M	145	1300	1	10M	350	3700	1	10M	145	1300
1	10M	145	1300	1	10M	350	3700	1	10M	145	1300
1	10M	145	1300	1	10M	350	3700	1	10M	145	1300
1	10M	145	1300	1	10M	350	3700	1	10M	145	1300
1	10M	145	1300	1	10M	350	3700	1	10M	145	1300
2	10M	145	1300	2	10M	300	3700	2	10M	145	1300
2	10M	145	1300	2	10M	350	3700	2	10M	145	1300
2	10M	145	1300	2	10M	350	3700	2	10M	145	1300

Table A III-11 Shear design of the beams – 9-storey frame (b)

Beam 2-3											
Beam's end				Middle				Beam's end			
#	Bar	s (mm)	L (mm)	#	Bar	s (mm)	L (mm)	#	Bar	s (mm)	L (mm)
1	10M	350	1300	1	10M	145	3700	1	10M	145	1300
1	10M	350	1300	1	10M	145	3700	1	10M	145	1300
1	10M	350	1300	1	10M	145	3700	1	10M	145	1300
1	10M	350	1300	1	10M	145	3700	1	10M	145	1300
1	10M	350	1300	1	10M	145	3700	1	10M	145	1300
1	10M	350	1300	1	10M	145	3700	1	10M	145	1300
2	10M	300	1300	2	10M	145	3700	2	10M	145	1300
2	10M	350	1300	2	10M	145	3700	2	10M	145	1300
2	10M	350	1300	2	10M	145	3700	2	10M	145	1300

Table A III-12 Column's reinforcement details – 9-storey frame

Storey	Dim. (mm)	B1 - B4		B2 - B3	
9th	700 × 700	20	20M	20	20M
8th	700 × 700	20	20M	20	20M
7th	700 × 700	20	20M	20	20M
6th	700 × 700	20	20M	20	20M
5th	700 × 700	20	20M	20	25M
4th	700 × 700	20	20M	20	25M
3rd	700 × 700	20	20M	20	25M
2nd	700 × 700	20	20M	20	25M
1st	700 × 700	20	20M	20	25M

Table A III-13 Shear design of the columns – 9-storey frame

Storey	Location	Stirrup Type	B1 - B4				B2 - B3			
			Num.	Bar	s (mm)	L (mm)	Num.	Bar	s (mm)	L (mm)
9th	top end	squared	3	15M	150	700	3	15M	150	700
		lozenge	0	15M			0	15M		
	middle	squared	3	15M	150	950	3	15M	150	950
		lozenge	0	15M			0	15M		
	bot. end	squared	3	15M	150	700	3	15M	150	700
		lozenge	0	15M			0	15M		
8th	top end	squared	3	15M	150	700	3	15M	150	700
		lozenge	0	15M			0	15M		
	middle	squared	3	15M	150	950	3	15M	150	950
		lozenge	0	15M			0	15M		
	bot. end	squared	3	15M	150	700	3	15M	150	700
		lozenge	0	15M			0	15M		
7th	top end	squared	3	15M	150	700	3	15M	150	700
		lozenge	0	15M			0	15M		
	middle	squared	3	15M	150	950	3	15M	150	950
		lozenge	0	15M			0	15M		
	bot. end	squared	3	15M	150	700	3	15M	150	700
		lozenge	0	15M			0	15M		
6th	top end	squared	3	15M	150	700	3	15M	150	700
		lozenge	0	15M			0	15M		
	middle	squared	3	15M	150	950	3	15M	150	950
		lozenge	0	15M			0	15M		
	bot. end	squared	3	15M	150	700	3	15M	150	700
		lozenge	0	15M			0	15M		

Table A III-14 Shear design of the columns – 9-storey frame - Continue

Storey	Location	Stirrup Type	B1 - B4				B2 - B3			
			Num.	Bar	s (mm)	L (mm)	Num.	Bar	s (mm)	L (mm)
5th	top end	squared	3	15M	150	700	3	15M	150	700
		lozenge	0	15M			0	15M		
	middle	squared	3	15M	150	950	3	15M	150	950
		lozenge	0	15M			0	15M		
	bot. end	squared	3	15M	150	700	3	15M	150	700
		lozenge	0	15M			0	15M		
4th	top end	squared	3	15M	150	700	3	15M	150	700
		lozenge	0	15M			0	15M		
	middle	squared	3	15M	150	950	3	15M	150	950
		lozenge	0	15M			0	15M		
	bot. end	squared	3	15M	150	700	3	15M	150	700
		lozenge	0	15M			0	15M		
3rd	top end	squared	3	15M	150	700	3	15M	150	700
		lozenge	0	15M			0	15M		
	middle	squared	3	15M	150	950	3	15M	150	950
		lozenge	0	15M			0	15M		
	bot. end	squared	3	15M	150	700	3	15M	150	700
		lozenge	0	15M			0	15M		
2nd	top end	squared	3	15M	150	700	3	15M	150	700
		lozenge	0	15M			0	15M		
	middle	squared	3	15M	150	950	3	15M	150	950
		lozenge	0	15M			0	15M		
	bot. end	squared	3	15M	150	700	3	15M	150	700
		lozenge	0	15M			0	15M		
1st	top end	squared	3	15M	150	700	3	15M	150	700
		lozenge	0	15M			0	15M		
	middle	squared	3	15M	150	950	3	15M	150	950
		lozenge	0	15M			0	15M		
	bot. end	squared	3	15M	150	700	3	15M	150	700
		lozenge	0	15M			0	15M		

Table A III-15 Flexural design of the beams – 12-storey frame

Storey	Dim. (mm)	Bars loc.	1-2		2-1		2-3		3-2	
12th	600 × 750	Top Bars	7	20M	7	20M	7	20M	7	20M
		Bottom Bars	5	20M	5	20M	5	20M	5	20M
11th	600 × 750	Top Bars	7	20M	7	20M	7	20M	7	20M
		Bottom Bars	5	20M	5	20M	5	20M	5	20M
10th	600 × 750	Top Bars	7	20M	7	20M	7	20M	7	20M
		Bottom Bars	5	20M	6	20M	6	20M	6	20M
9th	600 × 750	Top Bars	7	20M	7	20M	7	20M	7	20M
		Bottom Bars	5	25M	5	25M	5	25M	5	25M
8th	600 × 750	Top Bars	5	25M	4	25M	5	25M	5	25M
		Bottom Bars	6	25M	6	25M	7	25M	7	25M
7th	600 × 750	Top Bars	6	25M	6	25M	6	25M	6	25M
		Bottom Bars	8	25M	8	25M	8	25M	8	25M
6th	600 × 750	Top Bars	6	30M	5	30M	6	30M	6	30M
		Bottom Bars	7	30M	7	30M	7	30M	7	30M
5th	600 × 750	Top Bars	7	30M	7	30M	7	30M	7	30M
		Bottom Bars	8	30M	8	30M	8	30M	8	30M
4th	600 × 750	Top Bars	8	30M	8	30M	8	30M	8	30M
		Bottom Bars	9	30M	9	30M	9	30M	9	30M
3rd	600 × 750	Top Bars	9	30M	9	30M	9	30M	9	30M
		Bottom Bars	10	30M	10	30M	10	30M	10	30M
2nd	600 × 750	Top Bars	9	30M	9	30M	9	30M	9	30M
		Bottom Bars	10	30M	10	30M	10	30M	10	30M
1st	600 × 750	Top Bars	7	30M	6	30M	6	30M	6	30M
		Bottom Bars	8	30M	8	30M	8	30M	8	30M

Table A III-16 Shear design of the beams – 12-storey frame (a)

Beam 1-2											
Beam's end				Middle				Beam's end			
#	Bar	s (mm)	L (mm)	#	Bar	s (mm)	L (mm)	#	Bar	s (mm)	L (mm)
1	10M	150	1500	1	10M	300	3200	1	10M	150	1500
1	10M	150	1500	1	10M	300	3200	1	10M	150	1500
1	10M	150	1500	1	10M	300	3200	1	10M	150	1500
1	10M	150	1500	1	10M	300	3200	1	10M	150	1500
1	10M	150	1500	1	10M	300	3200	1	10M	150	1500
1	10M	150	1500	1	10M	300	3200	1	10M	150	1500
1	10M	150	1500	1	10M	300	3200	1	10M	150	1500
2	10M	150	1500	2	10M	300	3200	2	10M	150	1500
2	10M	150	1500	2	10M	300	3200	2	10M	150	1500
2	10M	150	1500	2	10M	300	3200	2	10M	150	1500
2	10M	150	1500	2	10M	300	3200	2	10M	150	1500
2	10M	150	1500	2	10M	300	3200	2	10M	150	1500

Table A III-17 Shear design of the beams – 12-storey frame (b)

Beam 2-3											
Beam's end				Middle				Beam's end			
#	Bar	s (mm)	L (mm)	#	Bar	s (mm)	L (mm)	#	Bar	s (mm)	L (mm)
1	10M	300	1500	1	10M	150	3200	1	10M	150	1500
1	10M	300	1500	1	10M	150	3200	1	10M	150	1500
1	10M	300	1500	1	10M	150	3200	1	10M	150	1500
1	10M	300	1500	1	10M	150	3200	1	10M	150	1500
1	10M	300	1500	1	10M	150	3200	1	10M	150	1500
1	10M	300	1500	1	10M	150	3200	1	10M	150	1500
1	10M	300	1500	1	10M	150	3200	1	10M	150	1500
2	10M	300	1500	2	10M	150	3200	2	10M	150	1500
2	10M	300	1500	2	10M	150	3200	2	10M	150	1500
2	10M	300	1500	2	10M	150	3200	2	10M	150	1500
2	10M	300	1500	2	10M	150	3200	2	10M	150	1500
2	10M	300	1500	2	10M	150	3200	2	10M	150	1500

Table A III-18 Column's reinforcement details – 12-storey frame

Storey	Dim. (mm)	B1 - B4		B2 - B3	
12th	800 × 800	24	20M	24	20M
11th	800 × 800	24	20M	24	20M
10th	800 × 800	24	20M	24	20M
9th	800 × 800	24	20M	24	20M
8th	800 × 800	24	20M	24	25M
7th	800 × 800	24	20M	24	25M
6th	800 × 800	24	20M	24	25M
5th	800 × 800	24	20M	24	25M
4th	800 × 800	24	20M	24	25M
3rd	800 × 800	24	20M	24	25M
2nd	800 × 800	24	20M	24	25M
1st	800 × 800	24	20M	24	25M

Table A III-19 Shear design of the columns – 12-storey frame

Storey	Location	Stirrup Type	B1 - C1 - B4 - C4				B2 - C2 - B3 - C3			
			Num.	Bar	s (mm)	L (mm)	Num.	Bar	s (mm)	L (mm)
12th	top end	squared	1	15M	125	800	1	15M	125	800
		lozenge	1	15M			1	15M		
	middle	squared	1	15M	125	650	1	15M	125	650
		lozenge	1	15M			1	15M		
	bot. end	squared	1	15M	125	800	1	15M	125	800
		lozenge	1	15M			1	15M		
11th	top end	squared	1	15M	125	800	1	15M	125	800
		lozenge	1	15M			1	15M		
	middle	squared	1	15M	125	650	1	15M	125	650
		lozenge	1	15M			1	15M		
	bot. end	squared	1	15M	125	800	1	15M	125	800
		lozenge	1	15M			1	15M		
10th	top end	squared	1	15M	125	800	1	15M	125	800
		lozenge	1	15M			1	15M		
	middle	squared	1	15M	125	650	1	15M	125	650
		lozenge	1	15M			1	15M		
	bot. end	squared	1	15M	125	800	1	15M	125	800
		lozenge	1	15M			1	15M		
9th	top end	squared	1	15M	125	800	1	15M	125	800
		lozenge	1	15M			1	15M		
	middle	squared	1	15M	125	650	1	15M	125	650
		lozenge	1	15M			1	15M		
	bot. end	squared	1	15M	125	800	1	15M	125	800
		lozenge	1	15M			1	15M		
8th	top end	squared	1	15M	125	800	1	15M	125	800
		lozenge	1	15M			1	15M		
	middle	squared	1	15M	125	650	1	15M	125	650
		lozenge	1	15M			1	15M		
	bot. end	squared	1	15M	125	800	1	15M	125	800
		lozenge	1	15M			1	15M		
7th	top end	squared	1	15M	125	800	1	15M	125	800
		lozenge	1	15M			1	15M		
	middle	squared	1	15M	125	650	1	15M	125	650
		lozenge	1	15M			1	15M		
	bot. end	squared	1	15M	125	800	1	15M	125	800
		lozenge	1	15M			1	15M		

Table A III-20 Shear design of the columns – 12-storey frame - Continue

Storey	Location	Stirrup Type	B1 - C1 - B4 - C4				B2 - C2 - B3 - C3			
			Num.	Bar	s (mm)	L (mm)	Num.	Bar	s (mm)	L (mm)
6th	top end	squared	1	15M	125	800	1	15M	125	800
		lozenge	1	15M			1	15M		
	middle	squared	1	15M	125	650	1	15M	125	650
		lozenge	1	15M			1	15M		
	bot. end	squared	1	15M	125	800	1	15M	125	800
		lozenge	1	15M			1	15M		
5th	top end	squared	1	15M	125	800	1	15M	125	800
		lozenge	1	15M			1	15M		
	middle	squared	1	15M	125	650	1	15M	125	650
		lozenge	1	15M			1	15M		
	bot. end	squared	1	15M	125	800	1	15M	125	800
		lozenge	1	15M			1	15M		
4th	top end	squared	1	15M	125	800	1	15M	100	800
		lozenge	1	15M			1	15M		
	middle	squared	1	15M	125	650	1	15M	125	650
		lozenge	1	15M			1	15M		
	bot. end	squared	1	15M	125	800	1	15M	100	800
		lozenge	1	15M			1	15M		
3rd	top end	squared	1	15M	125	800	1	15M	100	800
		lozenge	1	15M			1	15M		
	middle	squared	1	15M	125	650	1	15M	125	650
		lozenge	1	15M			1	15M		
	bot. end	squared	1	15M	125	800	1	15M	100	800
		lozenge	1	15M			1	15M		
2nd	top end	squared	1	15M	125	800	1	15M	100	800
		lozenge	1	15M			1	15M		
	middle	squared	1	15M	125	650	1	15M	125	650
		lozenge	1	15M			1	15M		
	bot. end	squared	1	15M	125	800	1	15M	100	800
		lozenge	1	15M			1	15M		
1st	top end	squared	1	15M	125	800	1	15M	125	800
		lozenge	1	15M			1	15M		
	middle	squared	1	15M	125	650	1	15M	125	650
		lozenge	1	15M			1	15M		
	bot. end	squared	1	15M	125	800	1	15M	125	800
		lozenge	1	15M			1	15M		

One example of determining the moment capacity of 400 mm x 600 mm concrete beam using Response2000.

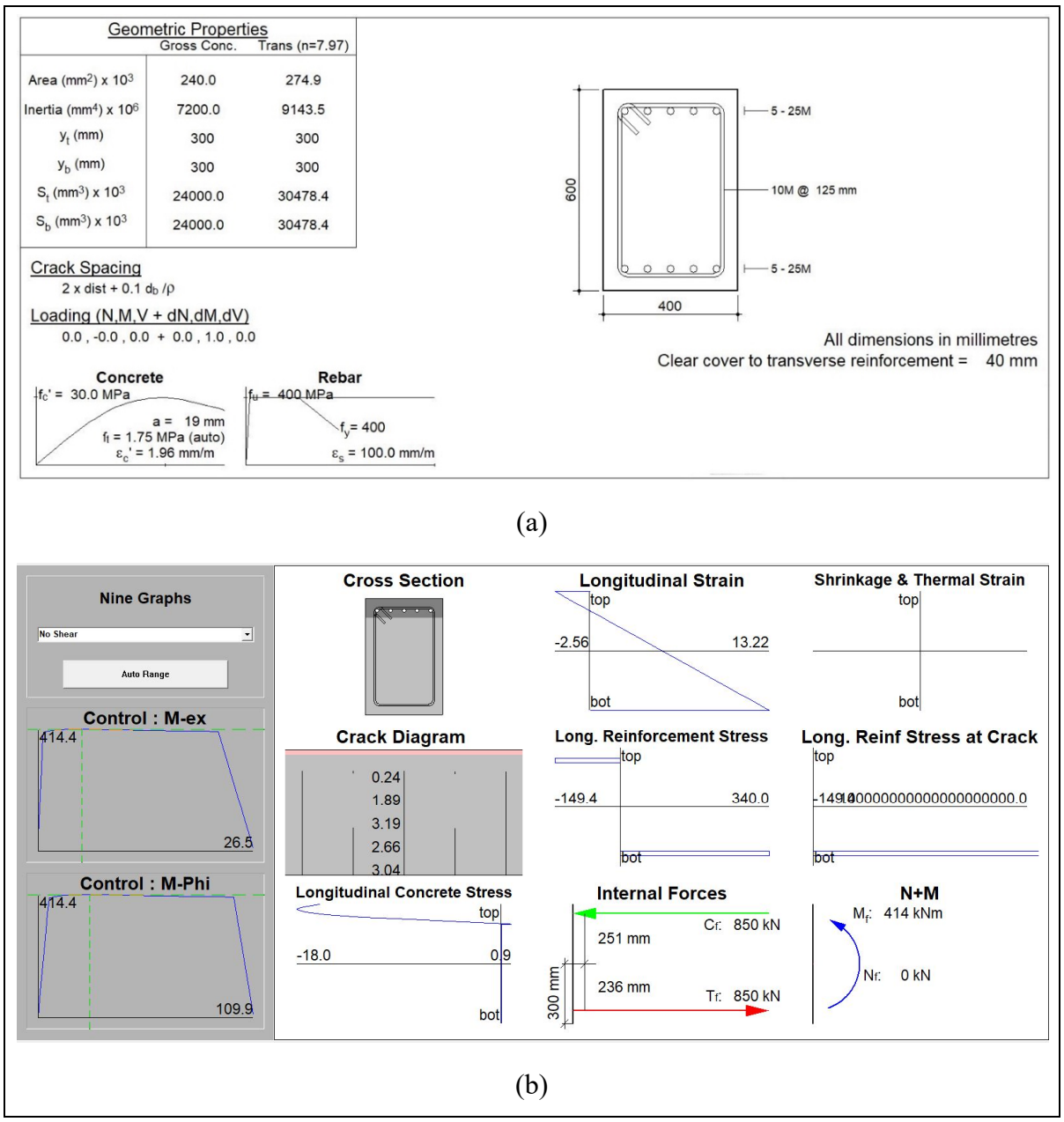

Figure A III.1 Section analysis using Response 2000: a) Input geometry and material of the section, b) Output of the moment-rotation relationship of the section

ANNEX IV

PLASTIC HINGE PROPERTIES AND ACCEPTANCE CRITERIA FOR BEAMS AND COLUMNS

Table IV.1 Acceptance criteria of plastic hinges in beams of the 3-storey frame

Hinge	a	b	c	IO	LS	CP
PHB01+	0.025	0.05	0.2	0.01	0.025	0.05
PHB01-	0.02	0.03	0.2	0.005	0.02	0.03
PHB02+	0.025	0.05	0.2	0.01	0.025	0.05
PHB02-	0.02	0.03	0.2	0.005	0.02	0.03
PHB03+	0.0181	0.0272	0.2000	0.0050	0.0181	0.0272
PHB03-	0.0192	0.0289	0.2000	0.0050	0.0192	0.0289
PHB04+	0.025	0.05	0.2	0.01	0.025	0.05
PHB04-	0.02	0.03	0.2	0.005	0.02	0.03
PHB05+	0.025	0.05	0.2	0.01	0.025	0.05
PHB05-	0.02	0.03	0.2	0.005	0.02	0.03
PHB06+	0.0192	0.0289	0.2000	0.0050	0.0192	0.0289
PHB06-	0.0192	0.0289	0.2000	0.0050	0.0192	0.0289

Table IV.2 Properties of plastic hinges in beams of the 3-storey frame

Hinge	My	θy	Mc/My	θc/θy	MD/My	θD/θy	ME/My	θE/θy
PHB01+	198.7	0.004953	1.1	6.0480	0.2	6.0480	0.2	11.0959
PHB01-	198.7	0.004953	1.1	5.0384	0.2	5.0384	0.2	7.0575
PHB02+	152.5	0.004953	1.1	6.0480	0.2	6.0480	0.2	11.0959
PHB02-	152.5	0.004953	1.1	5.0384	0.2	5.0384	0.2	7.0575
PHB03+	96.7	0.004953	1.1	4.6581	0.2	4.6581	0.2	6.4872
PHB03-	50.7	0.004953	1.1	4.8863	0.2	4.8863	0.2	6.8294
PHB04+	152.5	0.004953	1.1	6.0480	0.2	6.0480	0.2	11.0959
PHB04-	152.5	0.004953	1.1	5.0384	0.2	5.0384	0.2	7.0575
PHB05+	152.5	0.004953	1.1	6.0480	0.2	6.0480	0.2	11.0959
PHB05-	152.5	0.004953	1.1	5.0384	0.2	5.0384	0.2	7.0575
PHB06+	83.7	0.004953	1.1	4.8863	0.2	4.8863	0.2	6.8294
PHB06-	61.6	0.004953	1.1	4.8863	0.2	4.8863	0.2	6.8294

Units are in kN, m

Table IV.3 Acceptance criteria of plastic hinges in columns of the 3-storey frame

Hinge	a	b	c	IO	LS	CP
PHCE01	0.04255	0.08216	0.2	0.005	0.04108	0.05751
PHCE02	0.04255	0.08222	0.2	0.005	0.04111	0.05756
PHCE03	0.04255	0.08498	0.2	0.005	0.04249	0.05949
PHCE04	0.04255	0.08505	0.2	0.005	0.04252	0.05953
PHCE05	0.04255	0.08777	0.2	0.005	0.04388	0.06144
PHCE06	0.04255	0.08784	0.2	0.005	0.04392	0.06149
PHCI01	0.04255	0.08231	0.2	0.005	0.04116	0.05762
PHCI02	0.04255	0.08238	0.2	0.005	0.04119	0.05767
PHCI03	0.04255	0.08482	0.2	0.005	0.04241	0.05937
PHCI04	0.04255	0.08489	0.2	0.005	0.04244	0.05942
PHCI05	0.04255	0.08749	0.2	0.005	0.04375	0.06124
PHCI06	0.04255	0.08756	0.2	0.005	0.04378	0.06129

Table IV.4 Properties of plastic hinges in columns of the 3-storey frame

Hinge	My	θy	Mc/My	θc/θy	MD/My	θD/θy	ME/My	θE/θy
PHCE01	170.30	0.0062	1.1	7.919	0.2	7.919	0.2	14.3593
PHCE02	169.90	0.0062	1.1	7.919	0.2	7.919	0.2	14.3696
PHCE03	155.00	0.0062	1.1	7.919	0.2	7.919	0.2	14.8179
PHCE04	154.70	0.0062	1.1	7.919	0.2	7.919	0.2	14.8288
PHCE05	139.80	0.0062	1.1	7.919	0.2	7.919	0.2	15.2713
PHCE06	138.90	0.0062	1.1	7.919	0.2	7.919	0.2	15.2829
PHCI01	169.50	0.0062	1.1	7.919	0.2	7.919	0.2	14.3843
PHCI02	169.20	0.0062	1.1	7.919	0.2	7.919	0.2	14.3949
PHCI03	155.90	0.0062	1.1	7.919	0.2	7.919	0.2	14.7919
PHCI04	155.50	0.0062	1.1	7.919	0.2	7.919	0.2	14.8028
PHCI05	141.30	0.0062	1.1	7.919	0.2	7.919	0.2	15.2264
PHCI06	140.90	0.0062	1.1	7.919	0.2	7.919	0.2	15.2379

Units are in kN, m

Table IV.5 Acceptance criteria of plastic hinges in beams of the 6-storey frame

Hinge	a	b	c	IO	LS	CP
PHB01+	0.025	0.05	0.2	0.01	0.025	0.05
PHB01-	0.02	0.03	0.2	0.005	0.02	0.03
PHB02+	0.025	0.05	0.2	0.01	0.025	0.05
PHB02-	0.025	0.05	0.2	0.01	0.025	0.05
PHB03+	0.025	0.05	0.2	0.01	0.025	0.05
PHB03-	0.0197	0.0296	0.2	0.005	0.0197	0.0296
PHB04+	0.025	0.05	0.2	0.01	0.025	0.05
PHB04-	0.02	0.03	0.2	0.005	0.02	0.03
PHB05+	0.0192	0.0288	0.2	0.005	0.0192	0.0288
PHB05-	0.0192	0.0288	0.2	0.005	0.0192	0.0288
PHB06+	0.0187	0.0281	0.2	0.005	0.0187	0.0281
PHB06-	0.0187	0.0281	0.2	0.005	0.0187	0.0281
PHB07+	0.025	0.05	0.2	0.01	0.025	0.05
PHB07-	0.02	0.03	0.2	0.005	0.02	0.03
PHB08+	0.025	0.05	0.2	0.01	0.025	0.05
PHB08-	0.025	0.05	0.2	0.01	0.025	0.05
PHB09+	0.025	0.05	0.2	0.01	0.025	0.05
PHB09-	0.02	0.03	0.2	0.005	0.02	0.03
PHB10+	0.0244	0.0474	0.2	0.0094	0.0244	0.0474
PHB10-	0.0187	0.0281	0.2	0.005	0.0187	0.0281
PHB11+	0.0192	0.0288	0.2	0.005	0.0192	0.0288
PHB11-	0.0192	0.0288	0.2	0.005	0.0192	0.0288
PHB12+	0.0187	0.0281	0.2	0.005	0.0187	0.0281
PHB12-	0.0187	0.0281	0.2	0.005	0.0187	0.0281

Table IV.6 Properties of plastic hinges in beams of the 6-storey frame

Hinge	My	θy	M_c/M_y	θ_c/θ_y	M_D/M_y	$\theta_D/\theta y$	ME/My	θ_E/θ_y
PHB01+	414.4	0.003302	1.1	8.5719	0.2	8.5719	0.2	16.1439
PHB01-	414.4	0.003302	1.1	7.0575	0.2	7.0575	0.2	10.0863
PHB02+	496.6	0.003302	1.1	8.5719	0.2	8.5719	0.2	16.1439
PHB02-	496.6	0.003302	1.1	8.5719	0.2	8.5719	0.2	16.1439
PHB03+	414.4	0.003302	1.1	8.5719	0.2	8.5719	0.2	16.1439
PHB03-	414.4	0.003302	1.1	6.9910	0.2	6.9910	0.2	9.9865
PHB04+	336.7	0.003302	1.1	8.5719	0.2	8.5719	0.2	16.1439
PHB04-	336.7	0.003302	1.1	7.0575	0.2	7.0575	0.2	10.0863
PHB05+	208.8	0.003302	1.1	6.8579	0.2	6.8579	0.2	9.7869
PHB05-	160.2	0.003302	1.1	7.0575	0.2	7.0575	0.2	10.0863
PHB06+	159.5	0.003302	1.1	6.7248	0.2	6.7248	0.2	9.5873
PHB06-	79.3	0.003302	1.1	6.7248	0.2	6.7248	0.2	9.5873
PHB07+	414.4	0.006603	1.1	4.7860	0.2	4.7860	0.2	8.5719
PHB07-	414.4	0.006603	1.1	4.0288	0.2	4.0288	0.2	5.5432
PHB08+	496.6	0.006603	1.1	4.7860	0.2	4.7860	0.2	8.5719
PHB08-	496.6	0.006603	1.1	4.7860	0.2	4.7860	0.2	8.5719
PHB09+	414.4	0.006603	1.1	4.7860	0.2	4.7860	0.2	8.5719
PHB09-	414.4	0.006603	1.1	4.0288	0.2	4.0288	0.2	5.5432
PHB10+	336.7	0.006603	1.1	4.7028	0.2	4.7028	0.2	8.2392
PHB10-	256.1	0.006603	1.1	3.8624	0.2	3.8624	0.2	5.2936
PHB11+	208.8	0.006603	1.1	3.9290	0.2	3.9290	0.2	5.3934
PHB11-	160.2	0.006603	1.1	3.9290	0.2	3.9290	0.2	5.3934
PHB12+	159.5	0.006603	1.1	3.8624	0.2	3.8624	0.2	5.2936
PHB12-	79.3	0.006603	1.1	3.8624	0.2	3.8624	0.2	5.2936

Units are in kN, m

Table IV.7 Acceptance criteria of plastic hinges in columns of the 6-storey frame

Hinge	a	b	c	IO	LS	CP
PHCE01	0.0373	0.0681	0.2	0.005	0.0340	0.0476
PHCE02	0.04255	0.0682	0.2	0.005	0.0341	0.0477
PHCE03	0.0373	0.0716	0.2	0.005	0.0358	0.0501
PHCE04	0.0373	0.0717	0.2	0.005	0.0358	0.0502
PHCE05	0.0373	0.0758	0.2	0.005	0.0379	0.0530
PHCE06	0.0373	0.0759	0.2	0.005	0.0379	0.0531
PHCE07	0.0373	0.0800	0.2	0.005	0.0400	0.0560
PHCE08	0.0373	0.0801	0.2	0.005	0.0400	0.0561
PHCE09	0.0373	0.0838	0.2	0.005	0.0419	0.0587
PHCE10	0.0373	0.0840	0.2	0.005	0.0420	0.0588
PHCE11	0.0373	0.0872	0.2	0.005	0.0436	0.0611
PHCE12	0.0373	0.0874	0.2	0.005	0.0437	0.0612
PHCI01	0.0373	0.0743	0.2	0.005	0.0371	0.0520
PHCI02	0.0373	0.0744	0.2	0.005	0.0372	0.0521
PHCI03	0.0373	0.0765	0.2	0.005	0.0383	0.0536
PHCI04	0.0373	0.0767	0.2	0.005	0.0383	0.0537
PHCI05	0.0373	0.0789	0.2	0.005	0.0395	0.0553
PHCI06	0.0373	0.0791	0.2	0.005	0.0395	0.0553
PHCI07	0.0373	0.0815	0.2	0.005	0.0408	0.0571
PHCI08	0.0373	0.0816	0.2	0.005	0.0408	0.0571
PHCI09	0.0373	0.0843	0.2	0.005	0.0421	0.0590
PHCI10	0.0373	0.0844	0.2	0.005	0.0422	0.0591
PHCI11	0.0373	0.0872	0.2	0.005	0.0436	0.0610
PHCI12	0.0373	0.0873	0.2	0.005	0.0437	0.0611

Table IV.8 Properties of plastic hinges in columns of the 6-storey frame

Hinge	My	θy	Mc/My	θc/θy	MD/My	θD/θy	ME/My	θE/θy
PHCE01	612.8	0.0038	1.1	10.9027	0.2	10.9027	0.2	19.0703
PHCE02	611.9	0.0062	1.1	7.9187	0.2	7.9187	0.2	12.0827
PHCE03	579.4	0.0038	1.1	10.9027	0.2	10.9027	0.2	20.0035
PHCE04	578.5	0.0038	1.1	10.9027	0.2	10.9027	0.2	20.0308
PHCE05	539.3	0.0038	1.1	10.9027	0.2	10.9027	0.2	21.1159
PHCE06	538.3	0.0038	1.1	10.9027	0.2	10.9027	0.2	21.1461
PHCE07	499.8	0.0038	1.1	10.9027	0.2	10.9027	0.2	22.2313
PHCE08	498.6	0.0038	1.1	10.9027	0.2	10.9027	0.2	22.2645
PHCE09	464.1	0.0038	1.1	10.9027	0.2	10.9027	0.2	23.2606
PHCE10	462.8	0.0038	1.1	10.9027	0.2	10.9027	0.2	23.2967
PHCE11	433.9	0.0038	1.1	10.9027	0.2	10.9027	0.2	24.1593
PHCE12	432.6	0.0038	1.1	10.9027	0.2	10.9027	0.2	24.1981
PHCI01	777.4	0.0038	1.1	10.9027	0.2	10.9027	0.2	20.7139
PHCI02	776.5	0.0038	1.1	10.9027	0.2	10.9027	0.2	20.7430
PHCI03	759.7	0.0038	1.1	10.9027	0.2	10.9027	0.2	21.3195
PHCI04	758.7	0.0038	1.1	10.9027	0.2	10.9027	0.2	21.3502
PHCI05	740.5	0.0038	1.1	10.9027	0.2	10.9027	0.2	21.9592
PHCI06	739.5	0.0038	1.1	10.9027	0.2	10.9027	0.2	21.9916
PHCI07	719.9	0.0038	1.1	10.9027	0.2	10.9027	0.2	22.6400
PHCI08	718.9	0.0038	1.1	10.9027	0.2	10.9027	0.2	22.6743
PHCI09	460.4	0.0038	1.1	10.9027	0.2	10.9027	0.2	23.3679
PHCI10	459.1	0.0038	1.1	10.9027	0.2	10.9027	0.2	23.4044
PHCI11	434.2	0.0038	1.1	10.9027	0.2	10.9027	0.2	24.1493
PHCI12	432.9	0.0038	1.1	10.9027	0.2	10.9027	0.2	24.1881

Units are in kN, m

Table IV.9 Acceptance criteria of plastic hinges in beams of the 9-storey frame

Hinge	a	b	c	IO	LS	CP
PHB01+	0.0240	0.0461	0.2	0.0090	0.0240	0.0461
PHB01-	0.0181	0.0271	0.2	0.0050	0.0181	0.0271
PHB02+	0.0244	0.0477	0.2	0.0094	0.0244	0.0477
PHB02-	0.0244	0.0477	0.2	0.0094	0.0244	0.0477
PHB03+	0.0244	0.0477	0.2	0.0094	0.0244	0.0477
PHB03-	0.0244	0.0477	0.2	0.0094	0.0244	0.0477
PHB04+	0.0244	0.0477	0.2	0.0094	0.0244	0.0477
PHB04-	0.0244	0.0477	0.2	0.0094	0.0244	0.0477
PHB05+	0.0242	0.0468	0.2	0.0092	0.0242	0.0468
PHB05-	0.0184	0.0276	0.2	0.0050	0.0184	0.0276
PHB06+	0.0184	0.0276	0.2	0.0050	0.0184	0.0276
PHB06-	0.0184	0.0276	0.2	0.0050	0.0184	0.0276
PHB07+	0.0190	0.0285	0.2	0.0050	0.0190	0.0285
PHB07-	0.0190	0.0285	0.2	0.0050	0.0190	0.0285
PHB08+	0.0200	0.0300	0.2	0.0050	0.0200	0.0300
PHB08-	0.0200	0.0300	0.2	0.0050	0.0200	0.0300
PHB09+	0.0200	0.0300	0.2	0.0050	0.0200	0.0300
PHB09-	0.0200	0.0300	0.2	0.0050	0.0200	0.0300
PHB10+	0.0240	0.0461	0.2	0.0090	0.0240	0.0461
PHB10-	0.0181	0.0271	0.2	0.0050	0.0181	0.0271
PHB11+	0.0244	0.0477	0.2	0.0094	0.0244	0.0477
PHB11-	0.0244	0.0477	0.2	0.0094	0.0244	0.0477
PHB12+	0.0250	0.0500	0.2	0.0100	0.0250	0.0500
PHB12-	0.0250	0.0500	0.2	0.0100	0.0250	0.0500
PHB13+	0.0244	0.0477	0.2	0.0094	0.0244	0.0477
PHB13-	0.0244	0.0477	0.2	0.0094	0.0244	0.0477
PHB14+	0.0242	0.0468	0.2	0.0092	0.0242	0.0468
PHB14-	0.0184	0.0276	0.2	0.0050	0.0184	0.0276
PHB15+	0.0184	0.0276	0.2	0.0050	0.0184	0.0276
PHB15-	0.0184	0.0276	0.2	0.0050	0.0184	0.0276
PHB16+	0.0190	0.0285	0.2	0.0050	0.0190	0.0285
PHB16-	0.0190	0.0285	0.2	0.0050	0.0190	0.0285
PHB17+	0.0200	0.0300	0.2	0.0050	0.0200	0.0300
PHB17-	0.0200	0.0300	0.2	0.0050	0.0200	0.0300
PHB18+	0.0200	0.0300	0.2	0.0050	0.0200	0.0300
PHB18-	0.0200	0.0300	0.2	0.0050	0.0200	0.0300

Table IV.10 Properties of plastic hinges in beams of the 9-storey frame

Hinge	My	θy	Mc/My	θc/θy	MD/My	θD/θy	ME/My	θE/θy
PHB01+	758.1	0.003048	1.1	8.8835	0.2	8.8835	0.2	16.1283
PHB01-	551.2	0.003048	1.1	6.9236	0.2	6.9236	0.2	9.8853
PHB02+	987.1	0.003048	1.1	9.0166	0.2	9.0166	0.2	16.6606
PHB02-	886.3	0.003048	1.1	9.0166	0.2	9.0166	0.2	16.6606
PHB03+	879.4	0.003048	1.1	9.0166	0.2	9.0166	0.2	16.6606
PHB03-	759.2	0.003048	1.1	9.0166	0.2	9.0166	0.2	16.6606
PHB04+	758.1	0.003048	1.1	9.0166	0.2	9.0166	0.2	16.6606
PHB04-	637	0.003048	1.1	9.0166	0.2	9.0166	0.2	16.6606
PHB05+	635.7	0.003048	1.1	8.9368	0.2	8.9368	0.2	16.3412
PHB05-	461.1	0.003048	1.1	7.0300	0.2	7.0300	0.2	10.0450
PHB06+	461	0.003048	1.1	7.0300	0.2	7.0300	0.2	10.0450
PHB06-	284	0.003048	1.1	7.0300	0.2	7.0300	0.2	10.0450
PHB07+	337.5	0.003048	1.1	7.2429	0.2	7.2429	0.2	10.3644
PHB07-	231.8	0.003048	1.1	7.2429	0.2	7.2429	0.2	10.3644
PHB08+	231.6	0.003048	1.1	7.5623	0.2	7.5623	0.2	10.8435
PHB08-	231.6	0.003048	1.1	7.5623	0.2	7.5623	0.2	10.8435
PHB09+	231.6	0.003048	1.1	7.5623	0.2	7.5623	0.2	10.8435
PHB09-	231.6	0.003048	1.1	7.5623	0.2	7.5623	0.2	10.8435
PHB10+	758.1	0.003048	1.1	4.9418	0.2	4.9418	0.2	8.5641
PHB10-	551.2	0.003048	1.1	3.9618	0.2	3.9618	0.2	5.4427
PHB11+	987.1	0.003048	1.1	5.0083	0.2	5.0083	0.2	8.8303
PHB11-	886.3	0.003048	1.1	5.0083	0.2	5.0083	0.2	8.8303
PHB12+	879.4	0.003048	1.1	5.1015	0.2	5.1015	0.2	9.2029
PHB12-	759.2	0.003048	1.1	5.1015	0.2	5.1015	0.2	9.2029
PHB13+	758.1	0.003048	1.1	5.0083	0.2	5.0083	0.2	8.8303
PHB13-	637	0.003048	1.1	5.0083	0.2	5.0083	0.2	8.8303
PHB14+	635.7	0.003048	1.1	4.9684	0.2	4.9684	0.2	8.6706
PHB14-	461.1	0.003048	1.1	4.0150	0.2	4.0150	0.2	5.5225
PHB15+	461	0.003048	1.1	4.0150	0.2	4.0150	0.2	5.5225
PHB15-	284	0.003048	1.1	4.0150	0.2	4.0150	0.2	5.5225
PHB16+	337.5	0.003048	1.1	4.1215	0.2	4.1215	0.2	5.6822
PHB16-	231.8	0.003048	1.1	4.1215	0.2	4.1215	0.2	5.6822
PHB17+	231.6	0.003048	1.1	4.2812	0.2	4.2812	0.2	5.9218
PHB17-	231.6	0.003048	1.1	4.2812	0.2	4.2812	0.2	5.9218
PHB18+	231.6	0.003048	1.1	4.2812	0.2	4.2812	0.2	5.9218
PHB18-	231.6	0.003048	1.1	4.2812	0.2	4.2812	0.2	5.9218

Units are in kN, m

Table IV.11 Acceptance criteria of plastic hinges in columns of the 9-storey frame

Hinge	a	b	c	IO	LS	CP
PHCE01	0.0425	0.0753	0.1850	0.005	0.0377	0.0527
PHCE02	0.0425	0.0754	0.1852	0.005	0.0377	0.0528
PHCE03	0.0433	0.0770	0.1923	0.005	0.0385	0.0539
PHCE04	0.0433	0.0771	0.1925	0.005	0.0385	0.0539
PHCE05	0.0441	0.0789	0.2	0.005	0.0394	0.0552
PHCE06	0.0441	0.0789	0.2	0.005	0.0394	0.0552
PHCE07	0.0429	0.0789	0.2	0.005	0.0394	0.0552
PHCE08	0.0429	0.0789	0.2	0.005	0.0394	0.0552
PHCE09	0.0410	0.0789	0.2	0.005	0.0394	0.0552
PHCE10	0.0409	0.0789	0.2	0.005	0.0394	0.0552
PHCE11	0.0347	0.0748	0.2	0.005	0.0374	0.0524
PHCE12	0.0345	0.0748	0.2	0.005	0.0374	0.0524
PHCE13	0.0316	0.0748	0.2	0.0047	0.0374	0.0524
PHCE14	0.0316	0.0748	0.2	0.0047	0.0374	0.0524
PHCE15	0.0316	0.0748	0.2	0.0047	0.0374	0.0524
PHCE16	0.0316	0.0748	0.2	0.0047	0.0374	0.0524
PHCE17	0.0316	0.0748	0.2	0.0047	0.0374	0.0524
PHCE18	0.0316	0.0748	0.2	0.0047	0.0374	0.0524
PHCI01	0.0435	0.0789	0.2	0.005	0.0394	0.0552
PHCI02	0.0434	0.0789	0.2	0.005	0.0394	0.0552
PHCI03	0.0428	0.0789	0.2	0.005	0.0394	0.0552
PHCI04	0.0427	0.0789	0.2	0.005	0.0394	0.0552
PHCI05	0.0419	0.0789	0.2	0.005	0.0394	0.0552
PHCI06	0.0418	0.0789	0.2	0.005	0.0394	0.0552
PHCI07	0.0406	0.0789	0.2	0.005	0.0394	0.0552
PHCI08	0.0406	0.0789	0.2	0.005	0.0394	0.0552
PHCI09	0.0389	0.0789	0.2	0.005	0.0394	0.0552
PHCI10	0.0388	0.0789	0.2	0.005	0.0394	0.0552
PHCI11	0.0363	0.0789	0.2	0.005	0.0394	0.0552
PHCI12	0.0361	0.0789	0.2	0.005	0.0394	0.0552
PHCI13	0.0349	0.0789	0.2	0.005	0.0394	0.0552
PHCI14	0.0349	0.0789	0.2	0.005	0.0394	0.0552
PHCI15	0.0349	0.0789	0.2	0.005	0.0394	0.0552
PHCI16	0.0349	0.0789	0.2	0.005	0.0394	0.0552
PHCI17	0.0349	0.0789	0.2	0.005	0.0394	0.0552
PHCI18	0.0349	0.0789	0.2	0.005	0.0394	0.0552

Table IV.12 Properties of plastic hinges in columns of the 9-storey frame

Hinge	My	θy	Mc/My	θc/θy	MD/My	θD/θy	ME/My	θE/θy
PHCE01	1081.4	0.00316	1.1	14.4648	0.1850	14.4648	0.1850	24.860
PHCE02	1080.3	0.00316	1.1	14.4712	0.1852	14.4712	0.1852	24.873
PHCE03	1037.9	0.00316	1.1	14.7142	0.1923	14.7142	0.1923	25.398
PHCE04	1037	0.00316	1.1	14.7197	0.1925	14.7197	0.1925	25.410
PHCE05	978.1	0.00316	1.1	14.9756	0.2	14.9756	0.2	25.987
PHCE06	976.5	0.00316	1.1	14.9687	0.2	14.9687	0.2	25.987
PHCE07	910.1	0.00316	1.1	14.5837	0.2	14.5837	0.2	25.987
PHCE08	908.5	0.00316	1.1	14.5725	0.2	14.5725	0.2	25.987
PHCE09	844.9	0.00316	1.1	13.9869	0.2	13.9869	0.2	25.987
PHCE10	843.5	0.00316	1.1	13.9697	0.2	13.9697	0.2	25.987
PHCE11	783.7	0.00316	1.1	11.9788	0.2	11.9788	0.2	24.706
PHCE12	782	0.00316	1.1	11.9404	0.2	11.9404	0.2	24.706
PHCE13	727.6	0.00316	1.1	11.0136	0.2	11.0136	0.2	24.706
PHCE14	725.7	0.00316	1.1	11.0136	0.2	11.0136	0.2	24.706
PHCE15	679.2	0.00316	1.1	11.0136	0.2	11.0136	0.2	24.706
PHCE16	677.1	0.00316	1.1	11.0136	0.2	11.0136	0.2	24.706
PHCE17	638.6	0.00316	1.1	11.0136	0.2	11.0136	0.2	24.706
PHCE18	636.5	0.00316	1.1	11.0136	0.2	11.0136	0.2	24.706
PHCI01	1205.5	0.00316	1.1	14.7731	0.2	14.7731	0.2	25.987
PHCI02	1203.9	0.00316	1.1	14.7617	0.2	14.7617	0.2	25.987
PHCI03	1179.8	0.00316	1.1	14.5478	0.2	14.5478	0.2	25.987
PHCI04	1178.2	0.00316	1.1	14.5331	0.2	14.5331	0.2	25.987
PHCI05	1152.6	0.00316	1.1	14.2590	0.2	14.2590	0.2	25.987
PHCI06	1151.4	0.00316	1.1	14.2395	0.2	14.2395	0.2	25.987
PHCI07	1125.1	0.00316	1.1	13.8724	0.2	13.8724	0.2	25.987
PHCI08	1123.6	0.00316	1.1	13.8454	0.2	13.8454	0.2	25.987
PHCI09	1100.1	0.00316	1.1	13.3286	0.2	13.3286	0.2	25.987
PHCI10	1098.3	0.00316	1.1	13.2887	0.2	13.2887	0.2	25.987
PHCI11	732.3	0.00316	1.1	12.5073	0.2	12.5073	0.2	25.987
PHCI12	730.4	0.00316	1.1	12.4434	0.2	12.4434	0.2	25.987
PHCI13	700.7	0.00316	1.1	12.0622	0.2	12.0622	0.2	25.987
PHCI14	698.8	0.00316	1.1	12.0622	0.2	12.0622	0.2	25.987
PHCI15	668.7	0.00316	1.1	12.0622	0.2	12.0622	0.2	25.987
PHCI16	666.8	0.00316	1.1	12.0622	0.2	12.0622	0.2	25.987
PHCI17	636.5	0.00316	1.1	12.0622	0.2	12.0622	0.2	25.987
PHCI18	634.5	0.00316	1.1	12.0622	0.2	12.0622	0.2	25.987

Units are in kN, m

Table IV.13 Acceptance criteria of plastic hinges in beams of the 12-storey frame

Hinge	a	b	c	IO	LS	CP
PHB01+	0.0246	0.0484	0.2	0.0096	0.0246	0.0484
PHB01-	0.0250	0.0500	0.2	0.0100	0.0250	0.0500
PHB02+	0.0246	0.0484	0.2	0.0096	0.0246	0.0484
PHB02-	0.0246	0.0484	0.2	0.0096	0.0246	0.0484
PHB03+	0.0246	0.0484	0.2	0.0096	0.0246	0.0484
PHB03-	0.0246	0.0484	0.2	0.0096	0.0246	0.0484
PHB04+	0.0246	0.0484	0.2	0.0096	0.0246	0.0484
PHB04-	0.0246	0.0484	0.2	0.0096	0.0246	0.0484
PHB05+	0.0246	0.0484	0.2	0.0096	0.0246	0.0484
PHB05-	0.0246	0.0484	0.2	0.0096	0.0246	0.0484
PHB06+	0.0246	0.0484	0.2	0.0096	0.0246	0.0484
PHB06-	0.0184	0.0275	0.2	0.0050	0.0184	0.0275
PHB07+	0.0244	0.0477	0.2	0.0094	0.0244	0.0477
PHB07-	0.0188	0.0282	0.2	0.0050	0.0188	0.0282
PHB08+	0.0194	0.0291	0.2	0.0050	0.0194	0.0291
PHB08-	0.0188	0.0282	0.2	0.0050	0.0188	0.0282
PHB09+	0.0195	0.0293	0.2	0.0050	0.0195	0.0293
PHB09-	0.0195	0.0293	0.2	0.0050	0.0195	0.0293
PHB10+	0.0200	0.0300	0.2	0.0050	0.0200	0.0300
PHB10-	0.0200	0.0300	0.2	0.0050	0.0200	0.0300
PHB11+	0.0200	0.0300	0.2	0.0050	0.0200	0.0300
PHB11-	0.0200	0.0300	0.2	0.0050	0.0200	0.0300
PHB12+	0.0200	0.0300	0.2	0.0050	0.0200	0.0300
PHB12-	0.0200	0.0300	0.2	0.0050	0.0200	0.0300

Table IV.14 Acceptance criteria of plastic hinges in beams of the 12-storey frame - continue

Hinge	a	b	c	IO	LS	CP
PHB13+	0.0242	0.0467	0.2	0.0092	0.0242	0.0467
PHB13-	0.0242	0.0467	0.2	0.0092	0.0242	0.0467
PHB14+	0.0246	0.0484	0.2	0.0096	0.0246	0.0484
PHB14-	0.0246	0.0484	0.2	0.0096	0.0246	0.0484
PHB15+	0.0246	0.0484	0.2	0.0096	0.0246	0.0484
PHB15-	0.0246	0.0484	0.2	0.0096	0.0246	0.0484
PHB16+	0.0246	0.0484	0.2	0.0096	0.0246	0.0484
PHB16-	0.0246	0.0484	0.2	0.0096	0.0246	0.0484
PHB17+	0.0246	0.0484	0.2	0.0096	0.0246	0.0484
PHB17-	0.0246	0.0484	0.2	0.0096	0.0246	0.0484
PHB18+	0.0246	0.0484	0.2	0.0096	0.0246	0.0484
PHB18-	0.0192	0.0288	0.2	0.0050	0.0192	0.0288
PHB019+	0.025	0.05	0.2	0.01	0.025	0.05
PHB019-	0.02	0.03	0.2	0.005	0.02	0.03
PHB20+	0.018828	0.028242	0.2	0.005	0.018828	0.028242
PHB20-	0.018828	0.028242	0.2	0.005	0.018828	0.028242
PHB21+	0.019531	0.029297	0.2	0.005	0.019531	0.029297
PHB21-	0.019531	0.029297	0.2	0.005	0.019531	0.029297
PHB22+	0.02	0.03	0.2	0.005	0.02	0.03
PHB22-	0.02	0.03	0.2	0.005	0.02	0.03
PHB23+	0.02	0.03	0.2	0.005	0.02	0.03
PHB23-	0.02	0.03	0.2	0.005	0.02	0.03
PHB24+	0.02	0.03	0.2	0.005	0.02	0.03
PHB24-	0.02	0.03	0.2	0.005	0.02	0.03

Table IV.15 Properties of plastic hinges in beams of the 12-storey frame

Hinge	My	θy	Mc/My	θc/θy	MD/My	θD/θy	ME/My	θE/θy
PHB01+	1197.1	0.002641	1.1	10.3097	0.2	10.3097	0.2	19.3088
PHB01-	1053	0.002641	1.1	10.4649	0.2	10.4649	0.2	19.9298
PHB02+	1489.6	0.002641	1.1	10.3097	0.2	10.3097	0.2	19.3088
PHB02-	1346.3	0.002641	1.1	10.3097	0.2	10.3097	0.2	19.3088
PHB03+	1489.6	0.002641	1.1	10.3097	0.2	10.3097	0.2	19.3088
PHB03-	1346.3	0.002641	1.1	10.3097	0.2	10.3097	0.2	19.3088
PHB04+	1343.8	0.002641	1.1	10.3097	0.2	10.3097	0.2	19.3088
PHB04-	1200.1	0.002641	1.1	10.3097	0.2	10.3097	0.2	19.3088
PHB05+	1197.1	0.002641	1.1	10.3097	0.2	10.3097	0.2	19.3088
PHB05-	1053	0.002641	1.1	10.3097	0.2	10.3097	0.2	19.3088
PHB06+	1052.3	0.002641	1.1	10.3097	0.2	10.3097	0.2	19.3088
PHB06-	907.2	0.002641	1.1	7.9509	0.2	7.9509	0.2	11.4263
PHB07+	864.1	0.002641	1.1	10.2431	0.2	10.2431	0.2	19.0426
PHB07-	655.4	0.002641	1.1	8.1283	0.2	8.1283	0.2	11.6925
PHB08+	655.3	0.002641	1.1	8.3501	0.2	8.3501	0.2	12.0252
PHB08-	550	0.002641	1.1	8.1283	0.2	8.1283	0.2	11.6925
PHB09+	550.1	0.002641	1.1	8.3945	0.2	8.3945	0.2	12.0917
PHB09-	465.6	0.002641	1.1	8.3945	0.2	8.3945	0.2	12.0917
PHB10+	339.4	0.002641	1.1	8.5719	0.2	8.5719	0.2	12.3579
PHB10-	465.8	0.002641	1.1	8.5719	0.2	8.5719	0.2	12.3579
PHB11+	339.4	0.002641	1.1	8.5719	0.2	8.5719	0.2	12.3579
PHB11-	465.8	0.002641	1.1	8.5719	0.2	8.5719	0.2	12.3579
PHB12+	339.4	0.002641	1.1	8.5719	0.2	8.5719	0.2	12.3579
PHB12-	465.8	0.002641	1.1	8.5719	0.2	8.5719	0.2	12.3579

Units are in kN, m

Table IV.16 Properties of plastic hinges in beams of the 12-storey frame - continue

Hinge	My	θy	Mc/My	θc/θy	MD/My	θD/θy	ME/My	θE/θy
PHB13+	1196.1	0.002641	1.1	5.5772	0.2	5.5772	0.2	9.8439
PHB13-	907.3	0.002641	1.1	5.5772	0.2	5.5772	0.2	9.8439
PHB14+	1489.6	0.002641	1.1	5.6548	0.2	5.6548	0.2	10.1544
PHB14-	1346.3	0.002641	1.1	5.6548	0.2	5.6548	0.2	10.1544
PHB15+	1489.6	0.002641	1.1	5.6548	0.2	5.6548	0.2	10.1544
PHB15-	1346.3	0.002641	1.1	5.6548	0.2	5.6548	0.2	10.1544
PHB16+	1343.8	0.002641	1.1	5.6548	0.2	5.6548	0.2	10.1544
PHB16-	1200.1	0.002641	1.1	5.6548	0.2	5.6548	0.2	10.1544
PHB17+	1197.1	0.002641	1.1	5.6548	0.2	5.6548	0.2	10.1544
PHB17-	1053	0.002641	1.1	5.6548	0.2	5.6548	0.2	10.1544
PHB18+	1052.3	0.002641	1.1	5.6548	0.2	5.6548	0.2	10.1544
PHB18-	907.2	0.002641	1.1	4.6307	0.2	4.6307	0.2	6.4461
PHB19+	864.1	0.002641	1.1	5.73246	0.2	5.732458	0.2	10.46492
PHB19-	655.4	0.002641	1.1	4.78597	0.2	4.785967	0.2	6.67895
PHB20+	759.9	0.002641	1.1	4.56416	0.2	4.564164	0.2	6.346246
PHB20-	549.9	0.002641	1.1	4.56416	0.2	4.564164	0.2	6.346246
PHB21+	550.1	0.002641	1.1	4.69725	0.2	4.697246	0.2	6.545868
PHB21-	465.6	0.002641	1.1	4.69725	0.2	4.697246	0.2	6.545868
PHB22+	402	0.002641	1.1	4.78597	0.2	4.785967	0.2	6.67895
PHB22-	465.6	0.002641	1.1	4.78597	0.2	4.785967	0.2	6.67895
PHB23+	339.4	0.002641	1.1	4.78597	0.2	4.785967	0.2	6.67895
PHB23-	465.8	0.002641	1.1	4.78597	0.2	4.785967	0.2	6.67895
PHB24+	339.4	0.002641	1.1	4.78597	0.2	4.785967	0.2	6.67895
PHB24-	465.8	0.002641	1.1	4.78597	0.2	4.785967	0.2	6.67895

Units are in kN, m

Table IV.17 Acceptance criteria of plastic hinges in interior columns of the 12-storey frame

Hinge	a	b	c	IO	LS	CP
PHCI01	0.042827	0.0789	0.2	0.005	0.0394	0.0552
PHCI02	0.042725	0.0789	0.2	0.005	0.0394	0.0552
PHCI03	0.042327	0.0789	0.2	0.005	0.0394	0.0552
PHCI04	0.042287	0.0789	0.2	0.005	0.0394	0.0552
PHCI05	0.041729	0.0789	0.2	0.005	0.0394	0.0552
PHCI06	0.041682	0.0789	0.2	0.005	0.0394	0.0552
PHCI07	0.040995	0.0789	0.2	0.005	0.0394	0.0552
PHCI08	0.040938	0.0789	0.2	0.005	0.0394	0.0552
PHCI09	0.04007	0.0789	0.2	0.005	0.0394	0.0552
PHCI10	0.039999	0.0789	0.2	0.005	0.0394	0.0552
PHCI11	0.038872	0.0789	0.2	0.005	0.0394	0.0552
PHCI12	0.03878	0.0789	0.2	0.005	0.0394	0.0552
PHCI13	0.037263	0.0789	0.2	0.005	0.0394	0.0552
PHCI14	0.037138	0.0789	0.2	0.005	0.0394	0.0552
PHCI15	0.034994	0.0789	0.2	0.005	0.0394	0.0552
PHCI16	0.034925	0.0789	0.2	0.005	0.0394	0.0552
PHCI17	0.030988	0.0737	0.2	0.00465	0.0369	0.0516
PHCI18	0.030988	0.0737	0.2	0.00465	0.0369	0.0516
PHCI19	0.030988	0.0737	0.2	0.00465	0.0369	0.0516
PHCI20	0.030988	0.0737	0.2	0.00465	0.0369	0.0516
PHCI21	0.030988	0.0737	0.2	0.00465	0.0369	0.0516
PHCI22	0.030988	0.0737	0.2	0.00465	0.0369	0.0516
PHCI23	0.030988	0.0737	0.2	0.00465	0.0369	0.0516
PHCI24	0.030988	0.0737	0.2	0.00465	0.0369	0.0516

Table IV.18 Acceptance criteria of plastic hinges in exterior columns of the 12-storey frame

Hinge	a	b	c	IO	LS	CP
PHCE01	0.035964	0.0622	0.1607	0.005	0.0311	0.0435
PHCE02	0.035983	0.0622	0.1609	0.005	0.0311	0.0436
PHCE03	0.036843	0.0643	0.1689	0.005	0.0322	0.0450
PHCE04	0.036863	0.0644	0.1691	0.005	0.0322	0.0451
PHCE05	0.0379	0.0670	0.1787	0.005	0.0335	0.0469
PHCE06	0.037918	0.0671	0.1789	0.005	0.0335	0.0470
PHCE07	0.038951	0.0700	0.1885	0.005	0.0350	0.0490
PHCE08	0.03897	0.0700	0.1887	0.005	0.0350	0.0490
PHCE09	0.039938	0.0729	0.1977	0.005	0.0365	0.0511
PHCE10	0.039957	0.0730	0.1979	0.005	0.0365	0.0511
PHCE11	0.039314	0.0737	0.2	0.005	0.0369	0.0516
PHCE12	0.039285	0.0737	0.2	0.005	0.0369	0.0516
PHCE13	0.037773	0.0737	0.2	0.005	0.0369	0.0516
PHCE14	0.037725	0.0737	0.2	0.005	0.0369	0.0516
PHCE15	0.035451	0.0737	0.2	0.005	0.0369	0.0516
PHCE16	0.035367	0.0737	0.2	0.005	0.0369	0.0516
PHCE17	0.031726	0.0737	0.2	0.00476	0.0369	0.0516
PHCE18	0.031569	0.0737	0.2	0.00474	0.0369	0.0516
PHCE19	0.030988	0.0737	0.2	0.00465	0.0369	0.0516
PHCE20	0.030988	0.0737	0.2	0.00465	0.0369	0.0516
PHCE21	0.030988	0.0737	0.2	0.00465	0.0369	0.0516
PHCE22	0.030988	0.0737	0.2	0.00465	0.0369	0.0516
PHCE23	0.030988	0.0737	0.2	0.00465	0.0369	0.0516
PHCE24	0.030988	0.0737	0.2	0.00465	0.0369	0.0516

Table IV.19 Properties of plastic hinges in interior columns of the 12-storey frame

Hinge	My	θy	Mc/My	θc/θy	MD/My	θD/θy	ME/My	θE/θy
PHCI01	1772.3	0.002638	1.1	17.238	0.2	17.23776	0.2	30.9105
PHCI02	1765.9	0.002638	1.1	17.199	0.2	17.1991	0.2	30.9105
PHCI03	1746.3	0.002638	1.1	17.048	0.2	17.04809	0.2	30.9105
PHCI04	1744.7	0.002638	1.1	17.033	0.2	17.03309	0.2	30.9105
PHCI05	1716.5	0.002638	1.1	16.821	0.2	16.82148	0.2	30.9105
PHCI06	1714	0.002638	1.1	16.804	0.2	16.80354	0.2	30.9105
PHCI07	1686.9	0.002638	1.1	16.543	0.2	16.54318	0.2	30.9105
PHCI08	1684.5	0.002638	1.1	16.521	0.2	16.52148	0.2	30.9105
PHCI09	1652.4	0.002638	1.1	16.193	0.2	16.19258	0.2	30.9105
PHCI10	1650.1	0.002638	1.1	16.165	0.2	16.16532	0.2	30.9105
PHCI11	1619.2	0.002638	1.1	15.738	0.2	15.73816	0.2	30.9105
PHCI12	1617.1	0.002638	1.1	15.703	0.2	15.70318	0.2	30.9105
PHCI13	1584.1	0.002638	1.1	15.128	0.2	15.12834	0.2	30.9105
PHCI14	1581.5	0.002638	1.1	15.081	0.2	15.08074	0.2	30.9105
PHCI15	1545.6	0.002638	1.1	14.268	0.2	14.26784	0.2	30.9105
PHCI16	1543.2	0.002638	1.1	14.242	0.2	14.24171	0.2	30.9105
PHCI17	1025.9	0.002638	1.1	12.749	0.2	12.74882	0.2	28.9511
PHCI18	1023	0.002638	1.1	12.749	0.2	12.74882	0.2	28.9511
PHCI19	981.9	0.002638	1.1	12.749	0.2	12.74882	0.2	28.9511
PHCI20	979.3	0.002638	1.1	12.749	0.2	12.74882	0.2	28.9511
PHCI21	936.5	0.002638	1.1	12.749	0.2	12.74882	0.2	28.9511
PHCI22	933.7	0.002638	1.1	12.749	0.2	12.74882	0.2	28.9511
PHCI23	889.7	0.002638	1.1	12.749	0.2	12.74882	0.2	28.9511
PHCI24	886.7	0.002638	1.1	12.749	0.2	12.74882	0.2	28.9511

Units are in kN, m

Table IV.20 Properties of plastic hinges in exterior columns of the 12-storey frame

Hinge	My	θy	Mc/My	θc/θy	MD/My	θD/θy	ME/My	θE/θy
PHCE01	1714.5	0.002638	1.1	14.6355	0.1607	14.63546	0.1607	24.5748
PHCE02	1714	0.002638	1.1	14.6427	0.1609	14.64266	0.1609	24.5918
PHCE03	1680.7	0.002638	1.1	14.9691	0.1689	14.96909	0.1689	25.3841
PHCE04	1679.8	0.002638	1.1	14.9764	0.1691	14.97637	0.1691	25.4023
PHCE05	1621.7	0.002638	1.1	15.3695	0.1787	15.3695	0.1787	26.4208
PHCE06	1620.6	0.002638	1.1	15.3767	0.1789	15.37668	0.1789	26.44
PHCE07	1541.2	0.002638	1.1	15.7682	0.1885	15.76825	0.1885	27.5319
PHCE08	1539.8	0.002638	1.1	15.7755	0.1887	15.77552	0.1887	27.5529
PHCE09	1450.4	0.002638	1.1	16.1423	0.1977	16.14235	0.1977	28.654
PHCE10	1448.5	0.002638	1.1	16.1496	0.1979	16.14963	0.1979	28.6766
PHCE11	1354.5	0.002638	1.1	15.9059	0.2	15.90594	0.2	28.9511
PHCE12	1352.3	0.002638	1.1	15.895	0.2	15.89497	0.2	28.9511
PHCE13	1256.3	0.002638	1.1	15.3214	0.2	15.32144	0.2	28.9511
PHCE14	1253.7	0.002638	1.1	15.3034	0.2	15.3034	0.2	28.9511
PHCE15	1162.6	0.002638	1.1	14.4413	0.2	14.44127	0.2	28.9511
PHCE16	1160.2	0.002638	1.1	14.4092	0.2	14.40924	0.2	28.9511
PHCE17	1078.9	0.002638	1.1	13.0289	0.2	13.02892	0.2	28.9511
PHCE18	1076.4	0.002638	1.1	12.9692	0.2	12.96918	0.2	28.9511
PHCE19	1004.1	0.002638	1.1	12.7488	0.2	12.74882	0.2	28.9511
PHCE20	1001.1	0.002638	1.1	12.7488	0.2	12.74882	0.2	28.9511
PHCE21	940	0.002638	1.1	12.7488	0.2	12.74882	0.2	28.9511
PHCE22	936.9	0.002638	1.1	12.7488	0.2	12.74882	0.2	28.9511
PHCE23	887.3	0.002638	1.1	12.7488	0.2	12.74882	0.2	28.9511
PHCE24	884.1	0.002638	1.1	12.7488	0.2	12.74882	0.2	28.9511

Units are in kN, m

LIST OF BIBLIOGRAPHICAL REFERENCES

Abbati, S. D., Cattari, S., & Lagomarsino, S. (2018). Theoretically-based and practice-oriented formulations for the floor spectra evaluation. *Earthquakes and Structures*, *15*(5), 565–581. https://doi.org/10.12989/EAS.2018.15.5.565.

Achour, N., Miyajima, M., Kitaura, M., & Price, A. (2011). Earthquake-Induced Structural and Nonstructural Damage in Hospitals. *Earthquake Spectra*, *27*(3), 617–634. https://doi.org/10.1193/1.3604815.

Adam, C., Furtmüller, T., & Moschen, L. (2013). Floor Response Spectra for Moderately Heavy Nonstructural Elements Attached to Ductile Frame Structures. In M. Papadrakakis, M. Fragiadakis, & V. Plevris (Eds.), *Computational Methods in Earthquake Engineering* (Vol. 30, pp. 69–89). Springer Netherlands. https://doi.org/10.1007/978-94-007-6573-3_4.

Agrahari, R. K., & Pathak, K. K. (2021). Nonlinear Amplification Model in RC Frame Structures: Case Study for Chi-Chi Earthquake. *Civil Engineering and Architecture*, *9*(4), 1156–1169. https://doi.org/10.13189/cea.2021.090417.

Al Atik, L., & Abrahamson, N. (2010). An improved method for nonstationary spectral matching. *Earthquake Spectra*, *26*(3), 601–617.

American Society of Civil Engineers. (2017). *Minimum Design Loads and Associated Criteria for Buildings and Other Structures* (7th ed.). American Society of Civil Engineers. https://doi.org/10.1061/9780784414248.

American Society of Civil Engineers. & Structural Engineering Institute. (2017). *Seismic evaluation and retrofit of existing buildings.* American Society of Civil Engineers.

Anajafi, H., & Medina, R. A. (2018a). Uncertainties in using the spectrum matching technique for generating synthetic ground motions. *Proceedings of 11th National Conference in Earthquake Engineering, Earthquake Engineering Research Institute, Los Angeles, CA*.

Anajafi, H., & Medina, R. A. (2018b). Evaluation of ASCE 7 equations for designing acceleration-sensitive nonstructural components using data from instrumented buildings. *Earthquake Engineering & Structural Dynamics*, *47*(4), 1075–1094. https://doi.org/10.1002/eqe.3006.

Anajafi, H., & Medina, R. A. (2019a). Lessons Learned from Evaluating the Responses of Instrumented Buildings in the United States: The Effects of Supporting Building Characteristics on Floor Response Spectra. *Earthquake Spectra*, *35*(1), 159–191. https://doi.org/10.1193/081017EQS159M.

Anajafi, H., & Medina, R. A. (2019b). Damping modification factor for elastic floor spectra. *Bulletin of Earthquake Engineering*, 17(11), 6079-6108. https://doi.org/10.1007/s10518-019-00684-3.

Anajafi, H., Medina, R. A., & Adam, C. (2021). Evaluation of the Floor Acceleration Response Spectra of Numerical Building Models Based on Recorded Building Response Data. *Journal of Earthquake Engineering*, 1–25. https://doi.org/10.1080/13632469.2021.1927887.

Anajafi, H., Medina, R. A., & Santini-Bell, E. (2020). Inelastic floor spectra for designing anchored acceleration-sensitive nonstructural components. *Bulletin of Earthquake Engineering*, *18*(5), 2115–2147. https://doi.org/10.1007/s10518-019-00760-8.

Applied Technology Council. (2018). *Recommendations for improved seismic performance of nonstructural components* (NIST GCR 18-917-43; p. NIST GCR 18-917-43). National Institute of Standards and Technology. https://doi.org/10.6028/NIST.GCR.18-917-43.

ASCE. (2013). *Minimum Design Loads for Buildings and Other Structures* (7th ed.). American Society of Civil Engineers. https://doi.org/10.1061/9780784412916.

Asgarian, A., & McClure, G. (2017). b. New methodology for seismic assessment of non-structural building components based on ambient vibration measurements. *Proceedings of the 16th World Conference on Earthquake Engineering, Santiago, Chile, January 2017*, 9–13.

Asgarian, A., & McClure, G. (2020a). Direct generation of floor design spectra (FDS) from uniform hazard spectra (UHS) — Part I: Formulation of the method. *Canadian Journal of Civil Engineering*, *47*(12), 1372–1386. https://doi.org/10.1139/cjce-2018-0146.

Asgarian, A., & McClure, G. (2020b). Direct generation of floor design spectra (FDS) from uniform hazard spectra (UHS) — Part II: Extension and application of the method. *Canadian Journal of Civil Engineering*, *47*(12), 1387–1400. https://doi.org/10.1139/cjce-2018-0151.

Atkinson, G. M. (2009). Earthquake time histories compatible with the 2005 *National building code of Canada* uniform hazard spectrum. *Canadian Journal of Civil Engineering*, *36*(6), 991–1000. https://doi.org/10.1139/L09-044.

Bentz, E. (1999). *Response2000—Sectional analysis of reinforced concrete members*. [Computer software]. Toronto, Ontario, Canada: University of Toronto.

Berto, L., Bovo, M., Rocca, I., Saetta, A., & Savoia, M. (2020). Seismic safety of valuable non-structural elements in RC buildings: Floor Response Spectrum approaches. *Engineering Structures*, *205*, 110081. https://doi.org/10.1016/j.engstruct.2019.110081.

Bradley, B. A., Dhakal, R. P., Cubrinovski, M., MacRae, G. A., & Lee, D. S. (2009). Seismic loss estimation for efficient decision making. *Bulletin of the New Zealand Society for Earthquake Engineering*, *42*(2), 96–110. https://doi.org/10.5459/bnzsee.42.2.96-110.

Canadian Commission on Building Fire Codes, & National Research Council of Canada (2015). *National building code of Canada: 2015*; Issues 0-660-03633–5. Ottawa: National Research Council of Canada. https://doi.org/10.4224/40002005.

Canadian Commission On Building And Fire Codes. Standing Committee On Structural Design, & Canadian Commission On Building And Fire Codes. Standing Committee On Earthquake Design. (2017). *Structural Commentaries (User's Guide: NBC 2015: Part 4 of Division B)*. 312 p. https://doi.org/10.4224/40002023.

CEN. (2005). Eurocode 8: Design of structures for earthquake resistance-part 1: General rules, seismic actions and rules for buildings. *Brussels: European Committee for Standardization*.

Chaudhuri, S. R., & Villaverde, R. (2008). Effect of Building Nonlinearity on Seismic Response of Nonstructural Components: A Parametric Study. *Journal of Structural Engineering*, *134*(4), 661–670. https://doi.org/10.1061/(ASCE)0733-9445(2008)134:4(661).

Clayton, J. S., & Medina, R. A. (2012). Proposed method for probabilistic estimation of peak component acceleration demands. *Earthquake Spectra*, *28*(1), 55–75.

CSA. (2014a). *Design of concrete structures* (Sixth edition.). CSA Group.

CSA. (2014b). *Seismic risk reduction of operational and functional components (OFCs) of buildings*. Canadian Standard Association.

CSI. (2019). *SAP2000 Integrated Software for Structural Analysis and Design* (21.0.0) [Computer software]. Computers & Structures, Inc.

Fathali, S., & Lizundia, B. (2011). Evaluation of current seismic design equations for nonstructural components in tall buildings using strong motion records: SEISMIC DESIGN OF TALL BUILDING NONSTRUCTURAL COMPONENTS. *The Structural Design of Tall and Special Buildings*, *20*, 30–46. https://doi.org/10.1002/tal.736.

FEMA. (2009). *Quantification of building seismic performance factors (FEMA P695)*. US Department of Homeland Security, FEMA.

Fierro, E. A., Miranda, E., & Perry, C. L. (2011). Behavior of nonstructural components in recent earthquakes. In *AEI 2011: Building Integration Solutions* (pp. 369–377).

Filiatrault, A., & Sullivan, T. (2014). Performance-based seismic design of nonstructural building components: The next frontier of earthquake engineering. *Earthquake Engineering and Engineering Vibration*, *13*(S1), 17–46. https://doi.org/10.1007/s11803-014-0238-9.

GB50011-2010. (2010). Code for seismic design of buildings. *National Standards of the People's Republic of China*.

González, I., Silva, A., Macedo, L., Monteiro, R., & Castro, J. M. (2019). Critical Assessment of Estimation Procedures for Floor Acceleration Demands in Steel Moment-Resisting Frames. *Frontiers in Built Environment*, *5*, 139. https://doi.org/10.3389/fbuil.2019.00139.

Gupta, A., & McDonald, B. M. (2008). Performance of building structures during the October 15, 2006 Hawaii earthquake. *Proceedings of the 14th World Conference on Earthquake Engineering, Beijing, China, 12 Oct. 2008*.

Haymes, K., Sullivan, T., & Chandramohan, R. (2020). A practice-oriented method for estimating elastic floor response spectra. *Bulletin of the New Zealand Society for Earthquake Engineering*, *53*(3), 116–136.

Hur, J., Althoff, E., Sezen, H., Denning, R., & Aldemir, T. (2017). Seismic Assessment and Performance of Nonstructural Components Affected by Structural Modeling. *Special Issue on the 13th International Conference on Probabilistic Safety Assessment and Management (PSAM 13)*, *49*(2), 387–394. https://doi.org/10.1016/j.net.2017.01.004.

Kazantzi A. K., Vamvatsikos D., & Miranda E. (2020). Evaluation of Seismic Acceleration Demands on Building Nonstructural Elements. *Journal of Structural Engineering*, *146*(7), 04020118. https://doi.org/10.1061/(ASCE)ST.1943-541X.0002676.

Kazantzi, A., Vamvatsikos, D., & Miranda, E. (2018). Effect of yielding on the seismic demands of nonstructural elements. *Proceedings of 16th European Conference on Earthquake Engineering, Thessaloniki, Greece*.

Lagomarsino, S. (2015). Seismic assessment of rocking masonry structures. *Bulletin of Earthquake Engineering*, *13*(1), 97–128. https://doi.org/10.1007/s10518-014-9609-x.

Lin Jon & Mahin Stephen A. (1985). Seismic Response of Light Subsystems on Inelastic Structures. *Journal of Structural Engineering*, *111*(2), 400–417. https://doi.org/10.1061/(ASCE)0733-9445(1985)111:2(400).

Lucchini, A., Mollaioli, F., & Bazzurro, P. (2014). Floor Response Spectra for Bare and Infilled Reinforced Concrete Frames. *Journal of Earthquake Engineering*, *18*(7), 1060–1082. https://doi.org/10.1080/13632469.2014.916633.

Mazloom, S., & Assi, R. (2022). Estimation of the Vertical Peak Floor Acceleration Demands in Linear Elastic RC Moment-Resisting Frame Buildings. *Journal of Earthquake Engineering*.

Medina, R. A., Sankaranarayanan, R., & Kingston, K. M. (2006). Floor response spectra for light components mounted on regular moment-resisting frame structures. *Engineering Structures*, *28*(14), 1927–1940. https://doi.org/10.1016/j.engstruct.2006.03.022.

Merino, R. J., Perrone, D., & Filiatrault, A. (2020). Consistent floor response spectra for performance-based seismic design of nonstructural elements. *Earthquake Engineering & Structural Dynamics*, *49*(3), 261–284. https://doi.org/10.1002/eqe.3236.

Miranda, E., Mosqueda, G., Retamales, R., & Pekcan, G. (2012). Performance of nonstructural components during the 27 February 2010 Chile earthquake. *Earthquake Spectra*, *28*(1_suppl1), 453–471.

Miranda, E., & Taghavi, S. (2003). Estimation of seismic demands on acceleration-sensitive nonstructural components in critical facilities. *Proceedings of the Seminar on Seismic Design, Performance, and Retrofit of Nonstructural Components in Critical Facilities, ATC*, *292*.

MIT, M. delle I. (2019). Istruzioni per l'applicazione dell'Aggiornamento delle 'Norme Tecniche per le costruzioni'di cui al decreto ministeriale 17 gennaio 2018. *Gazz. Uffic. Rep. Ita*.

Naeim, F. (2004). Impact of the 1994 Northridge earthquake on the art and practice of structural engineering. *The Structural Design of Tall and Special Buildings*, *13*(5), 373–389. https://doi.org/10.1002/tal.280.

NIST. (2017). *GCR 17-917-44 (2017) Seismic analysis, design, and installation of nonstructural components and systems—Background and recommendations for future work*. Applied Technology Council.

NIST GCR 17-917-44. (2017). *Seismic analysis, design, and installation of nonstructural components and systems—Background and recommendations for future work*.

Obando, J. C., & Lopez-Garcia, D. (2018). Inelastic Displacement Ratios for Nonstructural Components Subjected to Floor Accelerations. *Journal of Earthquake Engineering*, *22*(4), 569–594. https://doi.org/10.1080/13632469.2016.1244131.

Petrone, C., Magliulo, G., & Manfredi, G. (2016). Floor response spectra in RC frame structures designed according to Eurocode 8. *Bulletin of Earthquake Engineering*, *14*(3), 747–767.

Prestandard, F. (2000). Commentary for the seismic rehabilitation of buildings (FEMA356). *Washington, DC: Federal Emergency Management Agency*, *7*(2).

Priestley, M. J. N., Calvi, G. M., & Kowalsky, M. J. (2007). *Displacement-based seismic design of structures*. IUSS Press : Distributed by Fondazione EUCENTRE.

Rashid, M., Sullivan, T., & Dhakal, R. (2021). *Seismic design of acceleration-sensitive non-structural elements in New Zealand: State-of-practice and recommended changes*.

Rodriguez, M. E., Restrepo, J. I., & Carr, A. J. (2002). Earthquake-induced floor horizontal accelerations in buildings. *Earthquake Engineering & Structural Dynamics*, *31*(3), 693–718. https://doi.org/10.1002/eqe.149.

Sankaranarayanan, R., & Medina, R. A. (2007). Acceleration response modification factors for nonstructural components attached to inelastic moment-resisting frame structures. *Earthquake Engineering & Structural Dynamics*, *36*(14), 2189–2210. https://doi.org/10.1002/eqe.724.

Sewell, R. T., Cornell, C. A., Toro, G. R., & McGuire, R. K. (1986). *Study of Factors Influencing Floor Response Spectra in Nonlinear Multi-Degree-of-Freedom Structures* (Issue 82). John A. Blume Earthquake Engineering Center.

Shang, Q., Li, J., & Wang, T. (2022). Floor acceleration response spectra of elastic reinforced concrete frames. *Journal of Building Engineering*, *45*, 103558. https://doi.org/10.1016/j.jobe.2021.103558.

Shang, Q., Wang, T., & Li, J. (2019). Seismic fragility of flexible pipeline connections in a base isolated medical building. *Earthquake Engineering and Engineering Vibration*, *18*(4), 903–916. https://doi.org/10.1007/s11803-019-0542-5.

Shooshtari, M., Saatcioglu, M., Naumoski, N., & Foo, S. (2010). Floor response spectra for seismic design of operational and functional components of concrete buildings in Canada. *Canadian Journal of Civil Engineering*, *37*(12), 1590–1599. https://doi.org/10.1139/L10-094.

Singh M. P., Moreschi L. M., Suárez L. E., & Matheu E. E. (2006). Seismic Design Forces. I: Rigid Nonstructural Components. *Journal of Structural Engineering*, *132*(10), 1524–1532. https://doi.org/10.1061/(ASCE)0733-9445(2006)132:10(1524).

Standard New Zealand (2016). *Structural design actions.* Part 5, *Earthquake actions* : New Zealand, (Reissued incorporating Amendment No. 1), September 2016.

Sullivan, T. J., Calvi, P. M., & Nascimbene, R. (2013). Towards improved floor spectra estimates for seismic design. *Earthquakes and Structures*, *4*(1), 109–132.

Surana, M. (2019). Evaluation of seismic design provisions for acceleration-sensitive non-structural components. *Earthquakes and Structures*, *16*(5), 611–623. https://doi.org/10.12989/EAS.2019.16.5.611.

Surana, M., Singh, Y., & Lang, D. H. (2018). Floor Spectra of Inelastic RC Frame Buildings Considering Ground Motion Characteristics. *Journal of Earthquake Engineering*, *22*(3), 488–519. https://doi.org/10.1080/13632469.2016.1244134.

Taghavi, S., & Miranda, E. (2005a). Approximate Floor Acceleration Demands in Multistory Buildings. II: Applications. *Journal of Structural Engineering*, *131*(2), 212–220. https://doi.org/10.1061/(ASCE)0733-9445(2005)131:2(212).

Taghavi, S., & Miranda, E. (2005b). Approximate Floor Acceleration Demands in Multistory Buildings. I: Formulation. *Journal of Structural Engineering*, *131*(2), 203–211. https://doi.org/10.1061/(ASCE)0733-9445(2005)131:2(203).

Taghavi, S., & Miranda, E. (2008). Effect of interaction between primary and secondary systems on floor response spectra. *14th World Conference on Earthquake Engineering*, *Beijing, China,* 12–17.

Takeda, T., Sozen, M. A., & Nielsen, N. N. (1970). Reinforced Concrete Response to Simulated Earthquakes. *Journal of the Structural Division*, *96*(12), 2557–2573. https://doi.org/10.1061/JSDEAG.0002765.

Tremblay, R., Atkinson, G. M., Bouaanani, N., Daneshvar, P., Léger, P., & Koboevic, S. (2015). Selection and scaling of ground motion time histories for seismic analysis using NBCC 2015. *11th Canadian Conference on Earthquake Engineering (11CCEE), Victoria, BC, Canada*, *99060*.

Villaverde, R. (1997). Seismic Design of Secondary Structures: State of the Art. *Journal of Structural Engineering*, *123*(8), 1011–1019. https://doi.org/10.1061/(ASCE)0733-9445(1997)123:8(1011).

Vukobratović, V., & Fajfar, P. (2015). A method for the direct determination of approximate floor response spectra for SDOF inelastic structures. *Bulletin of Earthquake Engineering*, *13*(5), 1405–1424. https://doi.org/10.1007/s10518-014-9667-0.

Vukobratović, V., & Fajfar, P. (2016). A method for the direct estimation of floor acceleration spectra for elastic and inelastic MDOF structures: A Method for the Direct Estimation of Floor Acceleration Spectra. *Earthquake Engineering & Structural Dynamics*, *45*(15), 2495–2511. https://doi.org/10.1002/eqe.2779.

Vukobratović, V., & Fajfar, P. (2017). Code-oriented floor acceleration spectra for building structures. *Bulletin of Earthquake Engineering*, *15*(7), 3013–3026. https://doi.org/10.1007/s10518-016-0076-4.

Wang, T., Shang, Q., & Li, J. (2021). Seismic force demands on acceleration-sensitive nonstructural components: A state-of-the-art review. *Earthquake Engineering and Engineering Vibration*, *20*(1), 39–62. https://doi.org/10.1007/s11803-021-2004-0.

Welch, D. P., & Sullivan, T. J. (2017). Illustrating a new possibility for the estimation of floor spectra in nonlinear multi-degree of freedom systems. *16th World Conference on Earthquake Engineering*, *Santiago, Chile, January 2017*, 9–13, (Vol. 212, p. 12).

Wieser, J., Pekcan, G., Zaghi, A. E., Itani, A., & Maragakis, M. (2013). Floor accelerations in yielding special moment resisting frame structures. *Earthquake Spectra*, *29*(3), 987–1002.

Yasui, Y., Yoshihara, J., Takeda, T., & Miyamoto, A. (1993). *Direct generation method for floor response spectra*.